IMPACT OF SHALLOW CONVECTIVE MOMENTUM TRANSPORT ON LARGE-SCALE DYNAMICS

Aquaplanet-Model Comparison Project

BY

Nicolaas J.M. Hoebe

STUDENT NUMBER: 5426391

Dr. Louise Nuijens
Prof. dr. A.P. Siebesma
Dr. Miren Vizcaino

Delft University of Technology, Faculty of Civil Engineering and Geosciences
Stevinweg 1, 2628 CN Delft, The Netherlands

June 24, 2023

Abstract

In the tropics, the character of the trade-winds is decisive for setting convergence and the large-scale circulation. Nevertheless, the vertical transport of momentum by shallow convection (SCMT) and yet its impact on trade-winds has not been investigated in depth yet. With this study, we aim to contribute in understanding the isolated effect SCMT has on the large scale circulations, setting the strength of the circulation and favouring zones of deep convection. Six climate models participated by each conducting three aquaplanet simulations, referring to a simplified climate model in which the entire planet's surface is covered by ocean, useful for studying fundamental atmosphere-ocean dynamics in the absence of complex land surface interactions. In three distinctive simulations, the models either turn off or exaggerate their SCMT scheme, alternatively by altering an approximate convective momentum scheme. We hypothesized that given the typical tropical wind profile, north-easterly flow at the surface and south-westerly flow aloft, the depth of mixing is determinative for the long-term reaction in setting the circulation. By deeper types if mixing, the scheme will likely bring opposite winds to the surface, affecting both the magnitude and direction of the trade-winds. A first analysis reveals that certain confine the mixing of surface friction to the sub-cloud layer, showing a clear cut-off of induced tendency between the mixed layer and the cloud layer. It is those models that favour a local response only in the shallow overturning circulation, opposite to the models that actively mix momentum between the mix-layer and cloud-layer and show adjustments in the deep overturning circulation. Further building earlier work showing that the horizontal advection of moist static energy (MSE) in the sub-tropics drives tropical convection, we analyzed to what extent enhanced SCMT leads to a change in atmospheric cooling rates by di- or convergence of MSE. Apparent differences by enhanced SCMT are observed in the in cooling rates by advection of MSE between the models that show strong responses in the deep overturning versus the models that do not.

Acknowledgements

Standing on the shoulders of giants, this research follows work by many devoted and extremely capable pioneers; scientists and modellers that over the last century have devoted decades of their life to understand how the tropical and global circulations operate, how atmospheric processes influence each other and have incorporated this in the construction of complex climate models. A special gesture of gratitude should be made to Dr. Louise Nuijens, whom has played a huge role in setting up and determining the simulation specifications and output requirements; directing the research and leading the many in-house discussions concerning the interpretation and hypotheses of what happens with the circulation and other key processes, failing to mention all her contributions. Last, the scientists and engineers active at the institutions and universities that participated with their knowledge and atmospheric models have been crucial in the creation of this research, moreover have been enormously valuable in the interpretation of their model behaviours and helpful in findings ways to distribute the data and providing additional data after the shifting of hypotheses: Niels Jansen (TUDelft); Brian Medeiros (NCAR); Adrian Lock (MetOffice); Pu Lin & Ming Zhao (NOAA); Ionela Musat & Florent Brient (IPSL).

1 Introduction

The latest state-of-the-art climate models for the Coupled Model Inter-Comparison Project Phases 5 and 6 (CMIP5 & CMIP6) still share troublesome systematic annual mean precipitation and sea surface temperature (SST) errors with respect to observations (Tian and Dong, 2020; Woelfle et al., 2018). Tropical precipitation and convective clouds are concentrated in planetary scale convergence zones. The Inter-Tropical Convergenze Zone (ITCZ) is a continuous zonal band fluctuating a few degrees north of the equator that is subjected to both the geometry of continents and atmosphere-ocean interaction (Bischoff and Schneider, 2014; Broccoli et al., 2006; Frierson, 2007; Marshall et al., 2014; Philander et al., 1996; Schneider et al., 2014).

Although the ITCZ tends to follow seasonal solstice cycles with both southern- and northern hemispheric maxima in climate models (Mitchell and Wallace, 1992; Waliser and Gautier, 1993)), observations clearly exhibit a single northern precipitation maximum. This single-ITCZ structure is generally misrepresented by Global Climate Models (GCMs), which simulate two zonally averaged maxima and an excessive depression over the equator - coined as the double-ITCZ problem (Hwang and Frierson, 2013; Li and Xie, 2014; Lin, 2007; Woelfle et al., 2018). Many GCMs simulate an extended, south-easterly oriented South Pacific Convergence Zone (SPCZ) ranging from the Eastern Pacific towards the Central Pacific that leads to the spurious southern hemispheric precipitation maximum in the zonal annual mean (Li and Xie, 2014; Woelfle et al., 2018)). In addition, the simulated precipitation along the equator tends to be weaker compared to observations, collocated with a cold bias in sea surface temperature (SST) ranging from the east Pacific to the edge of the west Pacific warm pool (Woelfle et al., 2018), referred to as the Pacific Cold Tongue bias (CT).

An extensive body of work analyses the sensitivity of these biases to model parametrizations and discrepancies in ocean-atmosphere coupling, such as cloud radiative forcings and convective parametrizations (de Szoeke et al., 2006; Yu and Mechoso, 1999)).

Less attention has been given to the role of parameterized wind transport, even though GCMs also exhibit a too strong easterly surface wind bias (Carr and Bretherton, 2001; Nuijens et al., 2022; Savazzi et al., 2022) along with the SST and precipitation biases (de Szoeke et al., 2006). It has been suggested that the too strong easterly wind bias originates in the free troposphere, where pressure gradients are influenced by errors in remote precipitation (Savazzi et al., 2022; Sobel and Neelin, 2006). Savazzi et al. (2022) indeed show that in the Integrated Forecasting System (IFS), easterly and meridional wind biases throughout the lower troposphere can be related to erroneous large-scale pressure gradients set by remote deep convection. The link between surface winds and winds in the free troposphere is established through the vertical transport of momentum by turbulence and convection (Back and Bretherton, 2009; Richter et al., 2014; Stevens et al., 2002). How momentum transport itself plays a role in setting wind and convergence biases is not understood thoroughly yet. For deep convection it is at least evident that convective momentum transport (CMT) is a key component to atmospheric circulation and needs to be included in GCMs (Richter and Rasch, 2008). Shallow convective momentum transport (hereafter sometimes referred to as SCMT) is also found to matter for setting lower tropospheric winds throughout the trades in weather forecasts (Carr and Bretherton, 2001; Sandu et al., 2020). Nonetheless, how SCMT influences the wind profile, and thus sets large-scale convergence and precipitation patterns is hardly documented and hence the objective of this work.

In the tropics, the typical trade-wind profile is dominated by the zonal wind component which tends to exhibit a local maximum near cloud base (Larson et al., 2019). Recent work suggests that the local jet is a result of dry convection that tends to introduce the largest deceleration in the upper sub-cloud layer, while shallow moist convection performs counter-gradient zonal momentum transport above cloud base, enhancing the zonal wind shear in the cloud layer. Both lead to a more pronounced wind maximum near cloud base (Dixit et al., 2021; Helfer et al., 2021; Nuijens et al., 2022). The results of Larson et al. (2019) and the aforementioned studies suggest that boundary layer and convection schemes should adequately capture the counter-gradient transport that is apparent in the sub-cloud layer and lower cloud layer.

Even less well documented in the literature is the profile of the meridional wind component and its associated momentum flux. For a predominantly zonal flow, this momentum flux controls the turning of the wind. Profiles of eddy momentum flux divergence calculated as the residual in the momentum budget constructed from airborne circular dropsonde arrays during EUREC4a (Nuijens et al., 2022) show that momentum fluxes contribute to a slowing down and turning of the wind across an Ekman layer approximately 1.5 km deep, however, the day to day (mesoscale) variability is large.

As the trade-wind layer deepens and more vigorous and organized shallow convection is observed, the component of friction in the along-wind direction decreases, and the cross-wind component of friction becomes relatively more important and veers the wind, reducing Ekman pumping. The wind veering is interpreted as the action of convective and mesoscale flows that introduce extra momentum near the surface, which may compensate for small-scale turbulent stresses.

In a 2007 study aiming to document to which extent sub-tropical shallow convection sets ITCZ width and intensity by means of vertical- and horizontal advection of MSE, conducted by Neggers et al. (2007). It is explained that with excluded presence of shallow convection they find that the oceanic ITCZ narrows but at the same time intensifies. Apparently shallow convection affects the tropical climate through more mechanisms than just by a change in moist and energy contained in the sub-tropical boundary layer. The found that changes in the surface winds impact the evaporation and thereby the transport of moisture into the deeper tropics, impacting deep convection. Inspired by their approach, we dissect the perturbed horizontal advection of MSE as a result of the inclusion of SCMT. Horizontal advection is influenced by the integrated meridional transport and by the latitudinal gradient of MSE. Hence, the dissection of it allows us to gain insight into what extent changes in the tropical MSE provisioning could be attributed to either dynamic changes as advection or to changes in evaporation.

Approximately one year later, Richter and Rasch (2008) investigated the effects of two convective momentum transport parameterizations (SL76 & GKI97) for CAM3. They found that changes in the upper branch of the Hadley circulation are small compared to changes in the lower branch, differing from the findings by Zhang and McFarlane (1995) and Kershaw and Gregory (1997), who actually found an intensification in the upper-troposphere. They speculate the difference to be caused by different vertical distributions of the convective mass flux and hence convective momentum transport.

To determine the range of sensitivity of low- and upper-level winds to SCMT across models, we carry out an inter-comparison case using different AGCMs in Aquaplanet configuration. Because the models use different SCMT schemes with different underlying convective mass flux parameterizations (Wu et al., 2007), we can distinguish fundamental steady-state (thermo-) dynamic adjustments for the different SCMT schemes. Changes in surface wind speed due to SCMT will affect surface evaporation and hence moisture advection, because surface evaporation is conventionally parameterized as a function of surface wind speed. Hence, we will also analyze whether changes in atmospheric moistening mediate the response to changes in wind patterns. Recent work suggests the bias results from deep convection parametrizations being too sensitive to SSTs and too insensitive to inhibitive large-scale dynamic forcings (Hirota et al., 2011; Oueslati and Bellon, 2015; Woelfle et al., 2018).

The simplified Aquaplanet configuration, using an all-water planet with prescribed SST pattern that is fixed-season and zonally symmetric, has proven to be very successful in highlighting differences in global mean cloud adjustment or feedbacks and zonal-mean circulation responses among models (Medeiros et al., 2015, 2008). This suggests that features as seasonality; land; geometry and ocean-atmosphere feedback processes might not be fundamental for understanding inter-model differences in, importantly, zonally-averaged precipitation and circulation characteristics (Bony et al., 2013; Stevens et al., 2012). Another major advantage of Aquaplanet configurations is that they are less computationally expensive and more straightforward to analyse, for instance in the zonal-mean (Webb et al., 2017).

2 Theory

The following sections conceptually discuss the tropical climatology including its circulation, typical wind profile and cloud structure. Next, we elaborate on what vertical transport of horizontal moment by shallow convection is, or in other words the vertical mixing of different winds by low-level clouds. We discuss its hypothetical effect on the typical wind profile and surface winds, and the implications for convergence and Ekman Pumping as an index for direct or indirect setting the circulation strength. Last, we discuss the change in the moist static energy (MSE) budget held by the atmosphere. Enhanced SCMT will lead to a change in the column-integrated energy budget and thereby the vertical and horizontal transport of energy, in the form of MSE.

Acronyms

Throughout the report, several terms or objects are referred to by acronyms, predominantly for reading efficiency. Table 1 lists the most important and most common ones:

Table 1: Acronyms & Description	
SCMT	Shallow Convective Momentum Transport
	Momentum mixing or mixing
CL	Convergence layer
	Layer where there is northerly (southerly) wind in NH (SH)
(s)CMTOFF	Run Without SCMT
CTRL	Control Run With SCMT
(s)CMTEXAG	Exaggerated Run With SCMT
(v)MSE	(Volumetric) Moist Static Energy
UKMOGK	UKMO With GKI Scheme
NH	Northern Hemisphere
SH	Southern Hemisphere

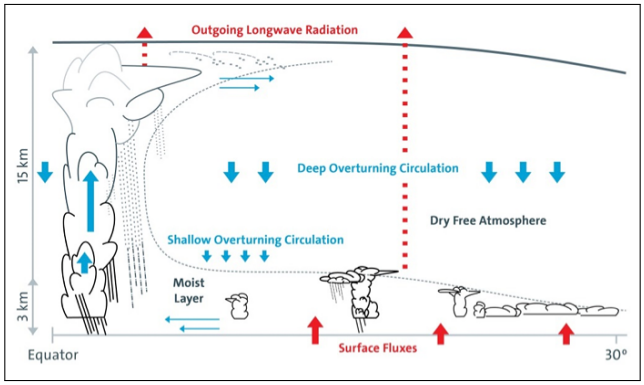

Figure 1: *Idealized Overturning Circulation Or Hadley Cell (University Of Hamburg).*

2.1 Tropical climatology

Tropical circulation refers to the large-scale atmospheric circulation pattern that exist in the tropics. It plays a crucial role in shaping global climate; weather patterns and poleward transport of heat. The primary drivers of the tropical circulation are solar heating, Earth's rotation, and oceanic circulation. It is important to note that tropical circulation is a complex system influenced by various factors, including ocean temperatures, land-sea distribution, and local topography. The interplay of these components contributes to the rich diversity of weather and climate patterns observed in tropical regions around the world. For the sake of this research, the circulation is confined to the direct- and indirect influence of low-level winds on driving the strength of the circulation and transport of scalars as heat and moisture.

2.1.1 Hadley circulation

The Hadley cell (Fig. 1) is a thermally-driven circulation that exists between the equator and about 30 degrees latitude in both hemispheres. It plays a crucial role in distributing heat and moisture between the equator and the poles. Intense solar radiation near the equator warms the air and surface in the tropics, causing it to rise and create a low-pressure zone. This ascending air cools as it gains altitude, leading to the formation of clouds and precipitation in the region known as the Intertropical Convergence Zone (ITCZ). As the air rises, it moves poleward in the upper atmosphere. Near the tropopause (the boundary between the troposphere and the stratosphere), it begins to cool and descend toward the subtropical latitudes (up to around 30^o N and S).

From there, the air flows back toward the equator near the surface and curls to the right (left) in the NH (SH) due to the Coriolis force, forming the trade winds (Fig. 2). While flowing towards the tropics, trade-winds attain a lot of moisture by their interaction with the warm sea surface that is heated by solar radiation. By the time the trade-winds enter the tropical zones, a warm, moist air mass is formed that fuels the circulation.

2.1.2 Winds

Sub-tropical surface winds or trade winds have a significant impact on the distribution of temperature, moisture and precipitation patterns in tropical and subtropical regions. They are closely linked with the surface fluxes through ocean-atmosphere interaction. Surface fluxes refer to the exchange of heat, moisture, and momentum between the Earth's surface (primarily the ocean) and the atmosphere. For the exchange of energy we distinguish between sensible and latent heat, the latter referring to the heat associated with the phase change of water, such as evaporation or condensation. The balance and interplay of these fluxes, along with other factors like wind speed, sea surface temperature and atmospheric stability, influences the dynamic behavior and properties of the mixed layer in the subtropics.

The trade winds play a crucial role in driving these surface fluxes and influencing the transfer of energy and moisture from the sub-tropics towards the tropics. As the trade winds approach the equator, they gain easterly momentum, causing the trade winds to gradually turn towards the west (Fig. 2). Advection of this warm, moist air mass towards the tropics, ultimately leads to equatorial convergence that drives uplifting and sets a zone of deep convection, also known as the ITCZ.

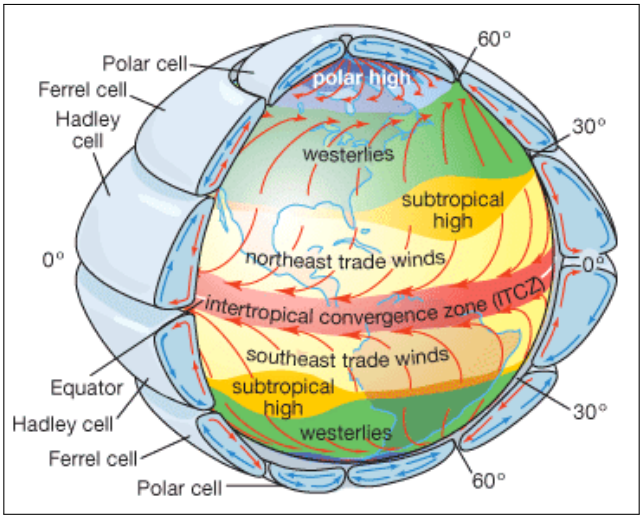

Figure 2: *Idealized Large-Scale Circulation On Earth (IAS, University of Amsterdam).*

2.1.3 Cloud structures

In the tropics, deeper types of convection and cloud formations are abundant due to the warm and moist atmospheric conditions. The primary form of convection observed in the tropics is deep convection that extents till the upper troposphere, characterized by large cumulonimbus-type clouds that form through the strong upward motion of air, giving rise to towering clouds and intense rainfall (left part in Fig. 3). Contrary, in the subtropics, convection and cloud formations are influenced by more stable atmospheric conditions. Hence, the prevailing type of convection observed in the subtropics is rather shallow convection (right part in Fig. 3), giving rise to cumulus-like cloud formations that are relatively less towering and less intense compared to the tropics.

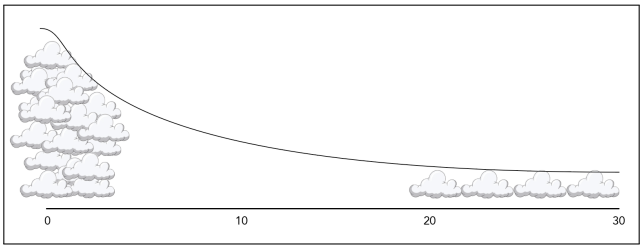

Figure 3: *Idealized Cloud Structure.*

2.2 Momentum transport by shallow convection

Shallow convective momentum transport (SCMT) refers to the vertical transport or vertical mixing of horizontal momentum by shallow convective clouds. This process has conventionally been parameterized in climate models because it is usually not numerically captured due to too large resolution. The influences of SCMT on the tropical wind profile and the atmospheric in general are rather complex and are interconnected with various processes.

2.2.1 Effect of SCMT on the wind profiles

The typical trade-wind profile consists of three layers, approximately halfway into the troposphere reversing direction from north-easterly towards a south-westerly component. In the boundary layer or the layer where surface friction is still experienced by winds, a local jet or local maximum in wind speed is apparent just below cloud base (Larson et al., 2019; Savazzi et al., 2022). In the tropics, trade-winds have reached their maximum zonal component and gain vertical velocity due to equatorial convergence or air masses from both hemispheres (Fig. 2).

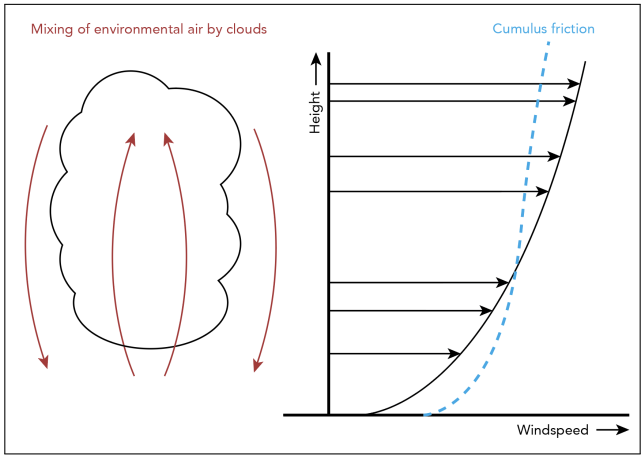

Figure 4: *Idealized Effect Of SCMT On An Idealized Wind-Profile).*

Typically, in the lower layers of the atmosphere, winds are slowed down by surface friction whereafter their speed increases with altitude (Fig. 4), known as vertical wind shear. SCMT will tend to mix these winds directly in the cloud layer, also directly or indirectly effecting winds at the surface and aloft. The mixing of wind shear by convection homogenizes the wind profile

in the cloud-layer, a process known as cumulus friction. The momentum flux that is directly affected by momentum transport affects the surface winds on a short time scale through finding a new wind vector balance, and through that on longer time scales by adjusting the circulation.

As explained by e.g. Back and Bretherton (2009); Richter et al. (2014); Stevens et al. (2002), the link between the winds at the surface and winds in the free troposphere is established through the vertical transport of momentum by turbulence and convection. Hence, the inclusion of SCMT in climate models is likely to have its effect on the surface winds, however yet not understood thoroughly.

2.2.2 Implications for tropical convergence

The strength of the deep overturning circulation could be indirectly measured through the intensity of upward motion due to the convergence of trade-winds and scalars as moist and energy. The magnitude and spatial distribution of convergence depends on the depth of the convergence layer; the meridional component or in other words the direction of the wind, and the strength of the winds.

2.2.3 Momentum fluxes

When we assume geostrophic balance in the steady state, there exists a balance between Coriolis, the pressure term and the vertical change of turbulent stresses in the mixed-layer. Following the work done by Back and Bretherton (2009); Richter et al. (2014); Stevens et al. (2002), explained in Section 2.2.1, the direct response to enhanced CMT will effectively change the winds at the top of the mixed layer and thereby affecting the winds in the free troposphere through the vertical momentum flux. This process adjusts the overall wind in the mixed-layer and through that, the strength of the Coriolis term and the non-linear response in surface stress, eventually finding a new vector wind balance. In other words, the direct response of vertically mixing the wind profile leads to an interaction of momentum between the free troposphere and the mixed layer, finding a new balance between Coriolis, the pressure term and the vertical change of the momentum flux. A complementary explanation and mathematical derivation could be found in Section 4.1.2.

2.2.4 Implications for Ekman Pumping

On larger time scales, the winds are indirectly adjusted through a change in circulation strength, as previously explained for convergence. Another way of measuring the strength of the circulation and distribution of upward motion as a driving mechanism for the circulation, is through Ekman Pumping - known as a term primarily used in the context of oceanography. When wind blows across the ocean surface, it imparts a force known as wind stress on the water. Due to the Coriolis effect, which is caused by the rotation of the Earth, the response of the water to the wind stress is deflected to the right in the Northern Hemisphere and to the left in the Southern Hemisphere, perpendicular to the direction of the winds. This deflection results in a spiral-like motion of water known as the Ekman spiral. In the atmosphere, we can define the same process within the Ekman layer - defined as the layer in the few first kilometers of the atmosphere where surface friction is still experienced. The curl of the surface stress sets zone of Ekman Pumping, driving upward motion of air. A mathematical derivation could be found in Section 4.1.3.

2.3 Double-ITCZ structure

A double Intertropical Convergence Zone (ITCZ) structure refers to a spurious phenomenon in climate models, characterized by two distinct bands or regions of enhanced atmospheric convection and low-level convergence. Observations exhibit a rather single, well-defined ITCZ, hence, this appears to be a persistent bias in climate models. In the ITCZ, there appears abundance of intense rainfall and thunderstorm activity near the equator, where the trade winds from the northern and southern hemispheres converge. The unequal distribution of sea surface temperatures (SSTs) could play a role in the formation of a double-ITCZ structure.

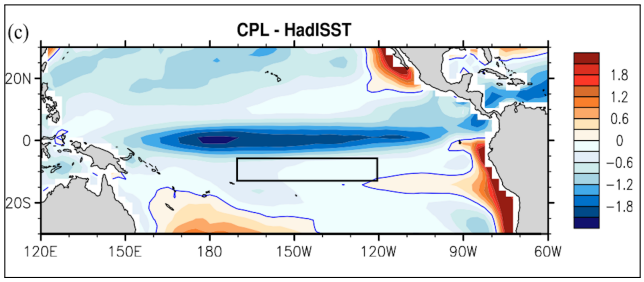

Figure 5: *Double-ITCZ Structure Shown As Sea Surface Temperature (SST) Anomaly Between Model (CPL) & Observations (HadlSST), Figure By Song and Zhang (2020)).*

If there is a pronounced temperature contrast across

equatorial oceans, it could lead to the formation of two distinct regions of enhanced convection and low-level convergence. Figure 5 shows an anomaly in sea surface temperature between simulations (CPL) and observations (HadlSST), obtained from a research done by Song and Zhang (2020). In coupled models, the SST is influenced by the surface winds through Ekman Pumping of cooler waters from below the subsurface. Hence, winds and SST distribution are narrowly linked, which rises the interest to see how SCMT affects surface winds.

3 Objectives

Our broad objective is to infer boundaries on the overall circulation response and the sensitivity of low-level equatorial trade-wind convergence to vertical transport of horizontal momentum by shallow convection (SCMT), which is of direct importance for improved future understanding of ocean-atmosphere feedback processes in coupled models (CMIP6 & 7):

1. How does the circulation respond to the inclusion of shallow convective momentum transport?

The overturning circulation is a very robust cell that is driven on longer time-scales by low layer convergence of winds; heat and moisture. The response in the circulation could be seen as an indirect result of altered winds that affect the convergence in the lower layers of the atmosphere. Hence, one of the first steps in dissecting the response in the circulation is through evaluating the response in the local wind profiles:

1a. What is the response in the wind profiles to enhanced SCMT?

Following, earlier suggestions by e.g. Richter and Rasch (2008) and Carr and Bretherton (2001) learned that the inter-model differences in large-scale circulation adjustment due to the change in winds by altered CMT, albeit shallow, could potentially be attributed to the vertical extent of the total convective mass flux. In this study we only twist the mixing of momentum by the shallow mass flux, hence, we still question and elaborate throughout the report to what extent the depth of shallow mass flux is affected and at play to directly or indirectly change the wind profiles. Profound changes in surface-wind direction and magnitude directly impact surface wind stresses, generally leading to Ekman Pumping of cooler waters from below the thermocline, directly influencing seasonal evolution of SSTs in coupled models. We adopt a similar atmospheric process where surface stress leads to Ekman Pumping at the top of the frictional layer:

1b. What is the long-term response, measured through wind convergence and Ekman Pumping as a reaction to the direct altering of low level winds?

The large-scale circulation and convergence zones are narrowly linked with deep convection, interested in consistency between the direct and indirect mechanisms and the surface precipitation as a proxy for the double-ITCZ structure that exists in climate models:

1c. To what extent does enhanced SCMT affect the positioning of convection zones?

Alternatively, the change of winds at the surface and in the mixed layer leads to a change in the atmospheric energy that is stored through a change in surface fluxes and to a change in the energy that is transported by horizontal divergence and vertical advection. Hence, aimed to retrieve insight into how models adjust their climate for the imbalance in energy caused by the inclusion of SCMT:

2. To what extent does enhanced SCMT lead to a change in the atmospheric MSE budget?

Changes in the surface winds due to the inclusion of SCMT might lead to differences in surface and energy fluxes such as evaporation, changing the amount of moist static energy stored in the mixed layer:

2a. Is there an influence on the sources and sinks of moist static energy?

Spatial changes in the distribution of available energy arise through the sum of net radiation and the surface fluxes and are balanced by changes in vertical advection & horizontal divergence. Following earlier work by Neggers et al. (2007), the horizontal advection of MSE sets the convective zones and fuels the tropics with moisture and heat. We question whether and to what extent the altering of surface winds affects this process:

2b. Is there an influence on the horizontal and vertical advection of moist static energy, leading to the cooling or warming of the troposphere?

4 Methods

The Ekman layer is defined as the layer where surface friction is communicated upward and experienced by the winds, making them ageostrophic. The direct response of momentum transport in the Ekman layer is causing the winds to directly establish a new vector wind balance in the steady-state - roughly confined to the mixed layer. On larger time scales, the winds are affected through changes in the circulation. Two powerful, alternative ways of indirectly assessing the driving mechanisms that set the strength of the circulation, are through boundary-layer convergence and Ekman Pumping. After thoroughly discussing model changes in the local wind profile and subsequently in the circulation, we question whether we can verify a similar trend in the convective precipitation pattern as a proxy for a double-ITCZ structure.

Next, interested into what extent changes in the width and intensity of the ITCZ could be attributed to either changes in dynamic nature such as the horizontal- and vertical advection of MSE, versus changes in physics, e.g. evaporation; radiation and moisture profiles - we adopt a formulation previously proposed by Neggers et al. (2007) that links the column-integrated available energy to the horizontal and vertical divergence of MSE.

4.1 Interpreting the circulation response

The deep- and shallow overturning circulations (Fig. 1) are complex systems influenced by many atmospheric processes. For directly evaluating the overall response of the circulation, the zonally averaged meridional stream function (ψ) is very suitable in showing the mass divergence in the meridional plane, assuming conservation of mass. Stream functions are arbitrary functions whose partial derivative at that point along a direction will give us the velocity in that direction. In other words, the stream function is constant for stream lines which are parallel to the flow, hence it represents the volumetric flux:

$$\psi_p(\phi, p) = \frac{2\pi cos(\phi)}{g} \int_p^{p_s} [v] dp \tag{1}$$

In the zonal plane, a positive stream flow ($\psi > 0$) refers to the clockwise rotation of mass in the meridional plane, whereas negative stream flow represents anti-clockwise rotation.

4.1.1 Interpreting changes in the local wind profiles

The influence of SCMT on the zonal, meridional and vertical wind profiles will be evaluated on vertical profiles at key locations (tropics, sub-tropics). In the tropics, the zonal wind and to a certain extent the meridional wind profile have a local maximum of momentum just below cloud base (explained earlier), expected to be more clearly present without vertical mixing processes. In the sub-tropics, the local jet is less pronounced. Overall, it will be assessed to what extent the inclusion of SCMT of is direct- or indirectly homogenizing the wind profiles and whether the changes are e.g. strong and remote or, alternatively, relatively weak and restricted to a certain part of the circulation.

Next, the change in winds will be compared with the tendency on the winds produced by the combined schemes of convection and turbulence. The reason for this is because the GFDL model only had available data from a diffusivity parameter that entails both schemes. For accurate inter-model comparison, the decision was made to combine the schemes for all models.

Last, the change in the surface winds due to enhanced SCMT will be evaluated in more depth, looking at both the change in strength and direction averaged over key locations (e.g. tropics, ($|0^o - 10^o|$), revealing a first grasp about whether the inclusion of SCMT might favour equatorial convergence.

4.1.2 Estimating changes in convergence

An indirect response in the circulation adjustment due to the inclusion of SCMT may be diagnosed through vertical motion set by horizontal convergence in the converging layer of the troposphere. With converging layer, we mean the layer in which there is still northerly (southerly) transport in the NH (SH). Using the conservation of mass and the continuity equation, integrated over the depth of the convergence layer, we may find an equation for the vertically integrated large-scale divergence $\hat{\mathcal{D}}$:

$$\hat{\mathcal{D}} = -w = \int_0^z \left(\frac{du}{dx} + \frac{dv}{dy} \right) dz \tag{2}$$

With z being the top of the converging layer and w the vertical velocity at z. Alternatively, rewritten in pressure notation:

$$\hat{\mathcal{D}} = \omega = \int_p^{p_s} \left(\frac{du}{dx} + \frac{dv}{dy} \right) dp \tag{3}$$

With ω the vertical velocity in pressure coordinates and

p & p_s referring to the pressure at z and at the surface respectively.

As the top of the convergence layer (z) is manually defined, we also check for sensitivity of setting the height of the layer. The reason behind this is that the real height of the layer is rather difficult to find or compute in GCMs. The models that provided a variable with the boundary layer height showed to be very chaotic of nature so could not be used.

4.1.3 The Ekman layer

Alternatively to wind convergence, a second way to infer the strength of the circulation is through Ekman Pumping. Using the mixed-layer framework applied to momentum, the steady-state geostrophic wind-balance in a horizontally homogeneous layer may be written as:

$$f\vec{k} \times \vec{u} + \rho_0^{-1}\vec{\nabla}p = \frac{\partial \vec{\tau}}{\partial z} \tag{4}$$

Where $\vec{U} = (u, v)$ and $\vec{\tau} = (-u'w', v'w')$ is the turbulent momentum flux.

In accordance with work previously done by Back and Bretherton (2009); Saggiorato et al. (2020); Stevens et al. (2002), integrating the geostrophic wind-balance over a well-mixed sub-cloud layer to express a formulation for the bulk wind speed and similar for the bulk pressure, gives us:

$$\vec{U} = \frac{1}{z}\int_o^z [\vec{u}]\, dz; \tag{5}$$

Such that the momentum flux at the top of the mixed-layer and surface is balanced by the Coriolis force and the hydro-static pressure term in bulk formulation:

$$f\vec{k} \times \vec{U} + \rho_0^{-1}\vec{\nabla}P = \frac{\vec{\tau}(z) - \vec{\tau}(0)}{z} \tag{6}$$

The momentum fluxes are parameterized by:

$$\begin{aligned} \vec{\tau}(0) &= (C_D\|\vec{U}\|)\vec{U} \\ \vec{\tau}(z) &= w_e(\vec{U}(z) - \vec{U}) \end{aligned} \tag{7}$$

In this notation, we find that the momentum flux at the surface, or surface stress, is a non-linear function of the wind speed at the surface. The momentum flux at the top of the mixed layer is expressed as an entrainment rate that is a function of the linear wind gradient within the mixed-layer ($\vec{U}(z) - \vec{U}$). When we include SCMT to the increments, we would find that the wind profile is directly adjusted in the cloud-layer. Hence, $\vec{U}(z)$ changes, effectively altering $\vec{\tau}(h)$ and thereby the right-hand side of Eq. 6. The Coriolis term will restore balance accordingly by altering its bulk wind speed $\vec{U}$ whereafter both the momentum flux at the top $\vec{\tau}(z)$ and surface $\vec{\tau}(0)$ iterate again, eventually finding balance with a steady-state bulk wind speed.

4.1.4 Estimating changes in Ekman Pumping

The indirect effects on the circulation through Ekman Pumping may be diagnosed by using the continuity equation, which establishes a link between the large-scale divergence $\mathcal{D}$ and the horizontal wind pattern:

$$\mathcal{D} = \frac{dw}{dz} = -\left(\frac{du}{dx} + \frac{dv}{dy}\right) \tag{8}$$

Rewriting Equation 6 into both its horizontal components and differentiating with respect to y and x respectively, gives the momentum balance for the mixed-layer model in two horizontal directions:

$$\begin{aligned} f\frac{\partial v}{\partial y} - \rho_0^{-1}\frac{\partial}{\partial y}\frac{\partial}{\partial x}p - \frac{\partial}{\partial z}\frac{\partial}{\partial y}u'w' = 0 \\ -f\frac{\partial u}{\partial x} - \rho_0^{-1}\frac{\partial}{\partial y}\frac{\partial}{\partial x}p - \frac{\partial}{\partial z}\frac{\partial}{\partial x}v'w' = 0 \end{aligned} \tag{9}$$

Combining the momentum equations with mass conservation described in Eq. 8, ultimately gives:

$$f\frac{dw}{dz} = \frac{\partial}{\partial z}\left(\frac{\partial u'w'}{\partial y} - \frac{\partial v'w'}{\partial x}\right) \tag{10}$$

The term within the large parentheses on the right hand side represents the curl of the momentum flux ($\nabla \times \vec{\tau}$, or $\mathrm{Curl}\,\vec{\tau}$). If the expression is integrated from the surface to the top of the Ekman layer h_E, defined as the height where $\vec{\tau}_{h_E} = 0$ (this appreciates that the Ekman layer extends beyond the mixed-layer h in the presence of shallow moist convection) the vertical velocity at the top of the frictional or Ekman layer is obtained:

$$w_{h_E} = -\frac{1}{f}\mathrm{Curl}\,\vec{\tau_0} \tag{11}$$

In other words, the Ekman pumping at the top of the frictional layer depends on the curl of the surface momentum flux. The indirect response of the meridional circulation measured through a change in Ekman pumping at h_E is thus felt through a difference in the distribution of $\vec{\tau_0}$. Budget analysis of Ekman pumping learned that the latitudinal gradient of the zonal surface stress (τ_{dy}) is the only dominant component, aligning with findings by Richter and Rasch (2008) who documented that the zonal momentum budget is primarily responsible for changes in the Hadley circulation by changing the Coriolis torque. This however differs from

Wu et al. (2003) who attribute changes in the tropical meridional flow to meridional convective momentum transport. An altering of surface winds due to the inclusion of SCMT that would have a latitudinal dependency would change the distribution of the zonal surface stress and favour Ekman Pumping at latitudes where the gradient enhances, at the expense of latitudes where the zonal surface stress is constant with latitude. Contrary, we would find that a consistent shift of the surface stress with latitude, or in other words a non-latitudinal dependence of the altering of surface winds, would have a minimal impact on changes in Ekman Pumping as a result to SCMT.

4.2 Estimating energetic changes

Altering surface winds and the winds in the mixed-layer by SCMT, effectively changes the energy stored in and above the mixed-layer. This is established through a change in the surface fluxes and the advection components. Complementary, the change in convergence zones also adjusts the amount of energy stored above the mixed layer, in the free troposphere. Energy is measured by moist static energy (MSE). MSE is a thermodynamic quantity used to describe the total energy content of a parcel of moist air. It takes into account the combined effects of temperature, water vapor content and pressure. It is defined as the sum of the sensible heat, latent heat and potential energy:

$$h = c_p T + L_v q + gz \tag{12}$$

With c_p the specific heat capacity; L_v the latent heat of vaporization and all other variables having their conventional meaning.

When we multiply MSE with density, we obtain a measure for the amount of energy per volume, or volumetric MSE (vMSE). This compensates for the linear increase of density with pressure (or likewise decrease with altitude) and moreover makes integration over height feasible in order to find the energy held by the atmosphere column in $[Jm^{-2}]$.

A 2007 study conducted by Neggers et al. (2007) proposed that the column-integrated net available energy, defined as the sum of the surface fluxes and the net radiation at the top of the atmosphere (TOA), is balanced by vertical- and horizontal integrated advection of MSE (Eq. 13). We would expect that convective zones of uprising warm, moist air, usually contain relatively more MSE in their atmospheric column than zones of subsidence. In other words, changes in surface fluxes coincide with changes in the amount of MSE stored in an atmospheric column.

$$\langle \mathcal{D}_H(h) \rangle + \langle \omega \partial_p(h) \rangle = F_{rad} + SH + LH \tag{13}$$

With $\mathcal{D}_H(h)$ the horizontal divergence of MSE (h); $\omega\partial_p(h)$ the vertical advection; F_{rad} the net radiation at the TOA ($LW_n + SW_n$); SH & LH being the sensible and latent heat fluxes at the surface respectively and $\langle\rangle$ referring to the vertical integration over the entire tropospheric column ($\int_p^{p_s} dp$).

We will first analyse how the amount of MSE held by the atmosphere changes by enhanced SCMT. Next, we see how this relates to the change of the surface fluxes and radiative balance at the TOA. Subsequently, we combine it with the horizontal- and vertical advection of (volumetric) MSE to show how, in an arbitrary simulation (e.g. control), horizontal- and vertical advection act to di- or convergence heat and moisture. Last, we show the change in cooling rates due to enhanced SCMT, driven by horizontal- and vertical divergence of MSE. Note that we partially adopt Equation 13 as we drop the vertical integration terms in order to reveal spatially where advection is at play.

4.2.1 Surface fluxes & energy budget

In climate models, the sensible and latent surface fluxes are parameterized formulas to account for the interaction and transport of moist and energy between the surface and the atmosphere, hence, they set the energy budget in the well-mixed layer for a large extent. These formulas are often based on empirical relationships derived from observations and can vary depending on the specific model or parameterization scheme employed. An approach commonly applied is to use a bulk aerodynamic formula that relates the fluxes to the difference in specific humidity along with other factors such as wind speed; temperature and surface roughness:

$$\begin{aligned} LH &\sim \rho_a L_v c_e (q_w - q_a)|U| \\ SH &\sim \rho_a c_p (T_w - T_a)|U| \end{aligned} \tag{14}$$

With ρ_a the density of air right at the surface or lowest model level; L_v and c_p being the latent heat of vaporization and the specific heat capacity of air respectively; $q_w; q_a; T_w$ & T_a the difference of specific humidity and temperature between the surface and the lowest model level and $|U|$ the absolute wind speed at the surface.

As shown, the surface fluxes are a function of the absolute wind speed at the surface or lowest model level, hence a change in windspeed due to vertical mixing of

horizontal momentum has its affect on the energy balance in the mixed layer.

4.2.2 Advection of MSE

Dismantling the two terms in the left hand side of Equation 13 would provide valuable insight in the divergence of vMSE through horizontal- and vertical advection, acting to either cool or warm atmospheric regions. The horizontal divergence is primarily measured through the meridional term as we are running an aquaplanet simulation which is approximately uniform in the longitudinal direction. Dropping the vertical integration and the zonal component of the first term in Equation 13 gives us:

$$\mathcal{D}_H(h) \sim \rho v \, \frac{d(h)}{dy} \tag{15}$$

Vertical advection of MSE is largely determined by the vertical wind vector, driven by horizontal convergence (Eq. 3). Dropping the vertical integral and combining this with density, we find an expression for the vertical advection or divergence of vMSE:

$$\omega \, \partial_p(h) \sim \rho\omega \, \frac{d(h)}{dz} \tag{16}$$

Both terms in Equations 15 & 16 provide inside in the cooling rate driven by either horizontal- or vertical transport of vMSE. By computing the perturbation and combining this with the energy fluxes discussed in Section 4.2.1, we reveal inter-model differences in the way both advective terms play a role in the provision or extraction of heat and moisture for zones in which we might find changes in atmospheric MSE content or changes in the energy fluxes.

4.3 Inter-model comparison

We start by discussing all findings for two models that showed very distinctive behaviour to SCMT: GFDL and UKMO. In order to show what the inclusion of SCMT enhances, we will later make use of perturbation plots that show the difference between the control run and the run without momentum mixing ($SCMT_{ctrl} - SCMT_{cmtoff}$). The reason for using the control run and not using the exaggerated run is that several models used a different factor (e.g. $x3$ or $x10$) to multiply the scheme with, which would make qualitative comparison rather spurious. After having discussed everything for GFDL and UKMO, we aim to see whether the comparison could be extended for the other participating models.

4.4 Conventions

The research contains multiple models and emphasizes on many variables; cross-sections and zones, therefore choices have been made to find an optimal balance between showing as much key findings while not overdoing the amount of figures nor the amount of space the figures make up in the report.

Using the approximate hemispheric similarity that an aquaplanet simulation induces, in this report it is sometimes decided to only show one hemisphere in the zonal average (e.g. $|0^o - 30^o|$), mainly for the purpose of saving space in the document or to show multiple models or multiple locations within one figure. Note that there is always checked for inter-hemispheric differences in terms in magnitude or conceptual changes, depending on what is discussed.

When showing a perturbation or change between two experiments, we subtract the run with an active SCMT scheme by the run without (e.g. $SCMT_{ctrl} - SCMT_{off}$). The reason behind this is is that an increase for a scalar or variable due to the inclusion for SCMT would result in a positive subtraction, whereas a decrease would result in a negative subtraction.

The line plots that reveal all experiments are shown by the convention that the darkest color together with the most solidity refer to the run with the most momentum mixing, in other words the exaggerated experiment. Contrary, the light colored plots with a dotted line refer to the experiment without SCMT. The legends show the experiments as well, together with the multiplication factor for the exaggerated run, depending on the model.

5 Models & Data

For this research, we worked with the data that is part of the Pan Gass Shallow Cumulus Friction Model Inter-Comparison Project. The simulations in this study are performed using Atmospheric Global Climate Models (AGCMs) consisting of fully dynamic atmospheric models. So far the models that participate include: CAM6 from NCAR (with two dynamical cores NE16 (CAM6NE) & FV2 (CAM6FV)) using a unified convection and turbulence scheme with K-theory for momentum transport; UKMO with two different parameterizations for convective momentum transport: GAL from Alan Grant (UKMO) and the Gregory-Kershaw scheme (GKI, UKMOGK) and the GFDL model from NOAA using separate schemes for shallow and deep convective

momentum transport.. All models are run at a horizontal resolution of 1^o or more for preferably 42 months, considering the 6 months to be spin-up time.

5.1 Aqua-planet simulation

In the simulations we run an idealized configuration of an atmospheric model, known as an aquaplanet mode - previously utilized by AMIP-II experiments (Medeiros et al., 2008; Webb et al., 2017). Aquaplanets are conventionally explained as an entirely symmetrical water-covered mathematically Earth-like planet, however with removed land masses; topography; sea-ice and other heterogeneity's (see also below for further description of the Aquaplanet experimental setup).

5.1.1 Model description

Models have been asked to make three distinctive runs with different configurations for (shallow) convective momentum transport:

1. Aqua-Control with default settings ($CTRL$).
2. Aqua-NOsCMT with momentum transport by shallow convection turned off or the tendency set equal to zero. ($CMTOFF$)
3. Aqua-sCMTx10 with tendencies by shallow convective momentum transport multiplied by a factor 10 or likewise. ($CMTEXAG$)

For most of the Aquaplanet experimental design we refer to previous CFMIP-2/CMIP5 experiments explained in detail by Webb et al. (2017) and Medeiros et al. (2015), and to the AquaPlanet Experimental (APE) protocol by Blackburn and Hoskins (2013). Hence, in the simulations SST is non-varying, zonally constant and does not vary with seasons. It is prescribed and varies with latitude only according to Neale and Hoskins (2000), meaning that if $|\phi| < \frac{\pi}{3}$, T it is prescribed by Equation 17 as a function of latitude (ϕ) and if else, temperature is set to zero ($T_s = 0$):

$$T_s(\phi) = \begin{cases} 27(1 - sin^2[\frac{3\phi}{2})]^o C & ; -\frac{\pi}{3} < \phi \frac{\pi}{3} \\ 0 & ; otherwise \end{cases} \quad (17)$$

No sea ice is prescribed, meaning that poleward of 60^o latitude, SST is equal to zero. All orbital parameters are set to perpetual equinox conditions, meaning that both eccentricity and obliquity have been set to zero in order to have global insolation independent of the non-circular orbit, being held constant at $1365\,Wm^{-2}$. All participating models that use a prognostic equation for the surface skin temperature are requested to set skin temperature equal to the prescribed surface temperature.

Radiatively active trace gases are well-mixed and prescribed following AMIP II: CO_2 : $348ppmv$; CH_4 : $1650ppbv$; N_2O : $306ppbv$ and halocarbon yield of $\approx 0.24Wm^{-2}$. Vertical ozone distribution is the same as the one that was derived from AMIP-II by Gates et al. (1999), and is provided in two netcdf data sets, online accessible via http://doi.org/10.5065/D64X5653.

5.1.2 Model parameterization

In practice, it is not possible for all models to carry out this precise set of experiments because they have no explicitly parameterized scheme for momentum transport by shallow convection or no parameterized shallow convection at all. Alternatively, momentum transport convection is generated through unified or deep convection only.

Table 2 lists all the participating models and their corresponding type of CMT parameterization (either deep, shallow or both) that is turned off and amplified in this research, and if so with what magnitude. For most models the amplification refers to the tendencies on the wind-profile induced by SCMT before the time-stepping takes place, alternations are documented.

Appearance of aerosols is set to zero in terms of direct (aerosol-radiative) and indirect (cloud-radiative) forcing. Models that rely on aerosols for cloud condensations are requested to use a constant ocean climatology (aerosol release by the ocean) that is zonally symmetric. Atmospheric dry mass is adjusted to a global mean of 1018 hPa and models are requested to adopt other geophysical constants equal to APE, as listed in Table 2 in Williamson et al. (2012).

5.2 Data correction

The data that was submitted by MetOffice for both UKMO models was originally provided on a height-grid ($[m]$). For plotting purposes, the data has intentionally been replaced by an averaged pressure-grid directly derived from the pressure variable within the data sets. The vertical pressure dimension is both zonally averaged and averaged over the tropical latitudes ($|0^o - 30^o|$).

Table 2: Models & Parameterizations			
Models CTRL		*NO CMT*	*CMT EXAG*
Main Report ↓			
Separate schemes for deep and shallow CMT.	GFDL	Shallow CMT turned off.	Shallow CMT Tendencies X10.
Non-Local K-Profile BL-scheme.	UKMO	Shallow CMT turned off.	Shallow CMT Tendencies X3.
Inter-Model Comparison ↓			
Unified convection and turbulence scheme with K-diffusion.	CAM6NE	CMT for both shallow and deep convection turned off by setting tuning parameter CK10 = 0.	Exaggerated by doubling scaling parameter.
Unified shallow convection and turbulence scheme.	CAM6FV	Deep CMT turned off.	Not available.
GKI-Scheme.	UKMOGK	Dropped Shallow Vertical Flux of Horizontal Momentum (uw_{conv}).	GKI increments for the SCMT by X10 .
No data.	LMDZ	No data.	No data.

As pressure gradients tend to be relatively relaxed in the tropics and this is for now our only domain of interest, the assumption has been made that the quantitative differences in the height-dimension for plotted variables are rather small for conceptual and qualitative understanding of the large-scale response. The consequence of averaging the pressure grid in latitudinal direction is that the shown pressure for the variables is actually overestimated in the tropics ($| < 20^o|$ and underestimated in the sub-tropics ($| > 20^o|$), with increasing underestimation towards the poles. Please note that the actual values of variables on the vertical intervals have not been changed, in other words all the figures for UKMO reveal exactly the same values, however with values on the y-axis representing height instead of pressure.

For integrating or differentiating in the vertical dimension on a pressure-grid, it is usually combined with the multiplication of omega, the vertical velocity on pressure scales. For both UKMO models, omega has been computed manually by vertical velocity and density directed retrieved from the data, as it was not originally provided.

Last, the geopotential height in the GFDL model, required for the computation of moist static energy, is central averaged as it was originally computed on interval levels of grid cells while temperature and humidity (and all other variables) were provided in the center of the grid cells - which makes multiplication erroneous. Looking at the vertical profile of MSE we find that it slightly increases with height in the troposphere. On the one hand this could be physically right, however compared to the other models that computed MSE directly from the data, it should be rather vertical, meaning that the vertical advection of MSE (Eq. 13) might slightly overestimated for this model.

6 Results

Considering the dynamic model responses, we start off by describing how the local wind profiles change, emphasizing on both the adjustment over the tropospheric column and at the surface. Next, we elaborate on the tendencies induced by activating and exaggerating SCMT in combination with the wind profiles. Shifting from the direct local response to rather long-term responses driving the circulation, we look at the convergence and Ekman Pumping. Last, we compare the meridional stream function together with what we found for e.g. the convergence patterns and see whether convective precipitation is in line with this. Secondly, the MSE budget and its components is elaborated, whereafter the perturbation ($SCMT_{ctrl} - SCMT_{off}$) in atmospheric MSE is shown as a result of altered surface winds and fluxes. To see what causes these differences, we dive further into the surface fluxes and the advection of MSE in both horizontal and vertical direction. Last, we compare all the findings confined to

UKMO and GFDL with both CAM6 (NE16 & FV2) models; UKMO with the GKI scheme (UKMOGK) and the LMDZ model.

6.1 Winds

Using changes in the upper tropospheric meridional wind as a first proxy for finding whether and to what extent both the local and remote winds adjusts to enhanced SCMT, we find that for the GFDL model (Fig. 6) both low level trade-winds and upper tropospheric westerly winds weaken. Also, we find that the depth of the tropical boundary layer slightly deepens for both models (Eq. 7), especially in the exaggerated experiment.

For UKMO, we find the poleward meridional wind in the upper troposphere to not show any significant change (Fig. 28). The strength of the trade-winds weakens, most probably as a response to the more local mixing of weaker, north-easterly geostrophic winds from the middle troposphere towards the friction layer. Agreeing with the GFDL model, the depth of the mixed layer deepens with the inclusion and exaggeration of SCMT, probably as a result of the enhanced momentum flux between the mixed layer and the free troposphere.

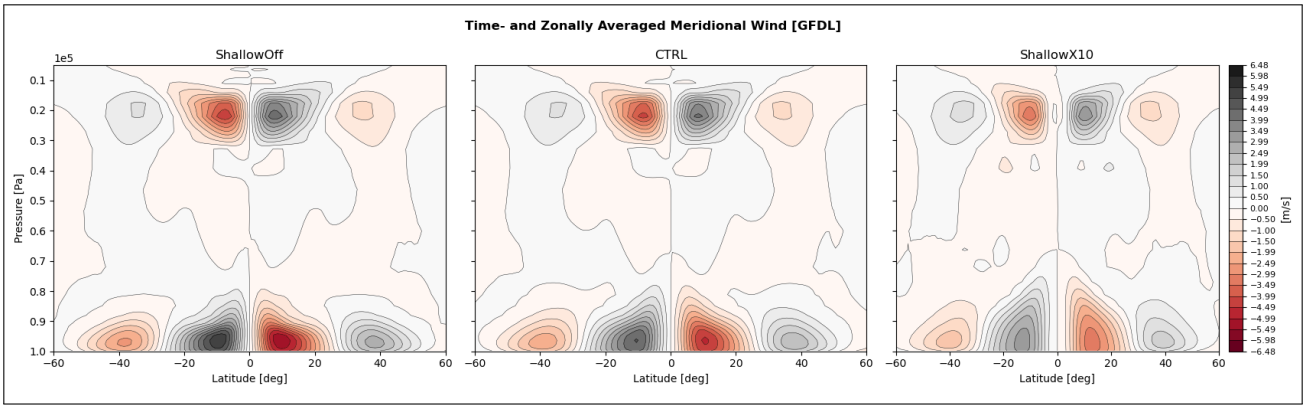

Figure 6: *Zonally Averaged Contour-Plot Of Meridional Wind In $SMCT_{off}$ (Left); $SCMT_{ctrl}$ (Centre) & $SCMT_{exag}$ (Right) For GFDL.*

6.1.1 Wind profiles

The tropics ($\sim |0^o - 10^o|$) are predominantly characterized by deep and strong types of convection, extending up till the beginning of the stratosphere. The typical horizontal wind profile is dominated by a strong zonal component, usually with a local maximum below below cloud base ($\sim 900 - 950\, hPa$) whereafter the winds decrease in strength with altitude. The meridional component is relatively weak as winds are obtaining vertical momentum by equatorial convergence, however, a smaller local jet below cloud base does exist to a certain extent. In the middle troposphere there is usually only zonal- and vertical transport, whereafter the upper troposphere is largely dominated by poleward movement.

Figure 7 shows the three wind components for the GFDL model for all three experiments, averaged over the tropics ($|2^o - 5^o|$) to make a representative tropical cross-section. The dotted light green line is the run without SCMT, whereas the dark solid green line refers to the run with the most abundant parameterization, see Section 4.4.

With regard to the zonal wind, which dominates the absolute wind speed in the tropics, we find that without vertical transport of momentum (dotted line), the local jet in the lower tropospheric layer is well pronounced, and that vertical wind shear is abundant. Enhanced SCMT weakens the wind over the entire depth of the troposphere and homogenizes the profile, thereby also getting rid of the local jet.

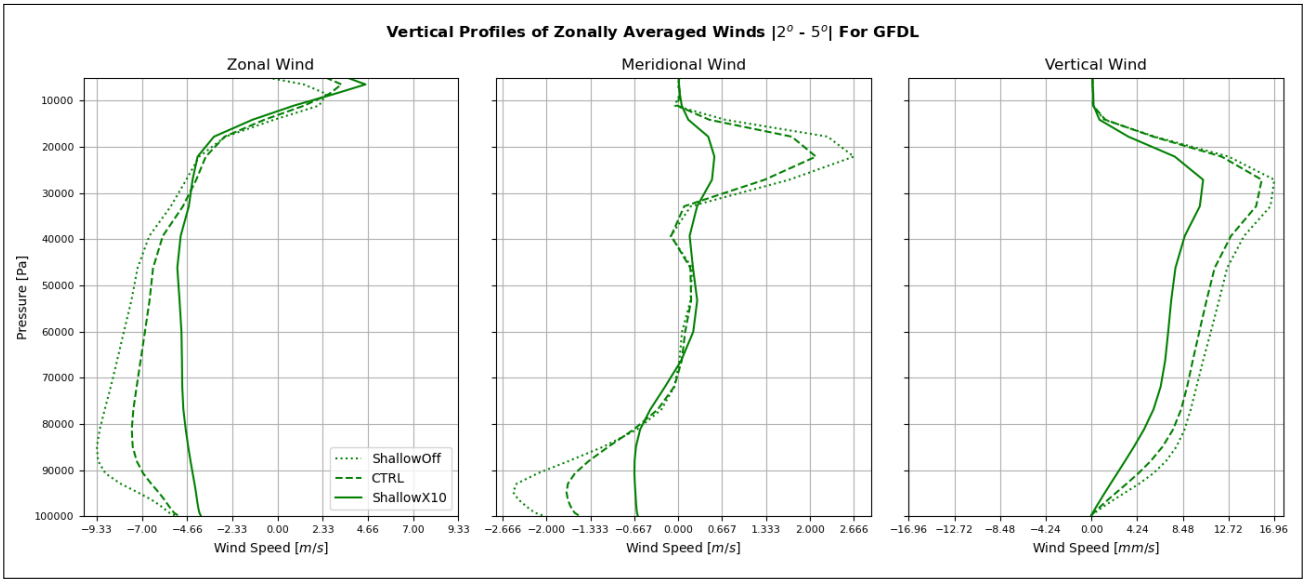

Figure 7: *Zonally Averaged Vertical Plots Of Tropical Winds, Averaged* $2^o - 5^o$ *For GFDL.*

Concerning the lower atmosphere, the meridional wind has a strong vertical wind shear and local jet in the converging layer ($> 700\,hPa$) whereas the profile tends to be homogenized and well-mixed by enhancing SCMT. The plot shows that the model shows a strong response in the upper tropospheric meridional wind as well, which we discussed in Section 6.1. In other words, both the vertical plots of the zonal and meridional seem to suggest that for GFDL the SCMT scheme appears to either directly or indirectly affect wind profiles over the depth of the entire troposphere.

The vertical wind profile, whatsoever, increases with height and reaches its maximum in the upper troposphere for all three experiments. We assume that the change of the vertical wind is rather an indirect result of low layer convergence, rather than a direct effect of SCMT itself.

When we consider the wind profiles for UKMO, shown in Figure 29, we find that overall the difference between the three runs is by far less pronounced. With regard to the zonal profile, the winds in the cloud layer are slightly weakened in easterly direction, whereas they are accelerated in the rest of the upper troposphere. The meridional profile shows barely no remote response. With the introduction and exaggeration of momentum transport, winds in the lower part of the free atmosphere ($\sim 900hPa - 700\,hPa$) are accelerated in easterly direction, at the expense of the trade-winds. In line with the small adjustments horizontal winds, the vertical wind profile reveals that large changes in low-level convergence are absent.

In the sub-tropics, we find for GFDL that the wind profiles are less affected between the three experiments (Fig. 30). The zonal wind slightly mixes the local jet below cloud base, and accelerates in easterly direction over the entire depth of the troposphere. The meridional wind decelerates at the surface, compensated for by acceleration in the cloud-layer ($\sim 950 - 850\,hPa$). In addition, a change in the depth of the mixed layer is observed, especially with the exaggeration of SCMT. Roughly the same findings apply for UKMO (Fig. 31) with deceleration of the zonal wind over the entire depth of the troposphere and mixing confined to the shallow overturning circulation ($1000-800hPa$), coinciding with an apparent deepening of the layer.

6.1.2 Tendencies & mass flux

We question here to what extent SCMT directly adjusts the wind profile by looking at the tendencies that act on both horizontal wind vectors. For GFDL, the original tendencies produced by SCMT only were reported to come from a process that was not turned on by the model, instead, a vertical diffusivity parameter that entails both the tendency by convection and turbulence was submitted and advice to evaluate as it was reported to come the closest to the effect SCMT has on the wind profile. To enable inter-comparison between models, all the tendencies shown represent the combined tendencies by both the convection and turbulence schemes.

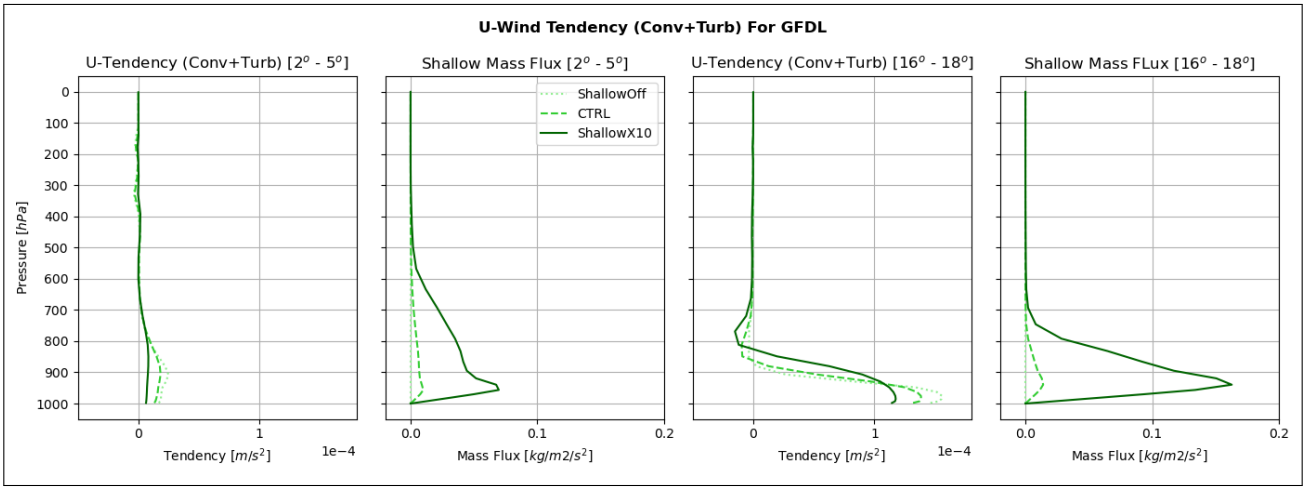

Figure 8: *Vertical Line-Plot Of Zonal Wind And Tendency Due To SCMT For GFDL, Cross-Sectional For Tropics ($|2^o - 5^o|$) And Sub-Tropics ($|16^o - 18^o|$).*

Following reports from NOAA, the shallow convective mass-flux that operates in the GFDL model is allowed for deeper mixing up to 200 hPa, therefore including congestus-type clouds present in the tropical latitudes. For GFDL, the tendency on the zonal wind and the mass flux are illustrated in Figure 8. It shows the zonal wind, total tendency on the zonal wind and the shallow convective mass flux for both the tropics (a-b) and the sub-tropics (c-d). The plotting convention is again that the most solid and dark lines coincide with the most abundance of SCMT (exaggerated run). After consultation with NOAA about the shallow mass flux, it was explained that after the convection scheme calculates the temperature and humidity tendency, it is multiplied by either $x0$ or $x10$, depending on the experiment, after passing it on to the momentum scheme. The mass flux output is also done after the amplification, which explains why it is absent for the CMTOFF experiment and nonphysically larger in the exaggerated run. In other words, only the control plot of the mass flux appears to be representative.

By looking at the tendencies for GFDL, we find that for the tropics, the total combined tendency is and remains positive, hence, it acts to decelerate the easterly winds for approximately the lower half of the atmosphere ($> 600\,hPa$). In the sub-tropics, it does the same in the cloud and sub-cloud layer ($> 800\ hPa$), however acts to accelerate the easterly winds in the lower free troposphere ($800 - 700\ hPa$). Assuming SCMT is at play here as turbulence is usually confined to the sub-cloud layer ($> 900\ hPa$), it looks like in the sub-tropics, the cloud layer is mixing faster easterly winds in the lower half of the cloud layer ($\approx 900 - 800 hPa$), with weaker easterly winds in the upper half ($\approx 800 - 700\,hPa$) of the cloud layer. The shallow convective mass flux reaches further into the tropical troposphere compared to the sub-tropics. This suggests that in line with reports from NOAA, the scheme uses the presence of deep convection to grow deeper, in other words it appears to be vertically rather unrestricted.

As we discussed earlier, the adjustment in the wind profiles due to enhanced SCMT is quite different for UKMO (Fig. 29 & 31) compared to the adjustment for GFDL (Fig. 7 & 30). For UKMO, it shows weaker changes in general, and most changes are largely confined to the lower troposphere. Figure 9 shows the combined tendency on the zonal wind and the shallow convective mass flux over the tropics and sub-tropics for UKMO. The largest difference in the zonal wind tendency between GFDL and UKMO is apparent in the tropics, finding that for UKMO the tendency by SCMT ($\approx 900 - 500 hPa$) is not smoothly connected to the tendency produced by the turbulence scheme ($> 920\,hPa$). In the sub-tropics, whatsoever, both the combined tendency and the shallow mass fluxes seem to be approximately equal for UKMO and GFDL. Being positive below $\approx 800 hPa$, it acts to add westerly momentum to the easterly trade-winds. Above this layer ($800 - 600\,hPa$), it adds easterly momentum to the zonal wind.

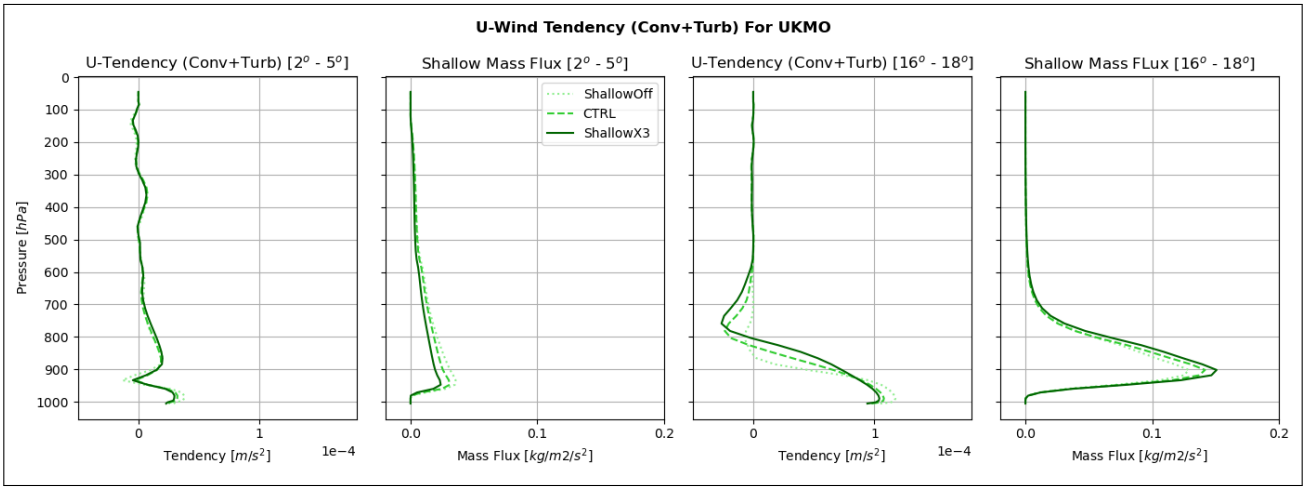

Figure 9: *Vertical Line-Plot Of Zonal Wind And Tendency Due To SCMT For UKMO, Cross-Sectional For Tropics* ($2^o - 5^o$) *And Sub-Tropics* ($16^o - 18^o$).

The fact that the combined tendency is approximately zero at cloud base ($\approx 920\,hPa$) for UKMO, means that both the SCMT scheme nor the turbulence scheme acts on the wind at this level. By applying the mixed-layer model, explained in Section 4.1.3, we find that the momentum flux at the top of the mixed layer ($\vec{\tau}(z)$), which more or less coincides with the cloud base, is a function of the bulk wind ($\vec{U}(z)$) at this level (Eq. 7). As for UKMO the tendency is close to zero here, we expect no changes in the momentum flux ($\vec{\tau}(z)$) nor in the linear gradient of the momentum flux over the mixed-layer ($[\vec{\tau}(z) - \vec{\tau}(0)]\, z^{-1}$). In other words, the amount of momentum leaving the mixed layer is not directly significantly affected by enhanced SCMT, therefore there is no need to dramatically establish a new wind vector balance according to Equation 6.

Opposite to UKMO, as discussed, the GFDL model shows a smooth connection between the turbulence and convection scheme, acting to add westerly momentum in the entire layer. As a result, the easterly bulk-wind at the top of the mixed layer ($\vec{U}(z)$) is weakened, therefore diminishing the momentum flux ($\vec{\tau}(z)$) that communicates momentum between the mixed layer and the free troposphere. Consequently, the gradient ($[\vec{\tau}(z) - \vec{\tau}(0)]\, z^{-1}$) adjusts whereafter a new wind vector (Eq. 6) balances by adjusting the bulk wind $\vec{U}$ in the layer. Ultimately this would reveal a change in both the direction and magnitude of the wind through $f\vec{k}\times\vec{U}$ and $\vec{U}$.

Interested in whether tropical surface winds are indeed veered and weakened for GFDL in comparison to UKMO, section 6.1.3 further discussed the wind vectors at the surface, averaged over the tropics ($0^o - 10^o$).

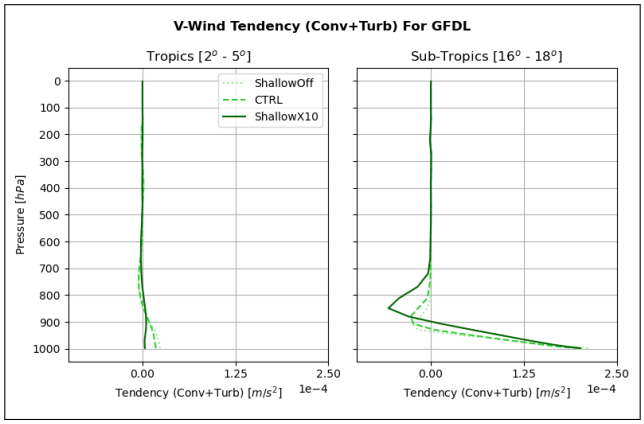

Figure 10: *Meridional-Wind Tendency Due To SCMT For GFDL, Cross-Sectional For Tropics* ($|2^o - 5^o|$) *And Sub-Tropics* ($|16^o - 18^o|$).

Complementary to the zonal tendencies, Figure 10 shows the combined tendencies for GFDL on the meridional wind component in both the tropics and sub-tropics. It shows that in the sub-tropics, momentum transport acts to decelerate the northerly trade-winds in the mixed layer ($> 900\,hPa$), which is likely predominantly the turbulence scheme at play. It acts to accelerate winds in and above the cloud layer ($< 900\,hPa$), which could largely be attributed to SCMT.

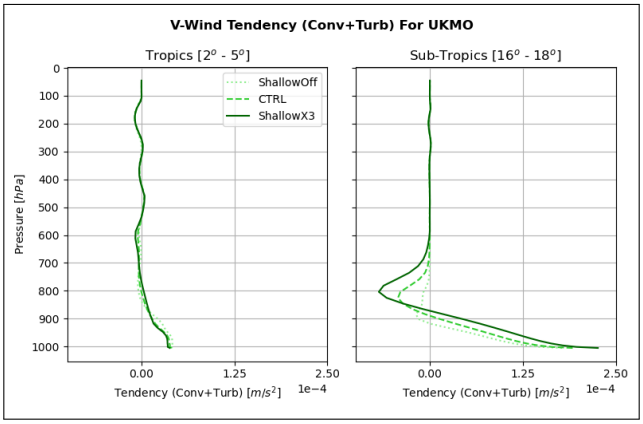

Figure 11: *Meridional-Wind Tendency Due To SCMT For UKMO, Cross-Sectional For Tropics ($|2^o - 5^o|$) And Sub-Tropics ($|16^o - 18^o|$).*

It is noteworthy that for all experiments, the height of the layer at which the scheme changes from decelerating to accelerating north-south winds remains stable. Contrary, in the tropics, we find that exaggeration of momentum mixing for GFDL leads to a raise of altitude at which its acting changes direction. Still, northerly winds are decelerated at the surface, however now accelerated in the middle part of the troposphere ($800 - 500\ hPa$). Figure 42 shows the combined tendency on the meridional wind component for UKMO. In the tropics, there appears to be significantly more adding of southerly momentum to the northerly trade-winds, acting to veer the winds more zonally. In the sub-tropics, it approaches the trend we discussed for the GFDL model.

6.1.3 Surface winds

Zooming in on the change of the surface winds or trade-winds at the lowest model level ($\sim 1000\ hPa$), Figure 12 shows zonally averaged averaged over the tropics ($|0.5^o - 10^o|$) in latitudinal direction for GFDL (left) and UKMO (right) for all three experiments.

We find that, on average over the tropics, the GFDL model indeed shows that the trade-winds are weakened by not only a smaller meridional component but by a significant decrease in absolute wind speed as well - dominated by the zonal component. In line with our earlier hypothesis, this could potentially be caused by the new vector wind balance and bulk wind speed $\vec{U}$ in the mixed layer as a result of weaker momentum flux ($\vec{tau}(z)$) between the mixed- and cloud layer. We hypothesize that both the geostrophic veering and the significant weakening in absolute wind speed will have its effect on the equatorial convergence driving the large circulation.3

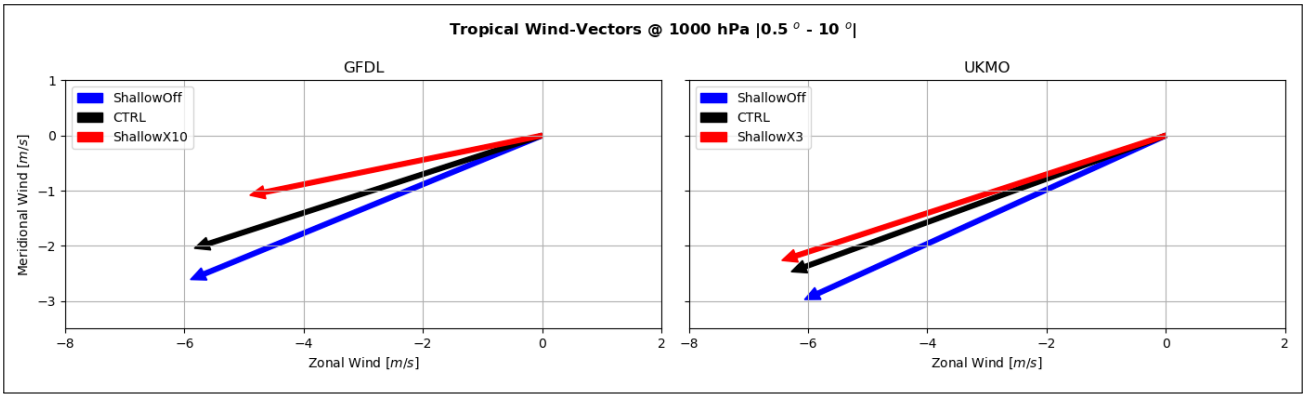

Figure 12: *Tropical Surface Wind Vectors For GFDL (Left) & UKMO (Right), Plotted For All Experiments.*

Contrary to GFDL, the tropical surface winds for the UKMO model show to have a weakened meridional component, coinciding with a slightly enhanced zonal wind. The weakening of the meridional component has been observed in the tendencies we discussed earlier. It might be important to note here that the scale of the zonal wind is larger compared to the y-axis. The surface winds veer towards a rather zonal, geostrophic direction however increase in absolute wind speed, suggesting small changes in equatorial convergence.

6.1.4 Convergence

Di- or convergence of winds, acting as a proxy for the concentration of moist and energy by winds, for

a large degree shows where scalars are transported to and moreover where vertical transport of such scalars is encouraged or obstructed. Through continuity of mass, peak zones of wind convergence coincide with peaks of vertical transport and hence peaks of convective precipitation and moist static energy. Figure 13 shows the zonally averaged wind convergence for GFDL (left) and UKMO (right), vertically integrated over a manually set convergence layer ($\approx 1000 - 750\,hPa$) for all three experiments.

For GFDL, we find a dampening of tropical peak convergence and an apparent poleward shift of the maxima, hinting at the convergence of scalars in the extratropics ($|6^o - 8^o|$) instead of at the equator. For UKMO, we find that both the intensity and location of tropical wind convergence are barely affected. If anything, equatorial wind convergence seems to be slightly encouraged whereas off-equatorial wind convergence ($|2^o - 3^o|$) is slightly dampened. What we find here is in accordance with the wind vectors we discussed earlier (Fig. 12) showed that for GFDL the winds at the surface are significantly weakened and turn zonal, encouraging weaker, off-equatorial convergence. In contrast to GFDL, the surface winds for UKMO showed a small zonal veering of the wind, coinciding with an increase in wind speed that balances convergence. What the figure shows is that the change in the surface-winds is quite a good proxy for the entire convergence layer as it appears to be well-mixed.

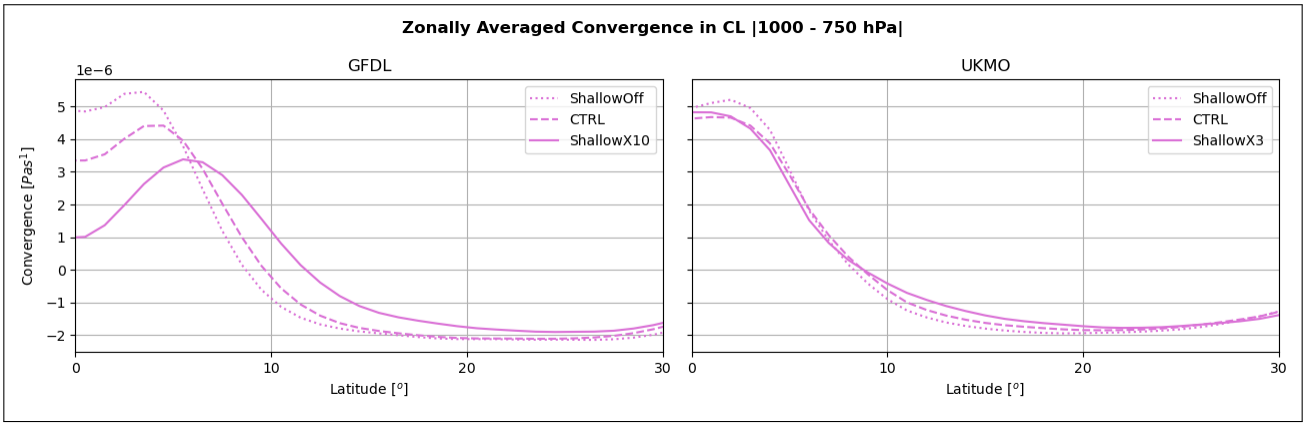

Figure 13: *Tropical Wind Convergence Averaged Over CL* ($1000 - 768\,hPa$) *For GFDL & UKMO.*

Shown in Figure 6, we explained that the depth of the layer with convergence visibly deepens with SCMT enhanced. This raises the question to what extent the layer-integrated convergence depends on the height over which we integrate the meridional transport. Figure 14 shows the integrated meridional wind for 4 different layer heights ($850 - 700\,hPa$) for UKMO & GFDL in the exaggerated experiment. We find that the total amount of convergence is rather insensitive for the depth of the layer, especially above $800\,hPa$ (red line). This is largely explained by the fact that the bulk of the strongest winds could be found below this layer. Or in other words that winds become geostrophic towards the top of the mixed layer, diminishing their meridional (converging) component.

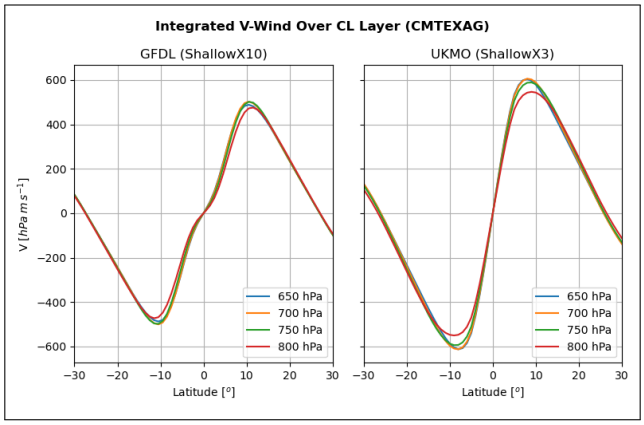

Figure 14: *Integrated Meridional Wind For Different Layer Heights, GFDL (Left) & UKMO (Right) For Exaggerated Run.*

6.1.5 Ekman Pumping

We showed earlier that Ekman Pumping is computed as the curl of the surface stresses. Budget analysis has shown that the zonal surface stress is the only dominant component leading to Ekman Pumping, most probably because of the nature of an aquaplanet simulation and the deflection of trade-winds. As the meridional surface stress is negligible, Figure 15 visualizes the zonal wind; zonal surface stress; latitudinal gradient of the surface stress and Ekman Pumping for the GFDL (left) and UKMO (right) models. The dark blue solid line is the exaggerated experiment with the most abundant parameterization, whereas the light blue dotted line is the run without SCMT, same convention as before.

The surface stress that is induced by the wind identically follows the surface wind velocity itself, as it is a function of wind speed only (Eq. 7). For GFDL, we find that the easterly wind and coinciding negative surface stress are reduced in the tropical latitudes, however actually accelerated and enforced in the sub-tropics. For UKMO a subtle acceleration is seen for both the tropics and sub-tropics, showing a small but very consistent change in surface winds over the entire span of the overturning circulation ($|0^o - 30^o|$).

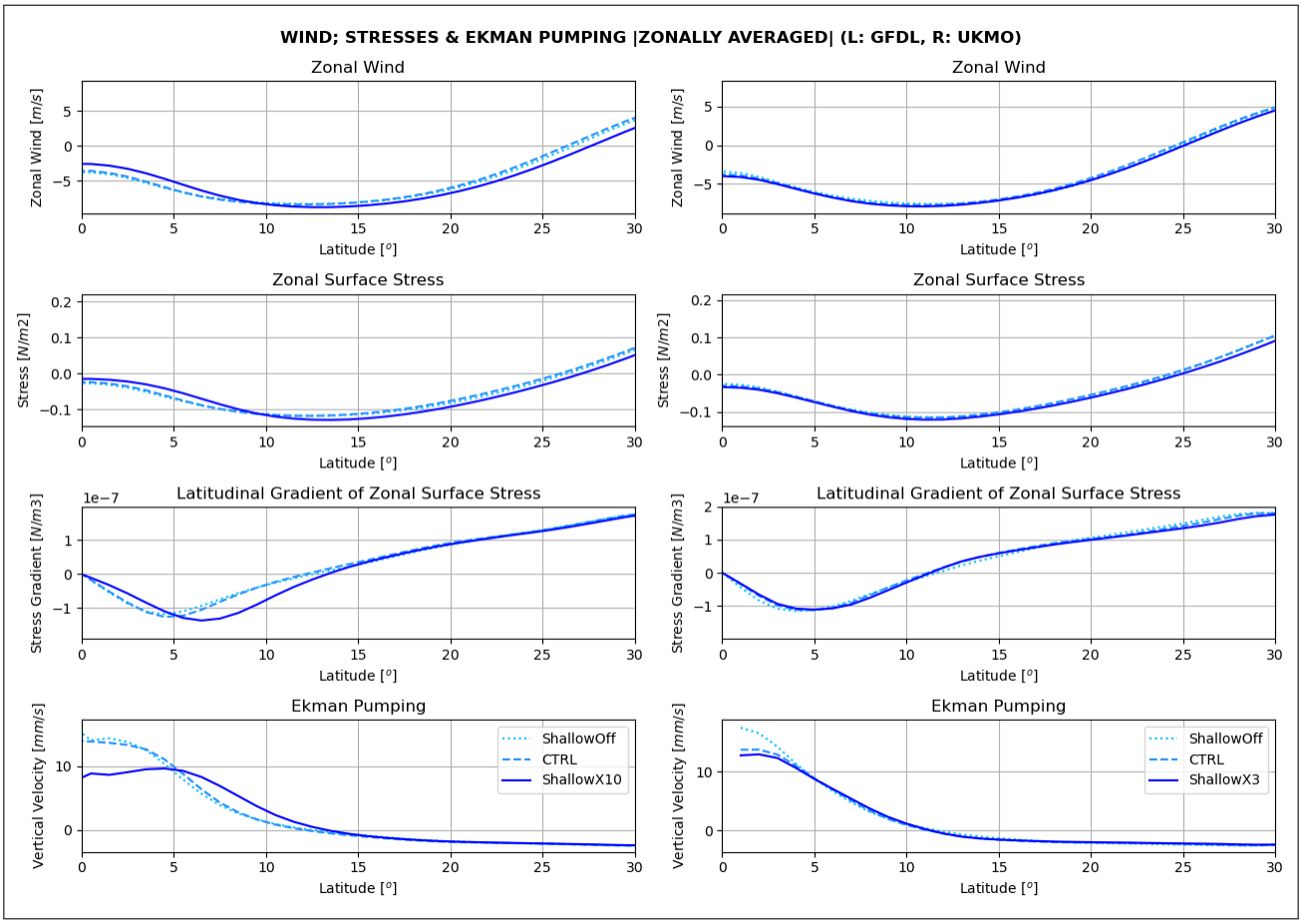

Figure 15: *Zonally Averaged Zonal Surface Wind; Zonal Surface Stress; Gradient Of Zonal Surface Stress & Ekman Pumping For GFDL (Left) & UKMO (Right)*

One very important implication for the GFDL model is that this apparent shift in surface wind adjustment from the tropics (decrease) towards the sub-tropics (increase) causes the the latitudinal gradient of the zonal surface stress to remain stronger in the outer tropical bands ($|6^o - 9^o|$), findings its peak moving poleward.

Hence, Ekman Pumping peaks at $|5^o|$ instead of at the equator, likely favouring two deep convective zones in the zonal mean coinciding with two convective precipitation maxima in both hemispheres.

The surface wind adjustment for UKMO is consistent over the entire latitudinal extent of the overturning circulation, or in other words independent of latitude. We find that the distribution of the surface stress gradient for the control and exaggerated runs approximately follows the run without SCMT. Hence, apart from a decrease of convergence at the equator, we find that Ekman pumping for all experiments is similar from $> |4^o|$ in both hemispheres for all three experiments.

6.2 Circulation

To reveal the global atmospheric circulation cells; their rotation and their respective magnitude, the meridional stream flow in a standard situation is a convincing way to start. Figure 16 shows the meridional stream-function for GFDL in the control situation. Positive (blue) values refer to clockwise rotation, whereas negative (red) values represent anti-clockwise rotation. Note how the circulation of the Hadley cells ($|0^o - 25^o|$) is significantly stronger compared to the circulation of the Ferrel cells ($|25^o - 55^o|$; not entirely shown).

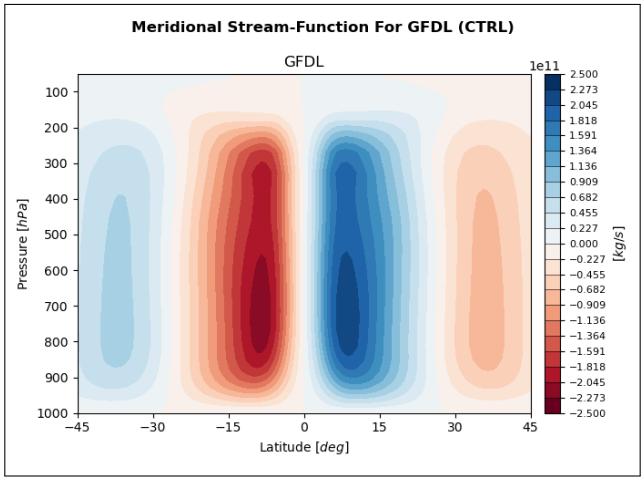

Figure 16: *Zonally Average Of The Meridional Stream-Flow In The Control Run For GFDL.*

Interested in the adjustment of the circulation response to SCMT, the perturbation between the control run and the run without SCMT provides valuable insight in how models adjust their meridional transport of scalars like moist and energy. Figure 17 shows a zonal average of the difference ($SCMT_{ctrl} - SCMT_{off}$) in meridional stream-flow for GFDL (left) and UKMO (right), plotted on the same scale to highlight inter-model differences.

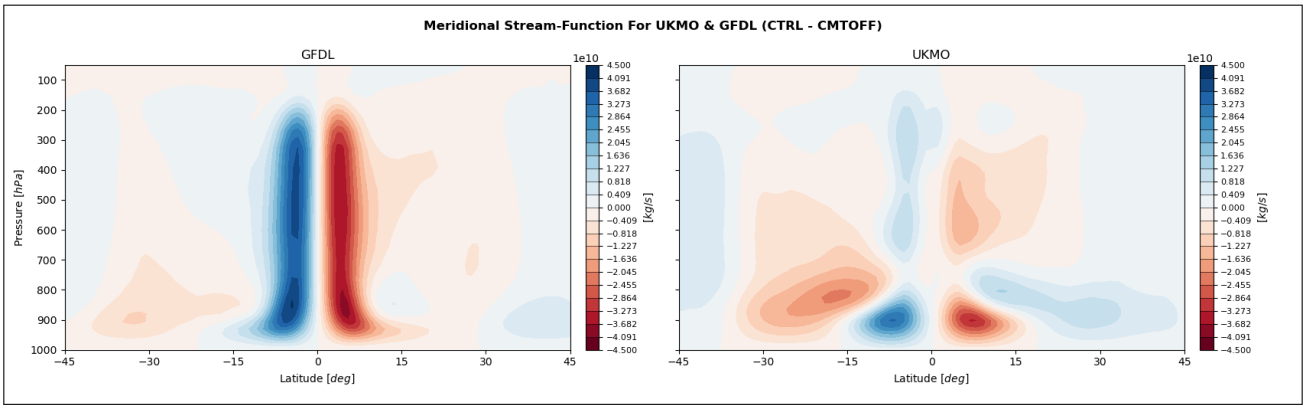

Figure 17: *Zonally Average Of The Meridional Stream-Flow Anomaly As A Result of Activated Shallow Convective Momentum Transport ($SCMT_{ctrl} - SCMT_{off}$) For GFDL (Left) And UKMO (Right).*

As the tropical cell rotates clockwise in the Northern Hemisphere (NH) and counter-clockwise in the Southern Hemisphere (SH), a negative (red) difference in the NH would indicate that the circulation is weakened with the inclusion and exaggeration of SCMT, whereas positive (blue) in the NH indicates that the circulation is enhanced in the control run, compared to the run without SCMT. The opposite is true for the SH, with positive (blue) indicating a weakening and negative (red) referring to a strengthening of the circulation.

We learn that for the GFDL model there is a strong weakening of the circulation over the entire depth of the ascending branch of the circulation. For UKMO, a weakening of the circulation is apparent in the tropical Ekman layer, somewhat weaker compared to GFDL in magnitude - which is partially compensated for with a strengthening of the shallow overturning circulation in the middle tropical troposphere and in the sub-tropics, a strong remote adjustment is absent.

6.2.1 Precipitation

The double-ITCZ structure that is persistent in climate models is directly referring to the bias in convective tropical surface precipitation. So far we have discussed that with by enhanced SCMT, the GFDL model favours both off-equatorial convergence and Ekman Pumping, usually coinciding with strong vertical motion of warm, moist air and therefore favouring deep convection. Overall, we expect the precipitation pattern to approximately follow peak convergence zones, or/and alternatively follow Ekman Pumping. In other words, the poleward migration of convergence and Ekman Pumping that we found for GFDL, is expected to be repeated in the convective precipitation pattern. Figure 18 shows the steady-state convective surface precipitation for GFDL in the exaggerated run (tendencies $x10$). We find that the precipitation is distributed in two bands, with an apparent depression at the equator. For more thorough analysis, Figure 19 shows the convective surface precipitation for GFDL and UKMO. The light turquoise dotted line refers to the experiment without SCMT, whereas the dark solid line represents the exaggerated experiment.

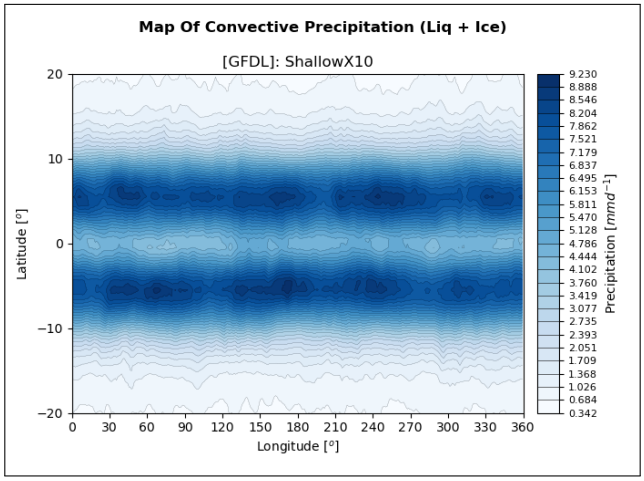

Figure 18: *Map (Lat-Lon) Of Convective Surface Precipitation For GFDL In The Exaggerated Run.*

What we see here is that the peak of convective surface precipitation roughly follows convergence (Fig. 13) and Ekman Pumping (Fig. 15) for both models. For GFDL is it showing a double precipitation structure with non-equatorial maxima at $|5^o - 6^o|$ in the control and exaggerated run, following the poleward migration of convergence. Contrary, for UKMO enhanced SCMT actually rather remains a single-ITCZ structure, aligning with what we saw for convergence and Ekman Pumping.

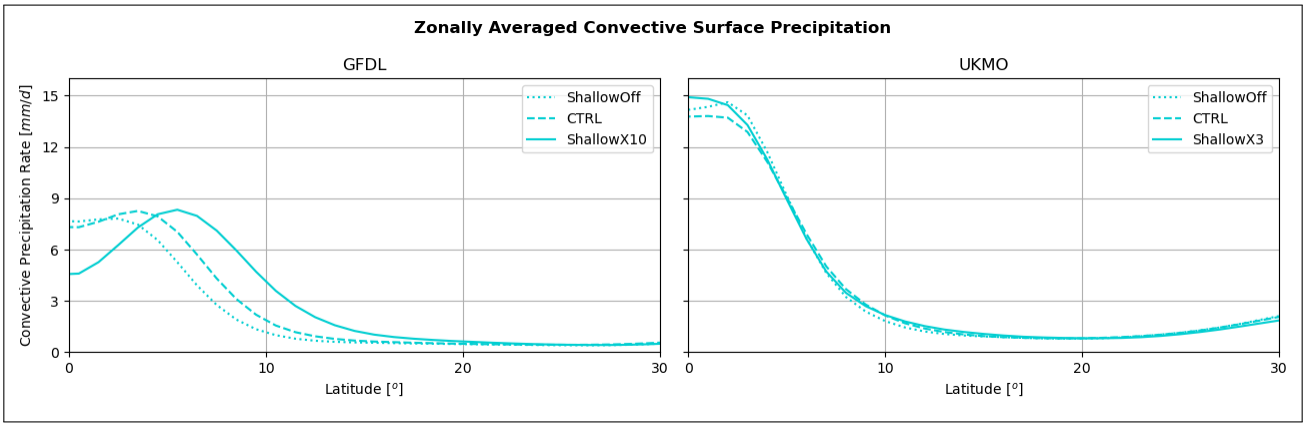

Figure 19: *Tropical Convective Surface Precipitation For GFDL (Left) & UKMO (Right).*

One notable difference with regard to convergence and Ekman Pumping, is that the weakening of maxima is not apparent in the surface precipitation. As the hydrological circle in an aqua-planet configuration is approximately closed and therefore the total amount water in the atmosphere is somewhat contained, the decrease in magnitude that is observed for e.g. wind convergence is not directly translated to a decrease in the maximum precipitation rate.

6.3 MSE budget

Moist static energy is the combined energy of the sensible heat; latent heat and potential energy of a parcel and is largely conserved with altitude for moist parcels. As the amount of moisture and the temperature in the troposphere decrease with height, the potential energy largely counterplays the latter two components. Figure 20 illustrates this by showing MSE and its three components in the tropics ($|2^o|$) for the GFDL model. Note that in the stratosphere ($< 100\ hPa$), MSE increases rapidly as temperature increases again and the linear pressure intervals gain a lot of height due to the strong nonlinear relation between pressure and height in this part of the atmosphere. Now interested in whether the amount of MSE that is contained in the tropospheric column changes due to the altering of surface winds, Figure 21 shows the zonally averaged perturbation between the CTRL and the CMTOFF run for GFDL (left) and UKMO (right).

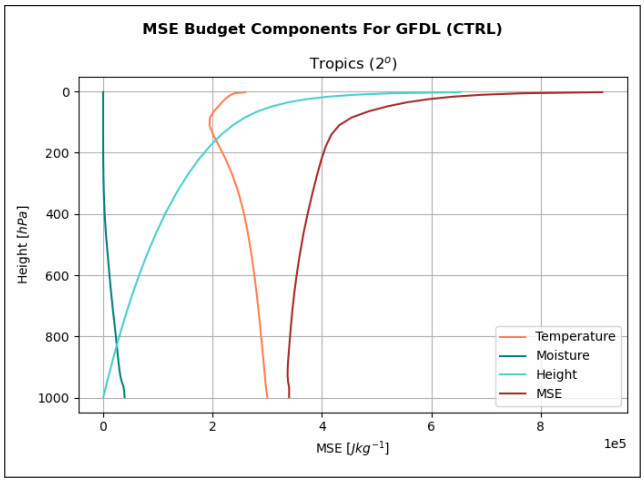

Figure 20: *Moist Static Energy And Its Components At $|2^o|$ For GFDL - Control Run.*

A negative value refers to an increase in MSE with the inclusion of SCMT. Note that, explained in Section 4.2, MSE is multiplied by density to obtain a volumetric quantity of MSE (h):

$$\Delta h_{vol} = \rho_{ctrl}(h_{ctrl} - h_{off}) \tag{18}$$

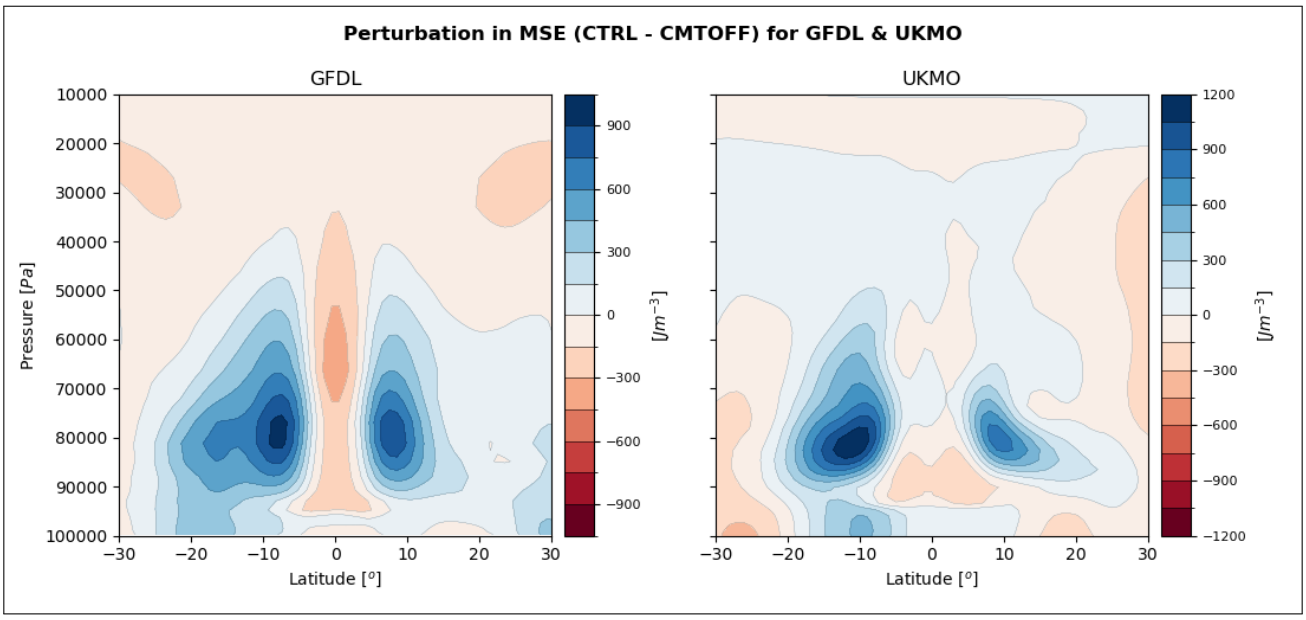

Figure 21: *Zonally Averaged Difference In MSE (CTRL - CMTOFF) For GFDL & UKMO.*

We find that for GFDL the amount of MSE increases in the outer- and extra-tropics ($|5^o - 15^o$), somewhat at the expense of MSE contained directly above the equator. This corresponds largely with the trend we discussed earlier for the poleward migration of convergence zones; Ekman Pumping and convective precipitation. In other words, it appears that enhanced SCMT for GFDL leads to the off-equatorial convergence favouring vertical transport of heat and moisture, thereby warming the sub-tropical free troposphere at these latitudes.

For UKMO, we find that that the inclusion of SCMT induces an increase in MSE in the sub-tropical latitudes as well. The difference is apparent in the first part of the free troposphere ($\sim 900 - 700\, hPa$) and appears somewhat larger in the SH compared to the NH, which might suggest that MSE is still not in equilibrium. In contrast to GFDL, there is no strong decrease in MSE in the equatorial column, in line with the trend we saw for convergence, although not in total accordance with the equatorial drop in Ekman Pumping.

6.3.1 Energy fluxes

Even in an aquaplanet configuration, differences in longitudinal direction exist. Figure 22 shows a map of the tropical and sub-tropical latent heat release for GFDL. It has been plotted as the difference or perturbation ($SCMT_{ctrl} - SCMT_{off}$), in which positive (blue) values indicate that there is an increase in LH in the control run compared to the run without SCMT. Negative (red) values indicate a drop in LH for the control run.

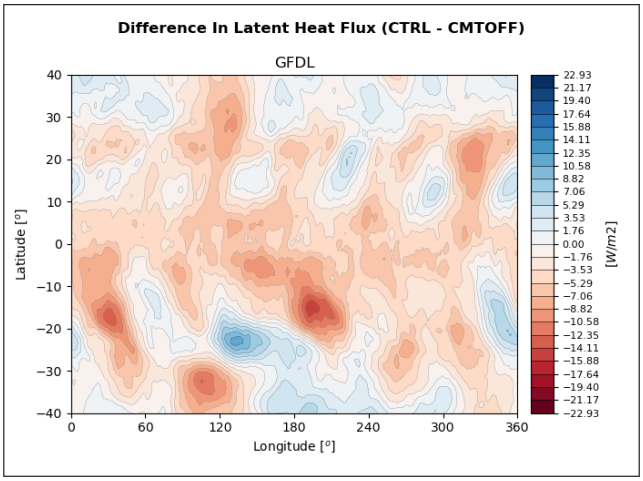

Figure 22: *Contourplot Of Difference In Latent Heat Flux (CTRL - CMTOFF) For GFDL.*

The map nicely shows that scalars are not as evenly distributed in longitudinal direction as one might expect, yet still, heterogeneity persists. For easier assessment in the zonal direction, Figure 23 shows the zonally averaged perturbation in energy fluxes for GFDL. Note that these are the fluxes entering and leaving the column, like we previously described in Section 4.2. In other words, according to Equation 13, a positive budget of energy fluxes would have to be compensated by column-integrated vertical or horizontal divergence of MSE.

Looking at an arbitrary experiment, the sensible heat flux entails a very similar spatial distribution with respect to the latent heat flux, especially in the zonal mean, although significantly smaller (not shown). The ratio between both surface heat fluxes is in the order of approximately $SH \approx 0.1LH$. The perturbation, shown in Figure 23, reveals that the change in the latent heat flux by enhanced SCMT is significantly larger as well. This suggests that the model is primarily adjusting the energy balance through net radiation at the TOA and by latent heat release, which would be a feasible response for an aquaplanet configuration.

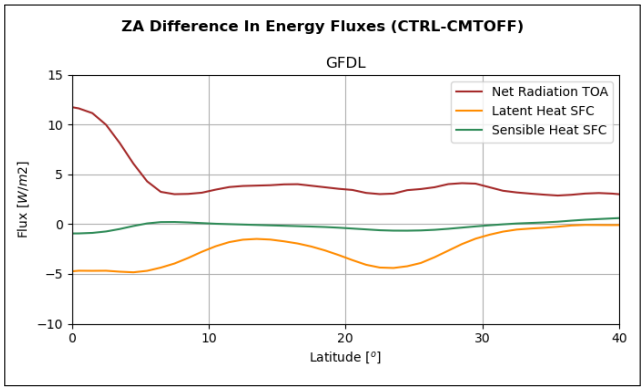

Figure 23: *Zonally Averaged Difference ($SCMT_{ctrl} - SCMT_{off}$) In Energy Fluxes For GFDL*

It becomes more clear that enhanced SCMT has its direct or indirect effect on the surface winds (Sec. 6.1.3) and thereby affects the release of latent heat (Eq. 14). Introduction of SCMT implicates for GFDL a reduction of the surface winds and stresses in the tropical latitudes ($\sim | < 10^o|$), and the sub-tropics ($\sim |15^o - 30^o$) coinciding with a drop in latent heat release.

Zooming in on the outer bands of the tropics ($|5^o - 10^o|$) for both models, we find that the local release of LH drops due to altered surface winds, while the amount of MSE stored in the atmospheric column

above increases. An explanation for this would be that the advection of latent heat from the sub-tropics towards the tropics, albeit in lesser amounts, is weakened. Complementary, the poleward migration of convergence zones we discussed earlier in Section 6.1.4 makes that, although less LH is released, more MSE is transported vertically in off-equatorial zones, at the expense of equatorial zones. This raises interest in how MSE is advected in both vertical and horizontal direction.

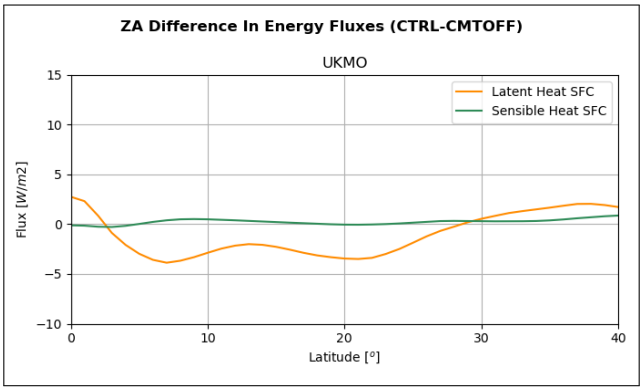

Figure 24: *Zonally Averaged Difference ($SCMT_{ctrl} - SCMT_{off}$) In Energy Fluxes For UKMO*

6.3.2 Advection of MSE

Explained in Section 4.2.2, the advection of MSE depends on both the wind vector and the gradient of MSE, or in other words the change of MSE with the corresponding spatial direction (either horizontal or vertical). Figure 60 shows a contour plot for the meridional wind (left) and the latitudinal gradient of MSE (right) for GFDL in the control run. Note that the gradient of MSE is multiplied with density to obtain a volumetric MSE (vMSE) gradient in $[J\ m^{-3}\ m^{-1}]$. The same plot for UKMO (not shown) looks very alike, true for all models. Negative (red) values indicate a decease of vMSE with latitude (northward), whereas positive (blue) values indicate an increase of vMSE with latitude. In the southern hemisphere latitude decreases when moving southward, which explains the positive gradient.

Expecting to find the largest amount of MSE close to the equator due to deep convection and the SST distribution (Eq. 17), we find that over approximately the entire lower troposphere MSE decreases consistently when we move poleward ($\partial h/\partial y < 0$), true for both hemispheres. Combining this with the direction of the meridional wind, we find that in the trade-wind layer, horizontal divergence of MSE is always positive. In other words, the trade-winds advect or diverge MSE towards the tropics, thereby cooling the sub-tropics and warming the tropics.

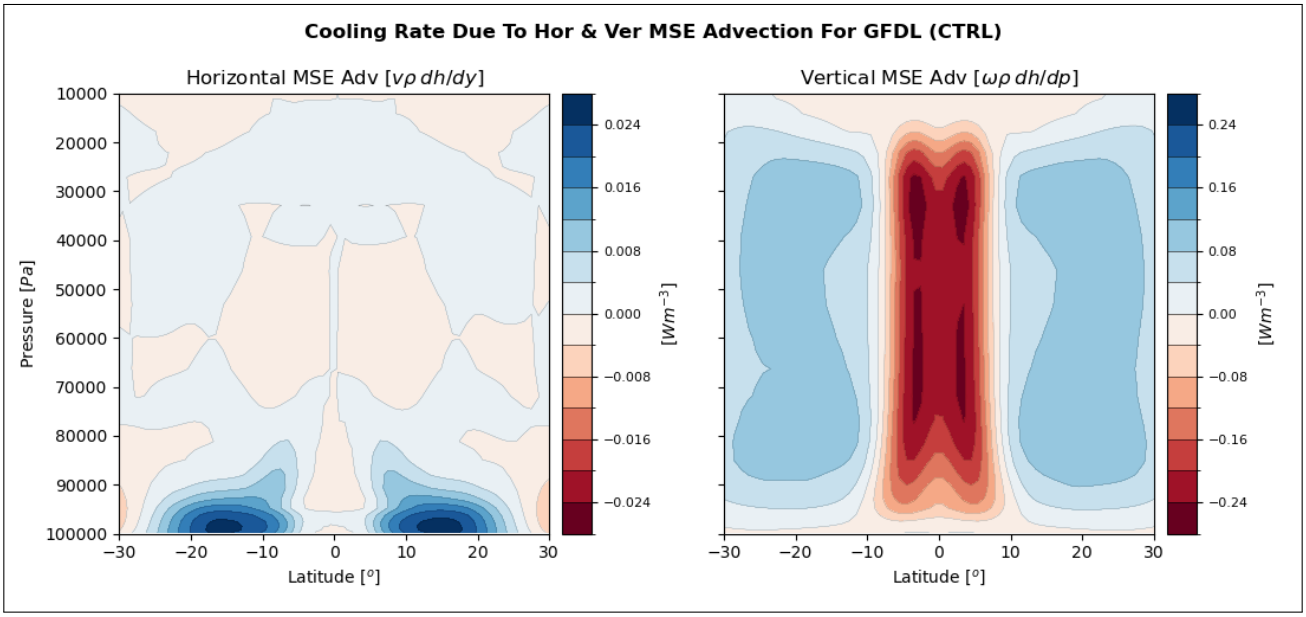

Figure 25: *Horizontal & Vertical Volumetric MSE Advection For GFDL (Control Experiment).*

Moving on to vertical advection, Figure 61 shows the vertical velocity on pressure coordinates (omega, ω, left) and the vertical change of vMSE (right) for the control run in GFDL. The same plot looks very alike for the other models (not shown). Note that pressure decreases with altitude, hence, omega appears negative in regions of upward motion and positive in regions of subsiding motion. For the vertical gradient, a positive ($\rho\ dh/dp > 0$) value indicates a volumetric decrease of MSE with height, or in other words and increase of vMSE with decreasing pressure. In the tropics, we find upward motion of air that contains relatively more MSE, hence the vertical advection of MSE is positive here and acts to warm the atmospheric column. For the sub-tropical regions ($> |10^o|$), the opposite is true as downward motion persists, subsiding air with relatively less MSE.

Combining the winds with their corresponding spatial gradients of MSE, we find the advection of vMSE in vertical and horizontal direction, showed by Figure 25 for GFDL and Figure 64 for UKMO. Alternatively, it could be regarded as a cooling rate in $[Wm^{-3}]$ driven by transport of MSE. The positive (blue) horizontal zones refer to sub-tropical divergence of MSE, e.g. by a southward motion ($v < 0$) with an increasing gradient along the wind direction ($\rho dh/dy < 0$). The figure reveals that horizontal advection generally cools ($Wm^{-3} > 0$) the trade-wind layer.

With regard to vertical transport of MSE, in the tropics, it acts to warm the atmospheric column in the tropical regions ($| < 10^o|$) by upward motion of air that contains relatively more vMSE. Contrary, in the subtropics, subsiding motion of air that contains relatively less vMSE cools the atmospheric column. For UKMO (Figure 64) we find very similar effects as the subtropics are cooled by both horizontal advection and vertical subsidence of air that contains less energy, whereas the tropical ascending branch is warmed by upward motion of air that contains relatively more MSE.

6.3.3 Change in the advection of MSE

We saw that the multiplication of the latitudinal gradient of vMSE $[J\ m^{-3}\ m^{-1}]$ with the meridional wind $[m^{-1}]$ provides a volumetric cooling rate $[W\ m^{-3}]$ as a result of horizontal transport of vMSE. For vertical advection, this works conceptually the same as the change of vMSE with pressure $[J\,m^{-3}\,Pa^{-1}]$ is multiplied with the vertical velocity in pressure coordinates $[Pa\ s^{-1}]$ to obtain a cooling rate as well $[W\ m^{-3}]$. Figure 26 shows the change ($SCMT_{ctrl} - SCMT_{off}$) of atmospheric cooling due to horizontal (left) and vertical advection (right) of vMSE for GFDL.

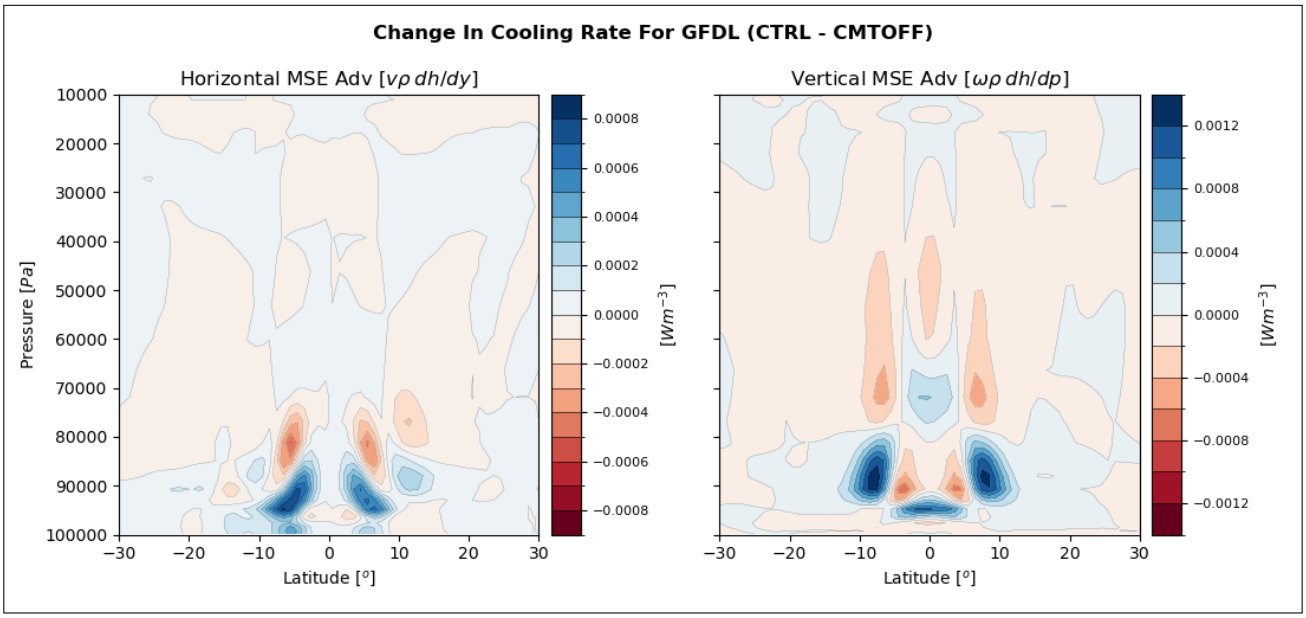

Figure 26: *Change In Cooling Rate ($SCMT_{ctrl} - SCMT_{off}$) Due To Horizontal & Vertical Advection For GFDL.*

We find that for GFDL, enhanced SCMT implies the horizontal advection of vMSE to cool a large part of the tropical mixed layer ($950-850\,hPa$), whereas it acts to warm right above ($850-750\,hPa$). With regard to vertical advection of vMSE, enhanced sCMT reveals that its effect through vertical energy transport is not confined to the lower layers only, but instead felt through the middle troposphere as well. It works to cool the outer-tropics ($\approx 900-800\,hPa$), and warms the layers above extending up till $450\,hPa$, albeit weaker.

UKMO, opposing to GFDL, shows differences in MSE content to be confined to the lower layers of the troposphere. Enhanced SCMT works to warm the lower troposphere ($\approx$ 800 − 900 hPa) in the outer tropics ($|5^o-10^o$) by horizontal advection. Contrary, enhanced SCMT works to actually cool approximately the same region by vertical advection, supplemented by cooling the tropical mixed layer $\approx 950hPa$. The change in cooling rates for UKMO are shown in Figure 27.

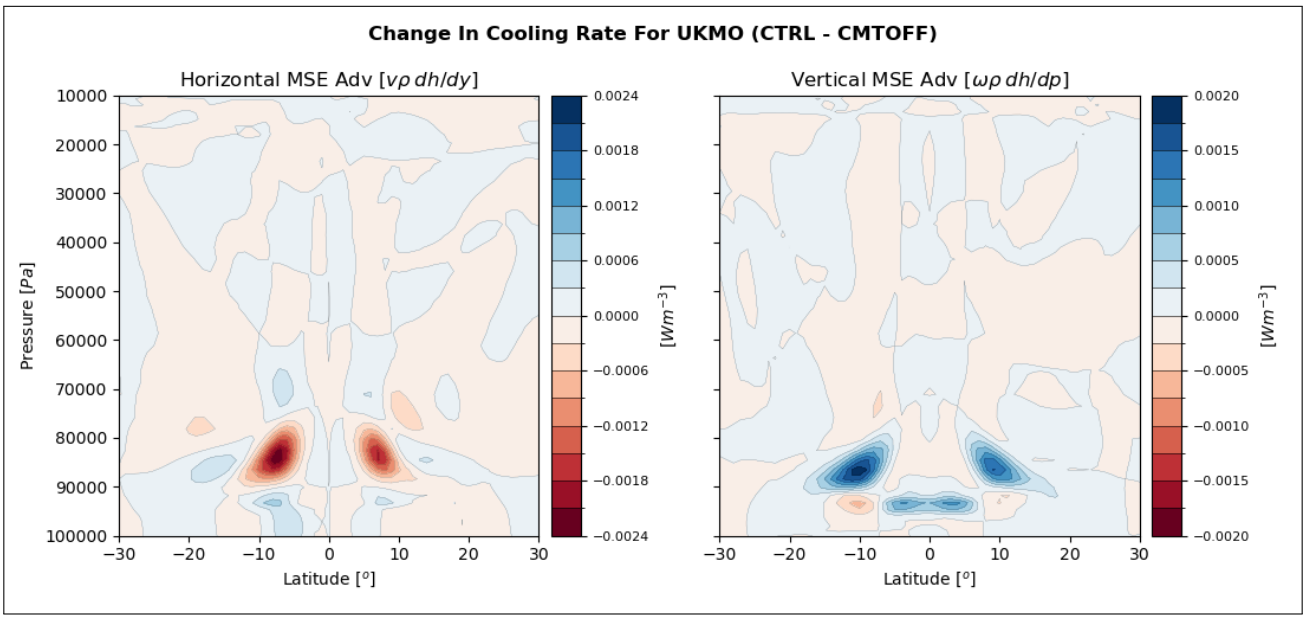

Figure 27: *Change In Cooling Rate ($SCMT_{ctrl}-SCMT_{off}$) Due To Horizontal & Vertical Advection For UKMO.*

6.4 Inter-model comparison

Supplementary to this section, Appendices A-J show all accompanying figures underlying the report and Table 3. Table 3 shortlists the inter-model responses for all findings previously discussed for GFDL and UKMO. We have distinguished between dynamic- and thermodynamic processes, the first one referring to the adjustments of wind profiles and surface winds in both the tropics and sub-tropics; tendencies of SCMT the schemes in combination with the extent of the shallow mass flux; responses in convergence and Ekman Pumping driving long-term adjustments; circulation differences and precipitation. The latter refers to the tropospheric energy budget through (v)MSE; the change in surface fluxes and the horizontal and vertical advection of MSE. Both CAM6 models (NE16 & FV2) have been combined as they contain very similar responses.

The convention in documenting the model responses is through describing changes by enhanced SCMT. In other words, if a scalar would decrease due to the inclusion of SCMT, it is documented as a weakened response.

6.4.1 Overall response

Complementary to the table, the overall responses and trends of both CAM6; UKMOGK and LMDZ models are briefly discussed below.

CAM6

Both CAM6 models (NE16 & FV2 cores) show their largest response in the upper troposphere. In the tropics, winds are accelerated in easterly direction and

northward transport is strongly reduced. In the sub-tropics, the effect on the zonal winds is similar, although weaker, whereas meridional wind profile is barely affected except for a small strengthening of northerly flow. In the long-term adjustment, we find that peaks of both convergence and Ekman Pumping migrate poleward and increase in magnitude at the expense of the equator, aligned with what has been found for precipitation. The overall circulation weakens in the upper tropical troposphere. All coincides with an increase of MSE in the off-equatorial convergence zones and a decrease of MSE in the equatorial branch. Surface fluxes are decreased in the tropics and enhanced in the sub-tropics. Overall, CAM6 models find differences in their large circulation due to enhanced CMT.

UKMOGK

UKMOGK shows a very similar response to UKMO, with the largest adjustment in the shallow overturning circulation. The zonal and meridional wind profiles are predominantly mixed over a rather shallow layer ($\sim 1000 - 800\, hPa$) both in the tropics and sub-tropics. Convergence and Ekman Pumping are slightly enhanced in the sub-tropics, while EP is only decreased at the equator. Precipitation largely follows the trend in convergence. Atmospheric MSE content is enhanced in the lower sub-tropical free troposphere, coinciding with an increase in LH. Overall no remote response in the deep circulation.

LMDZ

The LMDZ model shows a response in both the entire depth of the tropical troposphere as in the shallow overturning circulation, conceptually combining the responses we discussed for GFDL and both UKMO models. In the tropics, the easterly wind is decreased in strength and vertically well-mixed. Northerly trade-winds are weakened at the expense of upper-tropospheric southerly winds, coinciding with a deepening of the convergence layer. In the sub-tropics, the zonal wind is accelerated in easterly direction, except for the mixed-layer ($> 900\, hPa$). The meridional wind profile is only mixed in the lower half of the troposphere, leading to a decrease of northerly flow in the surface layer and an increase of the layer above, although not coinciding with a deepening of the converging layer. Peak convergence is weakened and migrated poleward, centered at the outer-tropics ($|8^o|$) with more convergence in the sub-tropics ($|10^o - 20^o|$), at the expense of equatorial convergence. Ekman Pumping largely follows this shift. Precipitation narrowly follows the trend we discussed for convergence, rather than follows Ekman Pumping. The amount of MSE and surface fluxes shift accordingly with enhanced release of latent heat and atmospheric MSE content in the sub-tropics, at the expense of the tropics and outer-tropics ($| < 11^o|$).

Table 3: Inter-Model Comparison

Dynamic Processes	*Thermodynamic Processes*
(1) Zonal Wind Profile Tropics	(9) MSE Budget
(2) Meridional Wind Profile Tropics	(10) Energy Fluxes
(3) Zonal Wind Profile Sub-Tropics	(11) Cooling Rate Due To Horizontal Advection
(4) Meridional Wind Profile Sub-Tropics	(12) Cooling Rate Due to Vertical Advection
(5) Convergence	
(6) Ekman Pumping	
(7) Circulation	
(8) Precipitation	

	CAM6
(1)	Easterly acceleration, predominantly apparent in the upper troposphere ($< 200\,hPa$). Effect stronger for control run compared to exaggerated run.
(2)	Decrease of both upper-tropospheric southerly flow and northerly flow at the lower layer. Increase of southerly flow in middle troposphere.
(3)	Slight easterly acceleration over the entire profile, with the largest effect at $200\,hPa$.
(4)	Apart from a very subtle increase of northerly wind at the surface, no significant changes.
(5)	Poleward migration of peak convergence ($\|7^o - 8^o\|$), at the expense of convergence the equator. Exaggerated run shows different behaviour, not consistent with control run.
(6)	Increased Ekman Pumping in outer-tropics ($\|6^o\|$), not necessarily at the expense of EP at the equator. Exaggerated run shows enhanced EP at the equator.
(7)	Upper-tropospheric ($600 - 200\,hPa$) weakening of the circulation in the tropics ($\|0^o - 10^o\|\|$).
(8)	Poleward migration of peak convective surface precipitation ($\|7^o - 8^o\|$), at the expense of convergence the equator, following convergence and Ekman Pumping. Exaggerated run shows different behaviour, not consistent with control run.
(9)	Decrease of MSE in the tropics, increase in the outer-tropics and sub-tropics ($\|8^o - 20^o\|$).
(10)	Enhanced release of latent heat in the sub-tropics ($\|10^o - 25^o\|$), while weakened in the tropics.
(11)	Most of the horizontal advection is centered in the sub-tropics ($\|8 - 30^o\|$) with barely no horizontal divergence of vMSE in the tropics. The middle troposphere is cooled in the ascending branch.
(12)	Predominantly warms the upper troposphere, apart from a centre spot ($\approx 500\,hPa$) right above the equator.

	UKMOGK
(1)	Barely no change in the zonal surface wind. Easterly acceleration in the middle and upper troposphere ($800 - 100\,hPa$)
(2)	Mixing of the profile in the shallow overturning circulation ($1000 - 750\,hPa$): Decrease of northerly surface winds at the expense of winds above this layer.
(3)	Easterly acceleration of westerly winds over the entire tropospheric profile, although weak at the surface layer ($1000 - 900\,hPa$)
(4)	Small increase in northerly surface winds, as well as northerly winds above this layer. Compensated by making middle tropospheric winds more westerly.
(5)	No significant change in the tropics. Enhanced convergence in outer-tropics & sub-tropics ($\|7^o - 20^o\|$).
(6)	Decrease of EP at the equator, slightly enhanced in the sub-tropics.
(7)	Vertically, the largest response is in the shallow overturning circulation. Weakening of the circulation in the tropics, whereas enhanced in the sub-tropics.
(8)	No significant change in precipitation pattern. Slightly enhanced both at the equator and at the outer-tropics ($\|8^o - 12^o\|$).
(9)	Predominantly an increase in MSE which is apparent in the free troposphere of the sub-tropical regions ($\|5^o - 20^o\|$). No decrease or change in MSE at the equator.
(10)	Northward migration of LH flux, coinciding with a decrease in the outer tropics ($\|4^o - 11^o\|$) and an increase in sub-tropics ($\|12^o - 25^o\|$). No significant change at the equator.
(11)	Confined to warming the lower atmosphere ($900 - 800\,hPa$) only in the outer-tropics ($8^o - 10^o$), much like UKMO.
(12)	Confined to roughly the same region as where horizontal advection is at play, slightly stretched towards the subtropics ($8^o - 13^o$), although now cooling. Much like the same effect as was described for UKMO.

	LMDZ
(1)	Mixing and weakening of easterly winds over the entire depth of the troposphere, apparent mixing of local jet at 920 hPa.
(2)	Strong mixing and weakening of northerly surface winds; deepening of the layer with convergence. Weakening of upper tropospheric southerly flow.
(3)	Gaining easterly momentum over entire depth of the troposphere, except for > 900 hPa as easterly winds are slightly weakened here.
(4)	Decrease of northerly flow, although significantly weaker compared to tropics. Barely no remote response in upper troposphere. Deepening of the layer with convergence.
(5)	Peak convergence dips at the equator and migrates poleward ($\|8^o - 9^o\|$). Coincides with more convergence in the sub-tropics.
(6)	Decrease of EP at the equator. Noteworthy enhanced in the outer tropics and sub-tropics ($\|7^o - 15^o\|$).
(7)	Shows both a relatively strong adjustment in the deep tropical troposphere as in the shallow overturning circulation. Conceptually combined response of GFDL and UKMO(GK).
(8)	Increase of sub-tropical precipitation ($\|8^o - 20^o\|$) at the expense of tropical precipitation. Hence, poleward migration of peak precipitation and slight decrease of maxima.
(9)	Very strong decrease of MSE at the tropics over the entire depth of the troposphere ($\|0^o - 10^o\|$), coinciding with an increase in free troposphere of the sub-tropics ($\| > 10^o\|$).
(10)	Small increase at the equator. Further decrease of LH in the outer-tropics and extra-tropics ($\|4^o - 15^o\|$), whereas it slightly increases poleward from $\| > 15^o\|$.
(11)	Divergence of MSE in the outer-tropical mixed layer (> 950 hPa), coinciding with a convergence of MSE in the layer right above ($950 - 850$ hPa).
(12)	Relatively small spot of cooling the cloud layer $920 - 875$ hPa in the inner sub-tropics ($\|10^o - 15^o\|$), partially making up for the warming by horizontal advection.

7 Discussion

We have discussed the multi-model response in large-scale circulation adjustment to momentum transport by shallow convection. Differences were apparent as the GFDL and LMDZ models showed strong responses in the strength and positioning of the entire circulation, whereas UKMO, ran with two different SCMT schemes, showed little to no remote responses despite an adjustment in the shallow overturning circulation. The CAM6 models, run with the NE16 and FV2 cores, did show circulation adjustments as well in the upper layers of the troposphere, however were not able to explicitly alter shallow convective momentum transport as the model utilises a unified scheme for shallow and deep convection.

7.1 Large-scale circulation

The inclusion of SCMT for GFDL; LMDZ and the CAM6 models caused the wind profile to adjust significantly, directly or indirectly affecting winds abroad. For both UKMO models, the change in local winds was modest in terms of magnitude and largely confined to the lower tropospheric layers. For the latter two models, in the tropics, the combined tendency produced by convective mixing and turbulence strongly diminishes at cloud base, even slightly acting to accelerate easterly winds at the top of the mixed layer. This is in pure contrast with GFDL and LMDZ, where the turbulence scheme that adds westerly momentum is rather smoothly transitioned into the tendency driven by convective mixing, consistently adding westerly momentum up to the free troposphere. We hypothesize that the difference in communicating momentum at the top of the mixed layer to the free troposphere has a profound effect on the wind vector balance in the mixed layer and hence on the direction and magnitude of the bulk wind itself, eventually setting convergence and deep convective zones.

Convective momentum transport is strongly dependent on the vertical extent of the convective mass flux, as explained by e.g. Richter and Rasch (2008). For our models the depth of the shallow mass flux shows a similar behaviour, if anything extends less deep for the models that show remote responses (GFDL & LMDZ). Hence, our findings suggest that the inter-model differences in the large-scale dynamics are independent, at least by direct alteration, on the depth of the shallow convective mass flux.

Responses in convergence and Ekman Pumping showed large inter-model differences. In general, enhanced SCMT showed a strong weakening of equatorial convergence and peak convergence for GFDL; LMDZ and CAM6, coinciding with a poleward movement of peak zones. Ekman Pumping largely followed this trend with enhanced upward motion in the outer-tropics and sub-tropics $(6 - 13^o)$ at the expense of the equator. Contrary, for UKMO we found no strong adjustment in convergence nor Ekman Pumping, apart from small changes at the equator itself. Ultimately linking this to convective zones, we found the convective surface precipitation to follow the long-term model adjustment of convergence and Ekman Pumping, favouring two precipitation maxima in both hemispheres with the inclusion and exaggeration of SCMT.

7.2 Energy budget & transport

All models largely agreed on an increase of MSE held by the sub-tropical free troposphere. For GFDL, CAM6 and LMDZ this coincided with a significant decrease in MSE held by the equatorial column, indicating a drop in the vertical transport of heat and moisture by enhanced SCMT. As we still found a hemispheric difference in the change in MSE held by the atmospheric column for UKMO, this could suggest that MSE is still not in equilibrium.

Concerning horizontal advection of MSE, the effects are largely confined to the lower atmosphere only $> 800\, hPa$ for GFDL; LMDZ and both UKMO models, whereas for CAM6 its effect dominates the middle tropical troposphere complementary. All models except UKMO and UKMOGK agreed on a divergence of MSE, or in other words, cooling tendency in the tropical mixed layer. All models that were able to twist SCMT (GFDL; UKMO(GK) & LMDZ) showed a warming of the lower free troposphere in the tropics $(900-800 hPa)$ due to horizontal convergence of MSE.

Opposite to the warming by horizontal advection, vertical advection plays to cool approximately the same zones as in which horizontal advection is warming the atmosphere, true for UKMO; UKMOGK and LMDZ. Considering the cooling rates, it is roughly compensating each other. For GFDL we find a strong cooling at $920 - 800\, hPa$ complementing the low level cooling by horizontal advection. It warms the middle troposphere to a smaller extent. The inclusion of CMT for CAM6 is predominantly warming the upper troposphere.

7.3 Data correction

Being aware that the current study assesses the circulation responses in an aquaplanet configuration with prescribed sea surface temperature, quantitative analysis of e.g. wind magnitude is complicated and in a way spurious. Complex processes as land-atmosphere interaction and geometry of land masses are excluded and will always happen to affect radiation; moisture; wind and pressure gradients. The study serves as a pilot in investigating the qualitative model sensitivity and response to enhanced SCMT. In line with this, the large amount of data and diversity of model output in terms of data structure and variable treatment led to choices in data processing that affected the quantitative analysis. The most important corrections are listed below.

1. The geopotential height in the GFDL model, required for the computation of moist static energy, is central averaged as it was originally computed on interval levels while all other variables were provided in the center of the grid cells. Looking at the vertical profile of MSE we find that it slightly increases with height, meaning that the quantitative vertical advection of MSE might be overestimated for this model through the vertical gradient.

2. All data from UKMO and UKMOGK was initially computed on height-grid $[m]$, which is for plot- and comparison purposes replaced with an averaged latitudinal and longitudinal pressure-grid between $-30^o and 30^o$, induced from the pressure variable within the data. We verified for conceptual differences in e.g. large scale circulation and wind direction adjustments. As pressure gradients in the tropics are by convention relatively weak we assume small qualitative differences, however they are present and underline the spuriosity of quantitative conclusions.

3. Computations in longitudinal direction are probably slightly underestimated as it is differentiated over degrees and consecutively divided by the distance of a longitude at the equator, meaning that e.g. at the subtropics one degree longitude becomes in terms of $[m^{\,o}]$.
4. It has proven to be very hard to manually compute the boundary layer height or alternatively the height of the converging layer. Some models provide these heights by default, however for the models that were able to do this, the data seemed very chaotic. A consequence of this is that vertical integration over a growing

boundary layer, as discussed in Section 6.1.4, should be done really carefully. Inadequate treatment of setting the vertical integration limits could lead to spurious under- or overestimation of e.g. convergence.

5. Omega from UKMO is computed by vertical velocity and density instead of directly retrieved from the data.

6. The air density for CAM6 was submitted on interval levels, after which it is central averaged to obtain density in the center of the grid cells.

7.4 Limitations

In general, looking at simulation averaged tendencies only provides an indication of what the convection and turbulence schemes have been doing over the entire simulation. Tendencies are usually conserved after each modelling time-step, as the model reaches a quasi steady-state, the magnitude of all tendencies will become smaller and hence averaging will only provide a qualitative idea of what the model has been doing.

Earlier analysis of the wind tendencies by convective mixing for the GFDL model revealed, after consultation, that although the output seemed correct the tendencies were actually not used to drive wind changes in the model and that the tendencies were coming from a process that was not turned on in the model. Alternatively, they advised to use a vertical diffusivity parameter that is used to calculate the wind tendency due to vertical diffusion as this was considered the most relevant variable. In doing so, the diffusivity is combined with diffusivity calculated in other parts of the model (e.g. deep convection and turbulence) - making it impossible to compare the influence of mixing momentum by shallow convection only with other models. As a solution to this, we had to decide to combine the momentum mixing from convection together with the mixing from turbulence for all the other models.

8 Recommendations

Two things that have by far taken the most attention and work within this research are the determination and discussion of what is actually happening with regards to the inter-model differences in circulation adjustment, and secondly, accordingly to what we wanted to analyse figuring out what data is required in terms of variables and structure (e.g. time dimension). For anyone intentioned to build further on this work, it could be beneficial to learn about both components following this section.

8.1 Future Work

The present research shows the steady-state or simulation-averaged responses to the inclusion of vertical mixing of horizontal momentum, being a first pilot of discussing how and to what extent shallow convection does with the circulation and all its key processes. However, for future work we would suggest to conduct a study that analyses model adjustments over time, with the purpose of revealing what occurs both in the short- and long-term.

8.1.1 Tendencies

The tendencies of the wind vectors induced by SCMT concerned simulation-averaged tendencies, which were only an qualitative indication of the influence SCMT has on the local wind profile. As the wind tendencies are fundamentally linked with the time dimension (change over time), this would require short-span data of both the wind profiles and the tendencies to evaluate the direct progression directly after the spin-up period. With this, one would be able to distinguish between the direct dynamic and thermodynamic responses due to the activation of momentum mixing, and the long-term response felt through the entire deep- or shallow overturning circulation.

In addition, although we specifically requested the tendencies induced by SCMT only, not all models were able to provide them isolated from the deep convection scheme or turbulence scheme. For the purpose of inter-model comparison, this should definitely be minded in a follow-up study.

8.1.2 Deep Convective Mass Flux

One of the last things we analysed was the response in the tropospheric energy budget, measured through (volumetric) MSE. As for approximately all models the shallow mass flux appeared to extent quite deep into the troposphere, especially at places of deep convection, we became interested in how the deep convective mass flux would behave while altering SCMT. For models that showed strong adjustments in the circulation (e.g. GFDL & LMDZ) we found that there was no significant difference in the depth of the shallow scheme compared to models that only showed a circulation adjustment in the shallow overturning cell (UKMO & UKMOGK). In

other words models that showed dampened remote responses in terms of the circulation had no fair difference in the shallow flux nor the tendencies induced by the shallow flux.

Our latest thought on this is that the sensitivity of the deep convective mass flux, known to be strongly determinative for setting convective zones and the circulation strength, might differ between models. An example of this would be that the deep flux is would be that the deep flux is rather parameterized as a function of surface fluxes, or either as a function of dynamics:

$$M_{DC} \sim F_{buoy}/F_{LH} \;\; or \;\; M_{DC} \sim \bigtriangledown u \cdot q \qquad (19)$$

As a first indication for this, we suggest to see whether the large-scale divergence is driven by changes in advective terms due to changed friction, or alternative by energetics (e.g. evaporation). Neggers et al. (2007) found that the column-integrated net available energy, defined as the sum of the surface fluxes and the net radiation at the top of the atmosphere (TOA), is balanced by vertical advection and horizontal divergence of MSE:

$$\langle \mathcal{D}_H(h) \rangle + \langle \omega \partial_p(h) \rangle = F_{rad} + SH + LH \qquad (20)$$

With $\mathcal{D}_H(h)$ the horizontal divergence of MSE (h); $\omega \partial_p(h)$ the vertical advection; F_{rad} the net radiation at the TOA ($LW_n + SW_n$); SH & LH being the sensible and latent heat fluxes at the surface respectively and $\langle\rangle$ referring to the vertical integration over the entire tropospheric column ($\int_p^{p_s} dp$).

In a first sensitivity analysis, we did not succeed in closing the energy budget. Potentially this could be a calculation error, however we rather believe it to be caused by the (nonphysically) strong increase in MSE at the highest vertical model levels. It sincerely seems like something is not numerically closing there.

The change in the structure and intensity of the large-scale circulation is driven by the changed friction due to SCMT on the one hand and through changes in energetics on the other hand. Much like Neggers et al. (2007) described, the overall circulation impact of both components could be diagnosed through w, defined as the large-scale divergence. By re-defining Eq. 13 as a perturbation from the control run (e.g. $SCMT_{off} - SCMT_{ctrl}$) and rewriting for $\langle w^{'} \rangle$ defined as the perturbation in vertically integrated vertical velocity due to large-scale di- or convergence, we find:

$$\langle \omega^{'} \rangle = \frac{F^{'}_{net} - \langle \omega_{ctrl} \partial_p(h)^{'} \rangle}{\langle \partial_p(h)^{noscmt} \rangle} - \frac{\langle \mathcal{D}_H(h) \rangle^{'}}{\langle \partial_p(h)^{noscmt} \rangle} \qquad (21)$$

Where the first term on the right-hand side refers to changes in physics and vertical fluxes, whereas the second term refers to rather dynamical changes in horizontal divergence or advection of energy.

8.2 Data

For our initial structure of model output and data requirements, we closely mirrored the clarification constructed by Webb et al. (2017) for CFMIP contributions to CMIP6, supplemented by CMOR and known (A)GCM output variables. Following the interpretation process of what was causing inter-model differences, additional data had to be requested as not all models were able to or were not requested to provide certain data we required for analysis, for the latter because we were not aware we needed it when we distributed the output requirements format. For example, we didn't request the tendencies and convective fluxes for CAM6, nor the radiative fluxes for both CAM6 and UKMO models.

Alternatively, we had to correct or compensate by manually computing variables leading to quality deficiencies. One clear example of this would be the fact that the UKMO and UKMOGK models submitted their data on a vertical height grid while all other models were provided on a vertical pressure axis, complicating inter-model comparison and computation. In an attempt of supporting future work, we would be benevolent to provide our most recent output requirements as a first backbone.
For remaining questions concerning the output requirements, model requirements or e.g. variable specification, please feel free to contact Nils Hoebe (n.j.m.hoebe@student.tudelft.nl) or Louise Nuijens (louise.nuijens@tudelft.nl).

References

Back, L. E. and Bretherton, C. S. (2009). On the relationship between sst gradients, boundary layer winds, and convergence over the tropical oceans. *Journal of Climate*, 22(15):4182–4196.

Bischoff, T. and Schneider, T. (2014). Energetic constraints on the position of the intertropical convergence zone. *Journal of Climate*, 27(13):4937–4951.

Blackburn, M. and Hoskins, B. J. (2013). Context and aims of the aqua-planet experiment. *Journal of the Meteorological Society of Japan. Ser. II*, 91:1–15.

Bony, S., Bellon, G., Klocke, D., Sherwood, S., Fermepin, S., and Denvil, S. (2013). Robust direct effect of carbon dioxide on tropical circulation and regional precipitation. *Nature Geoscience*, 6(6):447–451.

Broccoli, A. J., Dahl, K. A., and Stouffer, R. J. (2006). Response of the itcz to northern hemisphere cooling. *Geophysical Research Letters*, 33(1).

Carr, M. T. and Bretherton, C. S. (2001). Convective Momentum Transport over the Tropical Pacific: Budget Estimates. *Journal of the Atmospheric Sciences*, 58(13):1673–1693.

de Szoeke, S. P., Wang, Y., Xie, S.-P., and Miyama, T. (2006). Effect of shallow cumulus convection on the eastern pacific climate in a coupled model. *Geophysical Research Letters*, 33(17).

Dixit, V., Nuijens, L., and Helfer, K. C. (2021). Counter-gradient momentum transport through subtropical shallow convection in icon-lem simulations. *Journal of Advances in Modeling Earth Systems*, 13(6):e2020MS002352.

Frierson, D. M. (2007). The dynamics of idealized convection schemes and their effect on the zonally averaged tropical circulation. *Journal of the atmospheric sciences*, 64(6):1959–1976.

Gates, W. L., Boyle, J. S., Covey, C., Dease, C. G., Doutriaux, C. M., Drach, R. S., Fiorino, M., Gleckler, P. J., Hnilo, J. J., Marlais, S. M., et al. (1999). An overview of the results of the atmospheric model intercomparison project (amip i). *Bulletin of the American Meteorological Society*, 80(1):29–56.

Helfer, K. C., Nuijens, L., and Dixit, V. V. (2021). The role of shallow convection in the momentum budget of the trades from large-eddy-simulation hindcasts. *Quarterly Journal of the Royal Meteorological Society*, 147(737):2490–2505.

Hirota, N., Takayabu, Y. N., Watanabe, M., and Kimoto, M. (2011). Precipitation reproducibility over tropical oceans and its relationship to the double itcz problem in cmip3 and miroc5 climate models. *Journal of climate*, 24(18):4859–4873.

Hwang, Y.-T. and Frierson, D. M. (2013). Link between the double-intertropical convergence zone problem and cloud biases over the southern ocean. *Proceedings of the National Academy of Sciences*, 110(13):4935–4940.

Kershaw, R. and Gregory, D. (1997). Parametrization of momentum transport by convection. i: Theory and cloud modelling results. *Quarterly Journal of the Royal Meteorological Society*, 123(541):1133–1151.

Larson, V. E., Domke, S., and Griffin, B. M. (2019). Momentum transport in shallow cumulus clouds and its parameterization by higher-order closure. *Journal of Advances in Modeling Earth Systems*, 11(11):3419–3442.

Li, G. and Xie, S.-P. (2014). Tropical biases in cmip5 multimodel ensemble: The excessive equatorial pacific cold tongue and double itcz problems. *Journal of Climate*, 27(4):1765–1780.

Lin, J.-L. (2007). The double-itcz problem in ipcc ar4 coupled gcms: Ocean–atmosphere feedback analysis. *Journal of Climate*, 20(18):4497–4525.

Marshall, J., Donohoe, A., Ferreira, D., and McGee, D. (2014). The ocean's role in setting the mean position of the intertropical convergence zone. *Climate Dynamics*, 42(7):1967–1979.

Medeiros, B., Stevens, B., and Bony, S. (2015). Using aquaplanets to understand the robust responses of comprehensive climate models to forcing. *Climate Dynamics*, 44(7):1957–1977.

Medeiros, B., Stevens, B., Held, I. M., Zhao, M., Williamson, D. L., Olson, J. G., and Bretherton, C. S. (2008). Aquaplanets, climate sensitivity, and low clouds. *Journal of Climate*, 21(19):4974–4991.

Mitchell, T. P. and Wallace, J. M. (1992). The annual cycle in equatorial convection and sea surface temperature. *Journal of Climate*, 5(10):1140–1156.

Neale, R. B. and Hoskins, B. J. (2000). A standard test for agcms including their physical parametrizations: I: The proposal. *Atmospheric Science Letters*, 1(2):101–107.

Neggers, R. A., Neelin, J. D., and Stevens, B. (2007). Impact mechanisms of shallow cumulus convection on tropical climate dynamics. *Journal of Climate*, 20(11):2623–2642.

Nuijens, L., Savazzi, A., de Boer, G., Brilouet, P.-E., George, G., Lothon, M., and Zhang, D. (2022). The frictional layer in the observed momentum budget of the trades. *Quarterly Journal of the Royal Meteorological Society*, 148(748):3343–3365.

Oueslati, B. and Bellon, G. (2015). The double itcz bias in cmip5 models: Interaction between sst, large-scale circulation and precipitation. *Climate dynamics*, 44(3):585–607.

Philander, S., Gu, D., Lambert, G., Li, T., Halpern, D., Lau, N., and Pacanowski, R. C. (1996). Why the itcz is mostly north of the equator. *Journal of climate*, 9(12):2958–2972.

Richter, I., Behera, S. K., Doi, T., Taguchi, B., Masumoto, Y., and Xie, S.-P. (2014). What controls equatorial atlantic winds in boreal spring? *Climate dynamics*, 43:3091–3104.

Richter, J. H. and Rasch, P. J. (2008). Effects of convective momentum transport on the atmospheric circulation in the community atmosphere model, version 3. *Journal of Climate*, 21(7):1487–1499.

Saggiorato, B., Nuijens, L., Siebesma, A. P., de Roode, S., Sandu, I., and Papritz, L. (2020). The influence of convective momentum transport and vertical wind shear on the evolution of a cold air outbreak. *Journal of Advances in Modeling Earth Systems*, 12(6):e2019MS001991.

Sandu, I., Bechtold, P., Nuijens, L., Beljaars, A., and Brown, A. (2020). On the causes of systematic forecast biases in near-surface wind direction over the oceans.

Savazzi, A. C. M., Nuijens, L., Sandu, I., George, G., and Bechtold, P. (2022). The representation of the trade winds in ecmwf forecasts and reanalyses during eurec 4 a. *Atmospheric Chemistry and Physics*, 22(19):13049–13066.

Schneider, T., Bischoff, T., and Haug, G. H. (2014). Migrations and dynamics of the intertropical convergence zone. *nature*, 513(7516):45–53.

Sobel, A. H. and Neelin, J. D. (2006). The boundary layer contribution to intertropical convergence zones in the quasi-equilibrium tropical circulation model framework. *Theoretical and Computational Fluid Dynamics*, 20:323–350.

Song, X. and Zhang, G. J. (2020). Role of equatorial cold tongue in central pacific double-itcz bias in the ncar cesm1. 2. *Journal of Climate*, 33(24):10407–10418.

Stevens, B., Bony, S., and Webb, M. (2012). Clouds on-off klimate intercomparison experiment (cookie).

Stevens, B., Duan, J., McWilliams, J. C., Münnich, M., and Neelin, J. D. (2002). Entrainment, rayleigh friction, and boundary layer winds over the tropical pacific. *Journal of climate*, 15(1):30–44.

Tian, B. and Dong, X. (2020). The double-itcz bias in cmip3, cmip5, and cmip6 models based on annual mean precipitation. *Geophysical Research Letters*, 47(8):e2020GL087232.

Waliser, D. E. and Gautier, C. (1993). A satellite-derived climatology of the itcz. *Journal of climate*, 6(11):2162–2174.

Webb, M. J., Andrews, T., Bodas-Salcedo, A., Bony, S., Bretherton, C. S., Chadwick, R., Chepfer, H., Douville, H., Good, P., Kay, J. E., et al. (2017). The cloud feedback model intercomparison project (cfmip) contribution to cmip6. *Geoscientific Model Development*, 10(1):359–384.

Williamson, D., Blackburn, M., Hoskins, B., Nakajima, K., Ohfuchi, W., Takahashi, Y., Hayashi, Y.-Y., Nakamura, H., Ishiwatari, M., McGregor, J., et al. (2012). The ape atlas.

Woelfle, M., Yu, S., Bretherton, C., and Pritchard, M. (2018). Sensitivity of coupled tropical pacific model biases to convective parameterization in cesm1. *Journal of Advances in Modeling Earth Systems*, 10(1):126–144.

Wu, X., Deng, L., Song, X., and Zhang, G. J. (2007). Coupling of convective momentum transport with convective heating in global climate simulations. *Journal of the atmospheric sciences*, 64(4):1334–1349.

Wu, X., Liang, X.-Z., and Zhang, G. J. (2003). Seasonal migration of itcz precipitation across the equator: Why can't gcms simulate it? *Geophysical Research Letters*, 30(15).

Yu, J.-Y. and Mechoso, C. R. (1999). Links between annual variations of peruvian stratocumulus clouds and of sst in the eastern equatorial pacific. *Journal of Climate*, 12(11):3305–3318.

Zhang, G. J. and McFarlane, N. A. (1995). Role of convective scale momentum transport in climate simulation. *Journal of Geophysical Research: Atmospheres*, 100(D1):1417–1426.

Supplementary Material To:

IMPACT OF SHALLOW CONVECTIVE MOMENTUM TRANSPORT ON LARGE-SCALE DYNAMICS

Inter-Model Comparison Project of Steady-State Cumulus-Friction Adjustment on Tropical Dynamics

BY

Nicolaas J.M. Hoebe

Appendix A: Wind Profiles

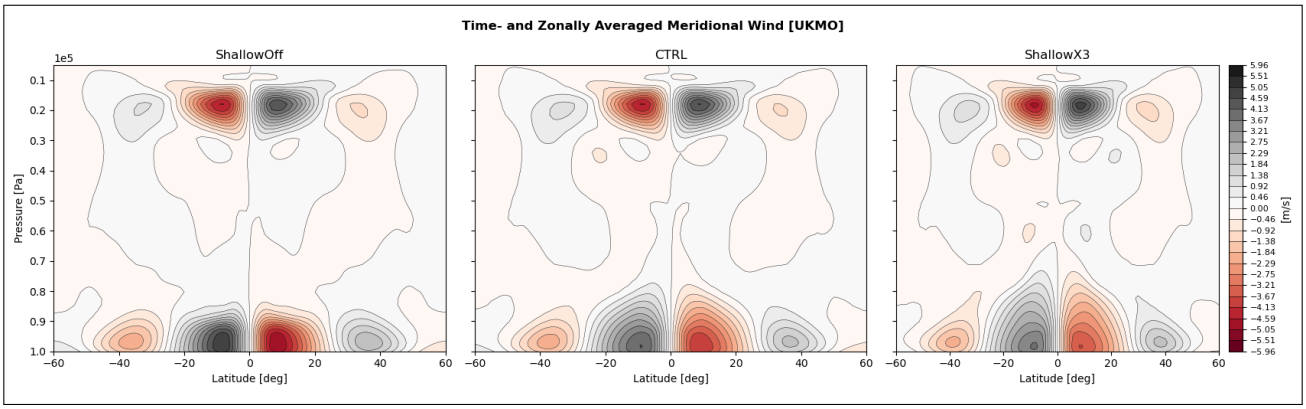

Figure 28: *Zonally Averaged Contour-Plot Of Meridional Wind In $SMCT_{off}$ (Left); $SCMT_{ctrl}$ (Centre) & $SCMT_{exag}$ (Right) For UKMO.*

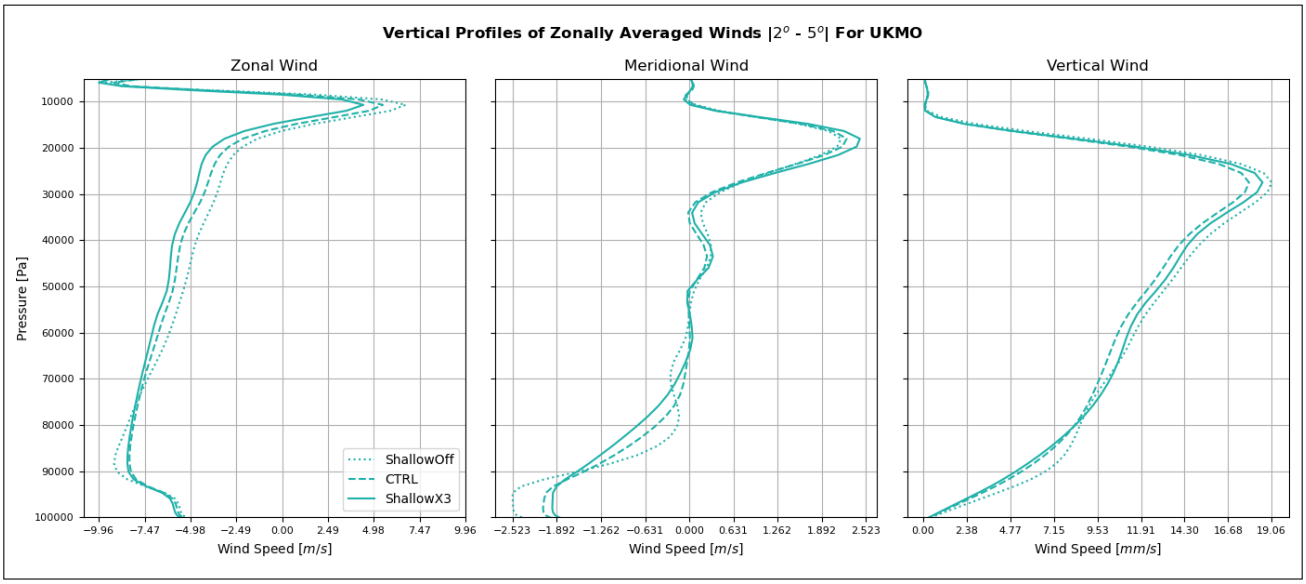

Figure 29: *Zonally Averaged Vertical Plots Of Tropical Winds, Averaged $2^o - 5^o$ For UKMO.*

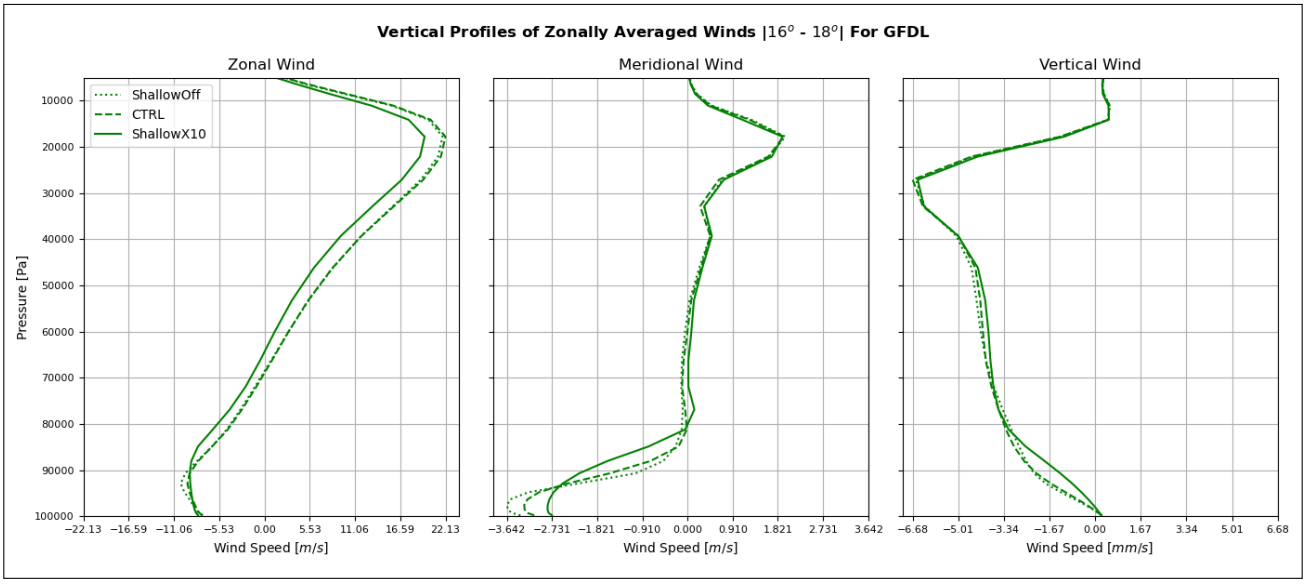

Figure 30: *Zonally Averaged Vertical Plots Of Sub-Tropical Winds, Averaged* $16^o - 18^o$ *For GFDL.*

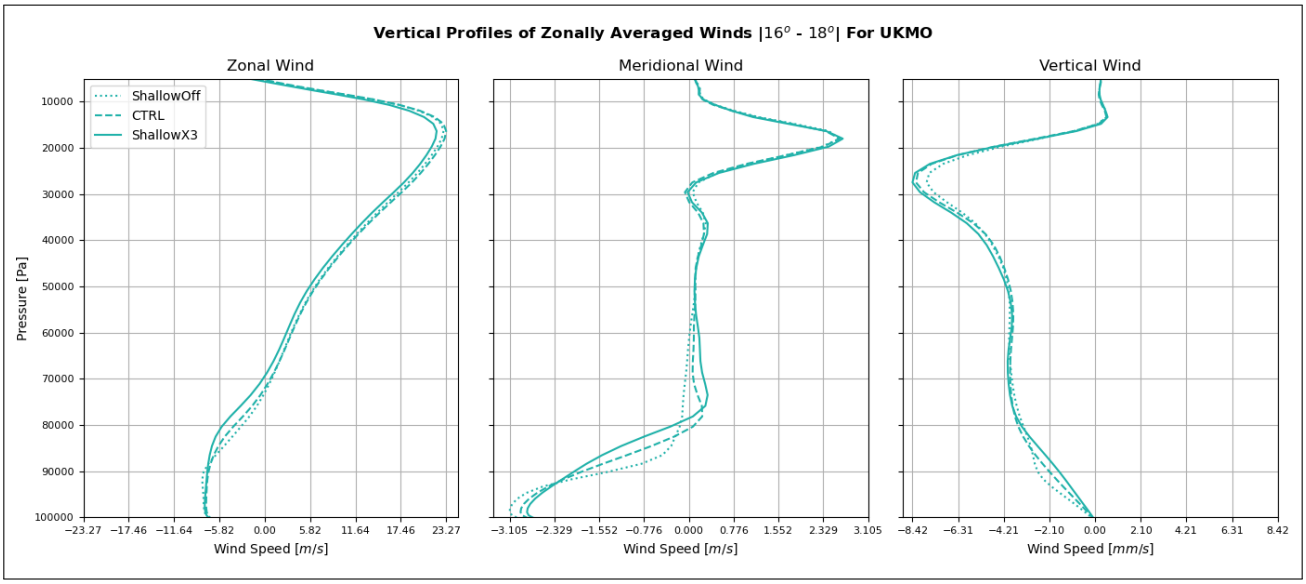

Figure 31: *Zonally Averaged Vertical Plots Of Sub-Tropical Winds, Averaged* $16^o - 18^o$ *For UKMO.*

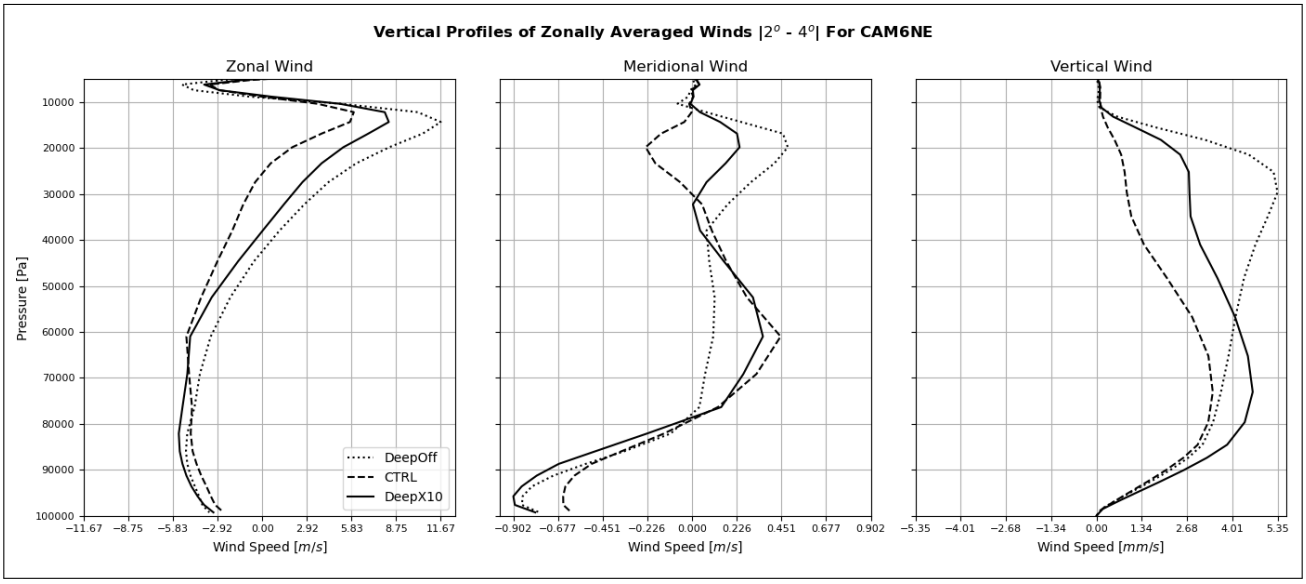

Figure 32: *Zonally Averaged Vertical Plots Of Tropical Winds, Averaged* $2^o - 4^o$ *For CAM6NE.*

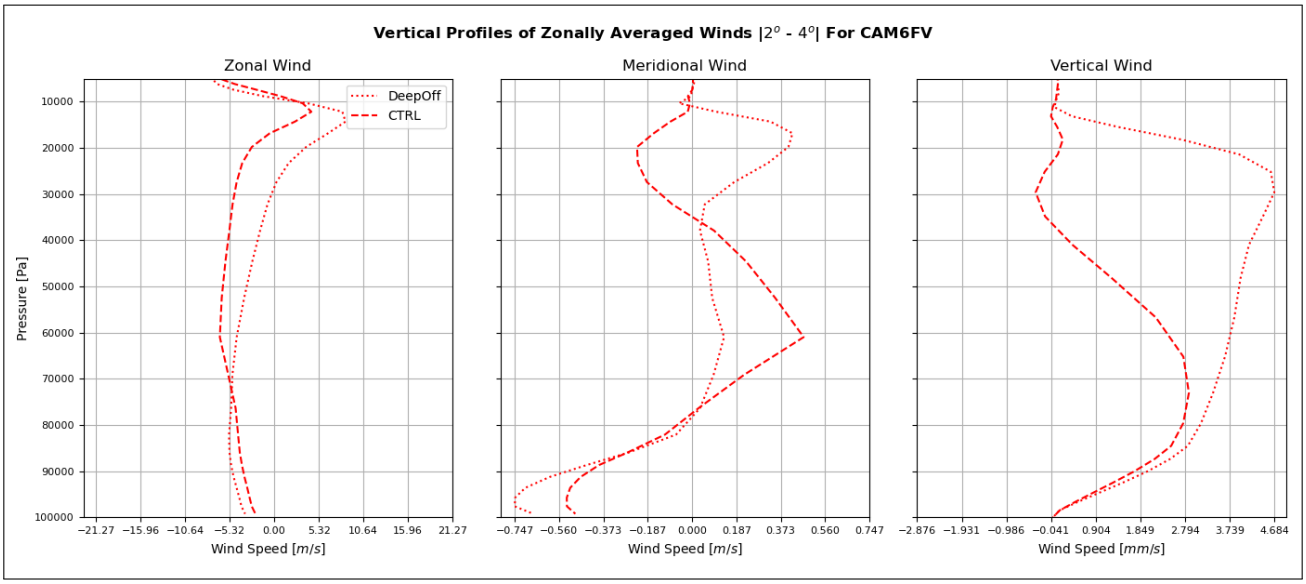

Figure 33: *Zonally Averaged Vertical Plots Of Tropical Winds, Averaged* $2^o - 4^o$ *For CAM6FV.*

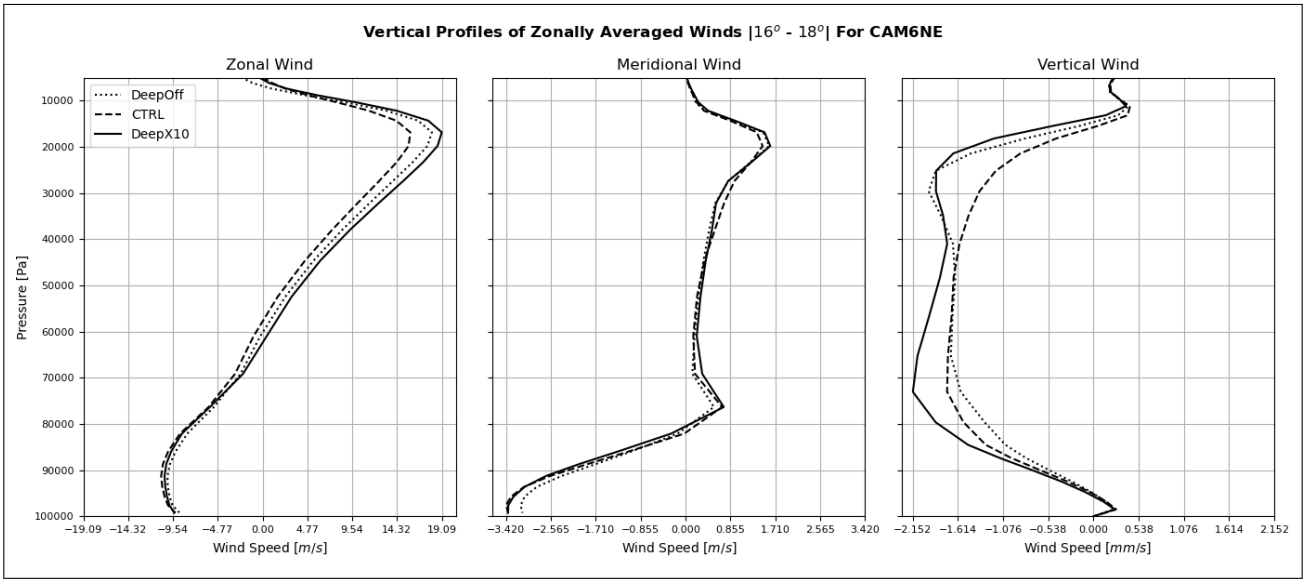

Figure 34: *Zonally Averaged Vertical Plots Of Sub-Tropical Winds, Averaged* $16^o - 18^o$ *For CAM6NE.*

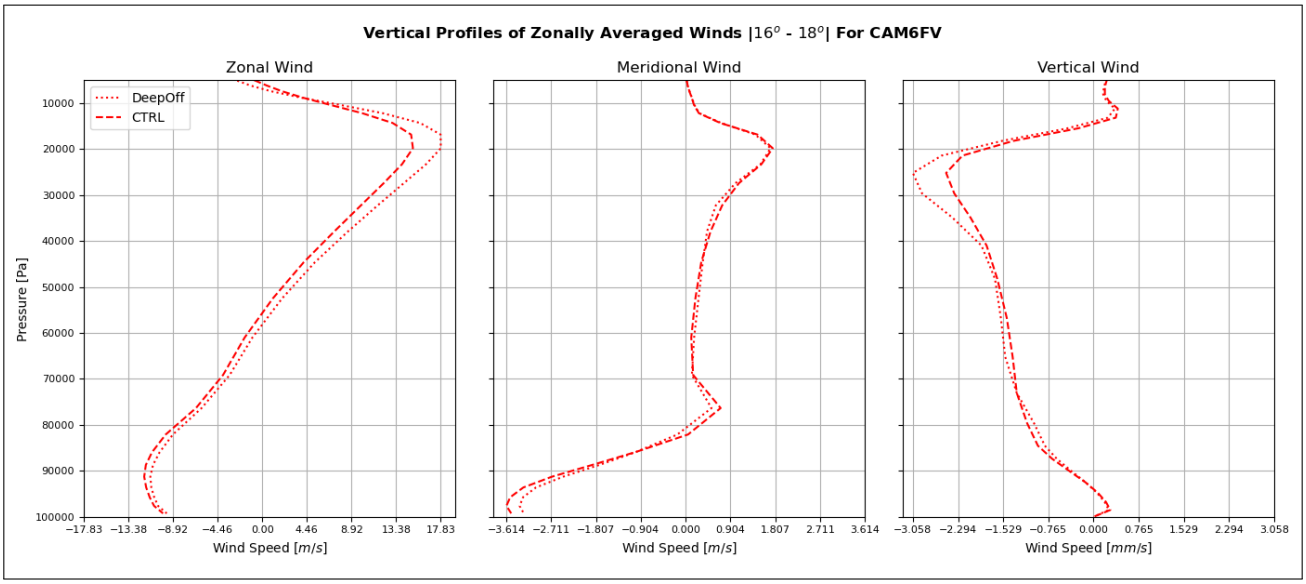

Figure 35: *Zonally Averaged Vertical Plots Of Sub-Tropical Winds, Averaged* $16^o - 18^o$ *For CAM6FV.*

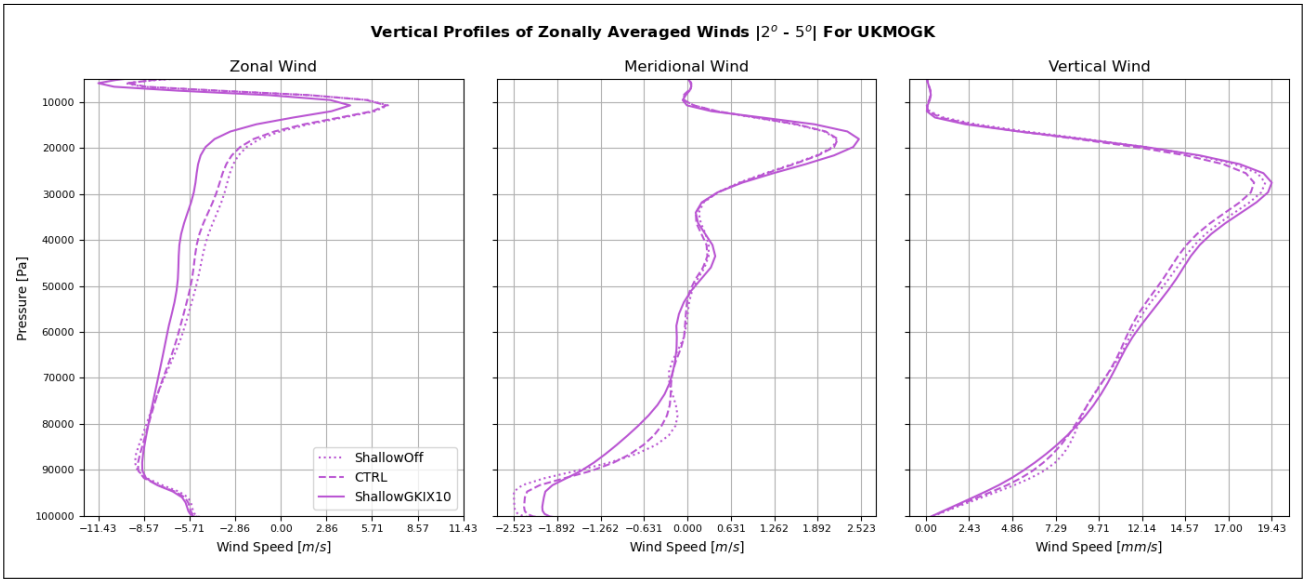

Figure 36: *Zonally Averaged Vertical Plots Of Tropical Winds, Averaged* $2^o - 5^o$ *For UKMOGK.*

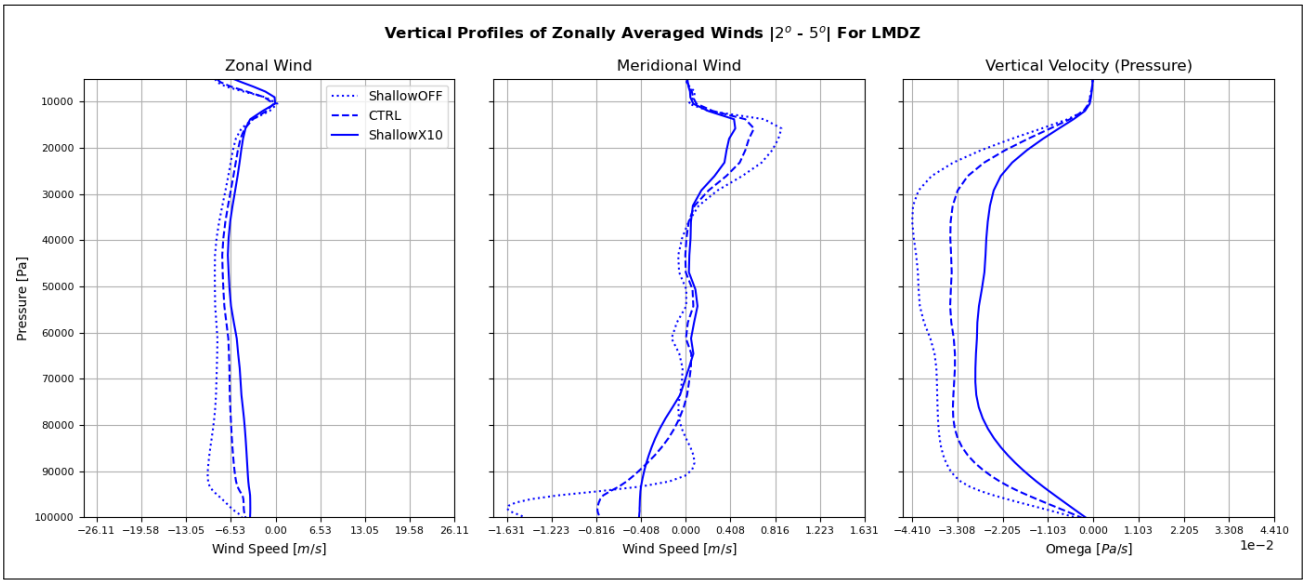

Figure 37: *Zonally Averaged Vertical Plots Of Tropical Winds, Averaged* $2^o - 5^o$ *For LMDZ.*

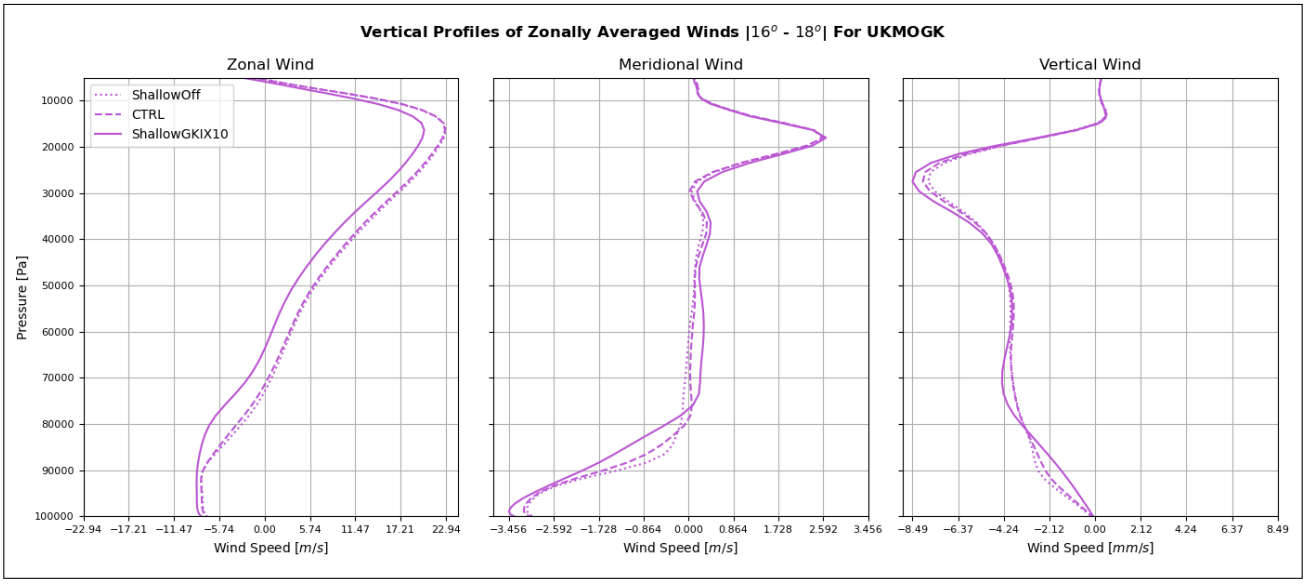

Figure 38: *Zonally Averaged Vertical Plots Of Sub-Tropical Winds, Averaged* $16^o - 18^o$ *For UKMOGK.*

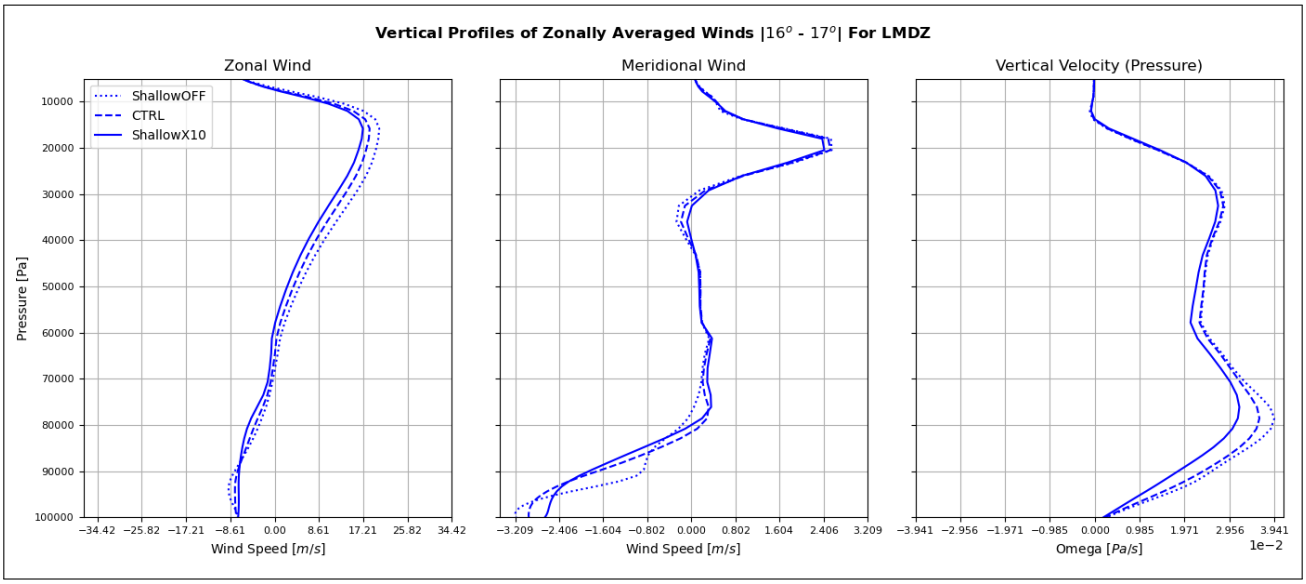

Figure 39: *Zonally Averaged Vertical Plots Of Sub-Tropical Winds, Averaged* $16^o - 18^o$ *For LMDZ.*

Appendix B: Tendencies & Convective Mass Fluxes

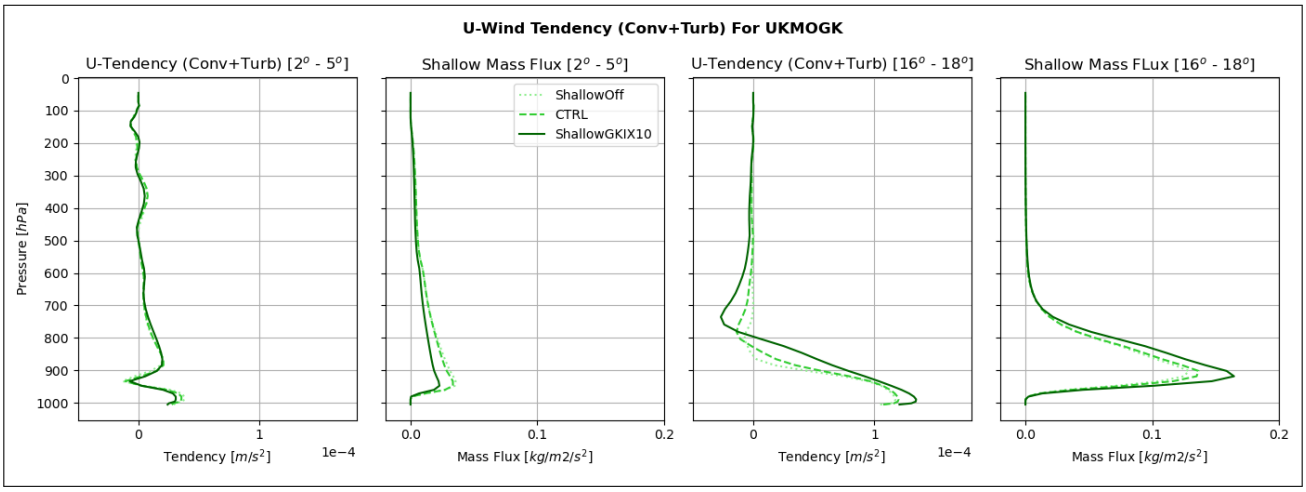

Figure 40: *Vertical Line-Plot Of Zonal Wind And Tendency Due To SCMT For UKMOGK, Cross-Sectional For Tropics* ($2^o - 5^o$) *And Sub-Tropics* ($16^o - 18^o$).

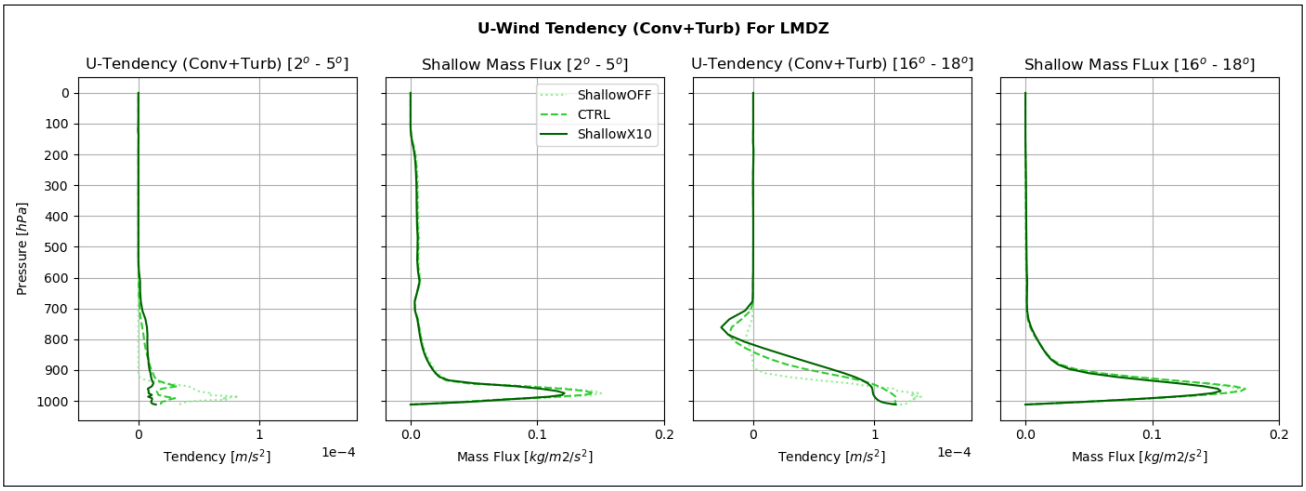

Figure 41: *Vertical Line-Plot Of Zonal Wind And Tendency Due To SCMT For LMDZ, Cross-Sectional For Tropics* ($2^o - 5^o$) *And Sub-Tropics* ($16^o - 18^o$).

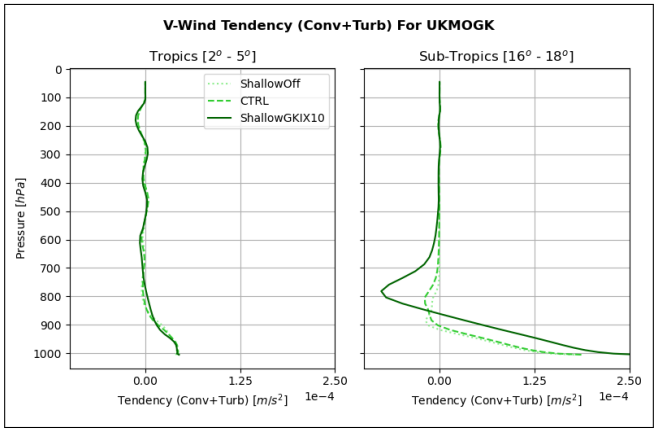

Figure 42: *Meridional-Wind Tendency Due To SCMT For UKMOGK, Cross-Sectional For Tropics* ($|2^o - 5^o|$) *And Sub-Tropics* ($|16^o - 18^o|$).

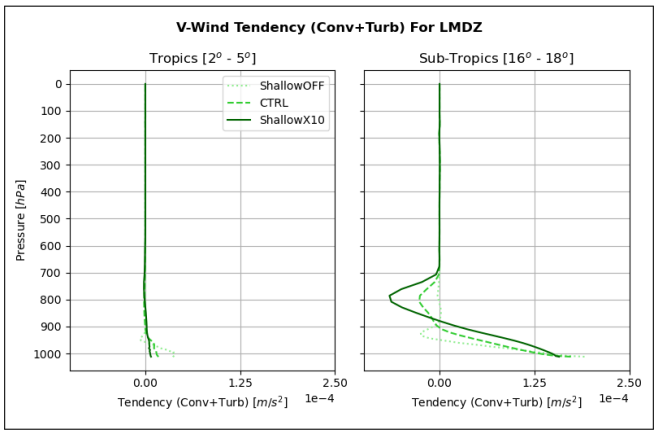

Figure 43: *Meridional-Wind Tendency Due To SCMT For LMDZ, Cross-Sectional For Tropics* ($|2^o - 5^o|$) *And Sub-Tropics* ($|16^o - 18^o|$).

Appendix C: Surface Winds

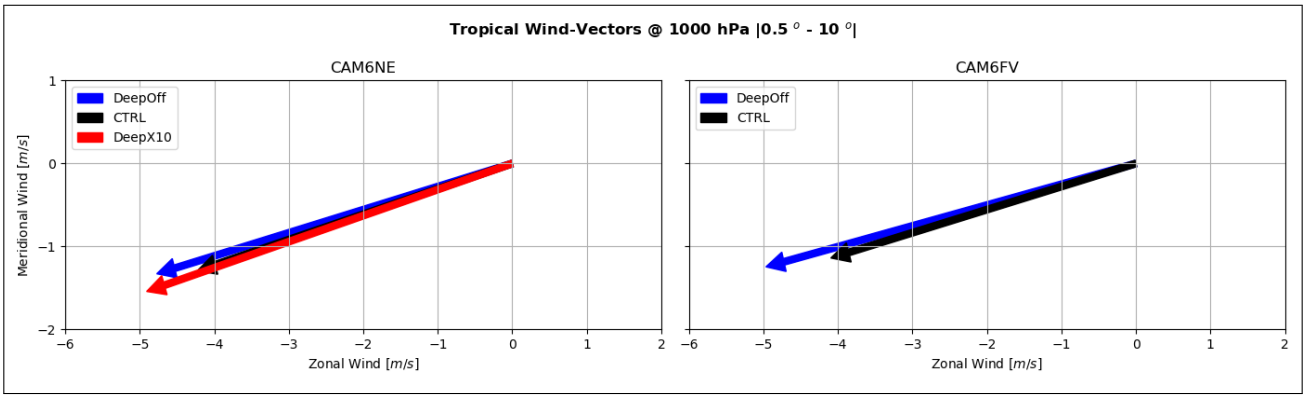

Figure 44: *Tropical Surface Wind Vectors For CAM6NE (Left) & CAM6FV (Right), Plotted For All Experiments.*

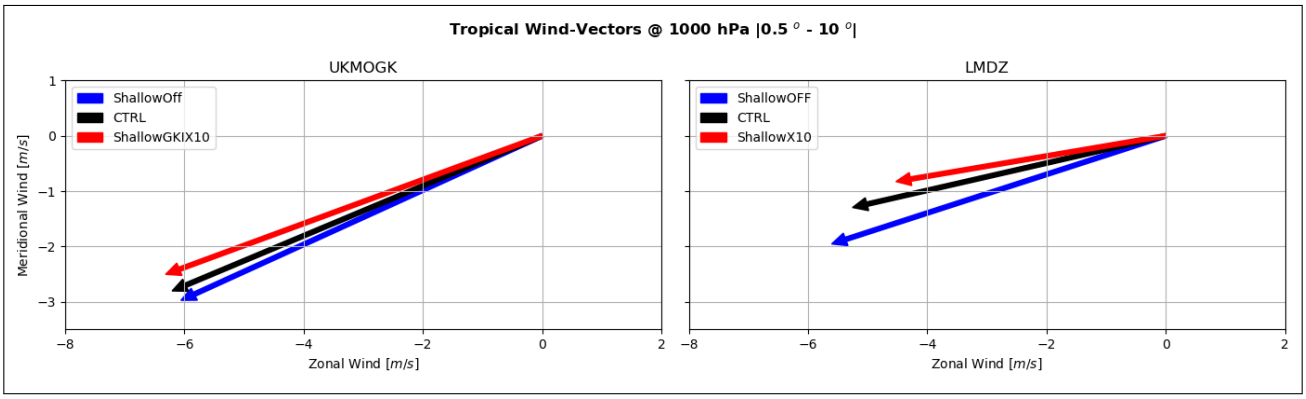

Figure 45: *Tropical Surface Wind Vectors For UKMOGK (Left) & LMDZ (Right), Plotted For All Experiments.*

Appendix D: Convergence & Ekman Pumping

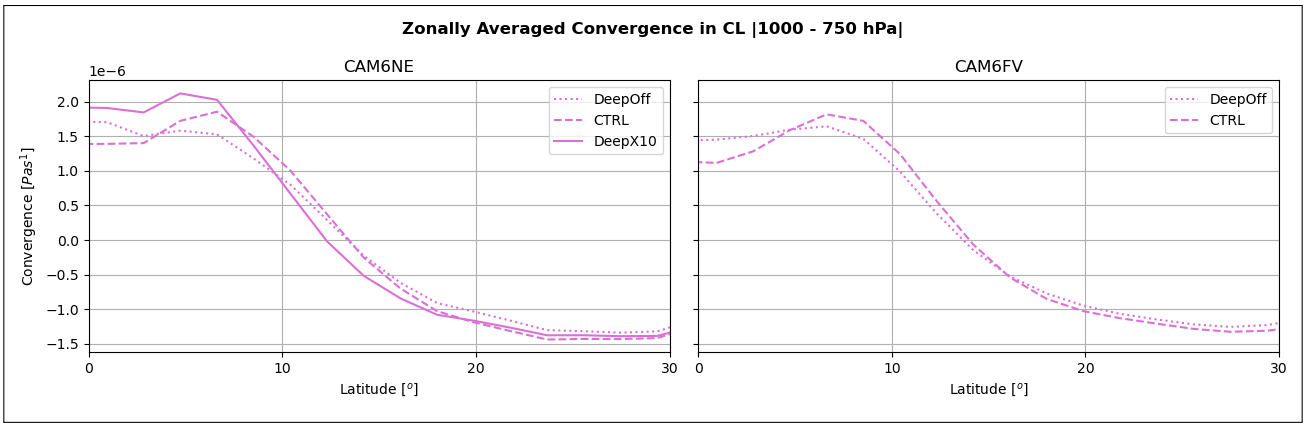

Figure 46: *Tropical Wind Convergence Averaged Over CL* $(1000 - 750hPa)$ *For CAM6NE & CAM6FV.*

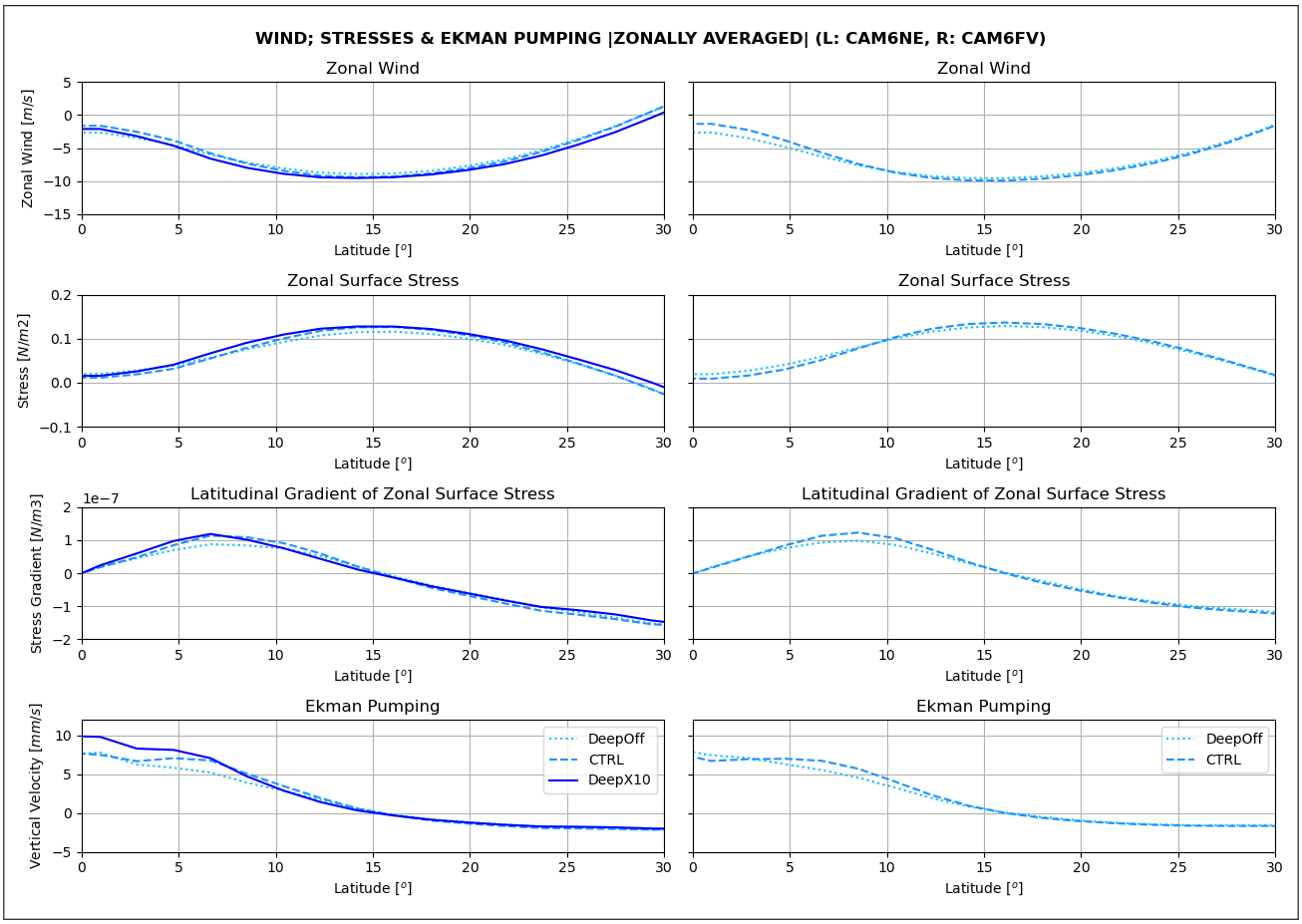

Figure 47: *Zonally Averaged Zonal Surface Wind; Zonal Surface Stress; Gradient Of Zonal Surface Stress & Ekman Pumping For CAM6NE (Left) & CAM6FV (Right)*

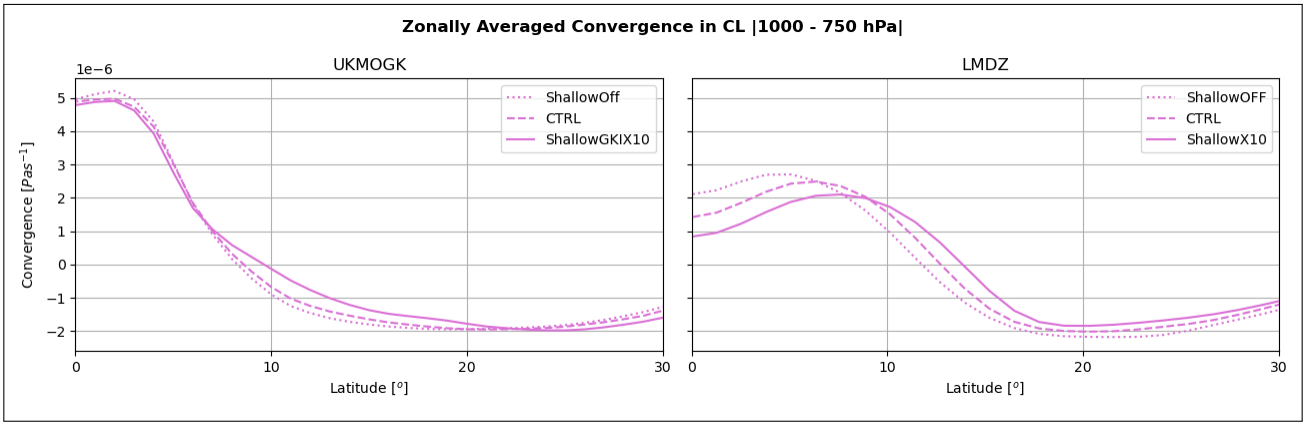

Figure 48: *Tropical Wind Convergence Averaged Over CL* $(1000 - 750hPa)$ *For UKMOGK (Left) & LMDZ (Right).*

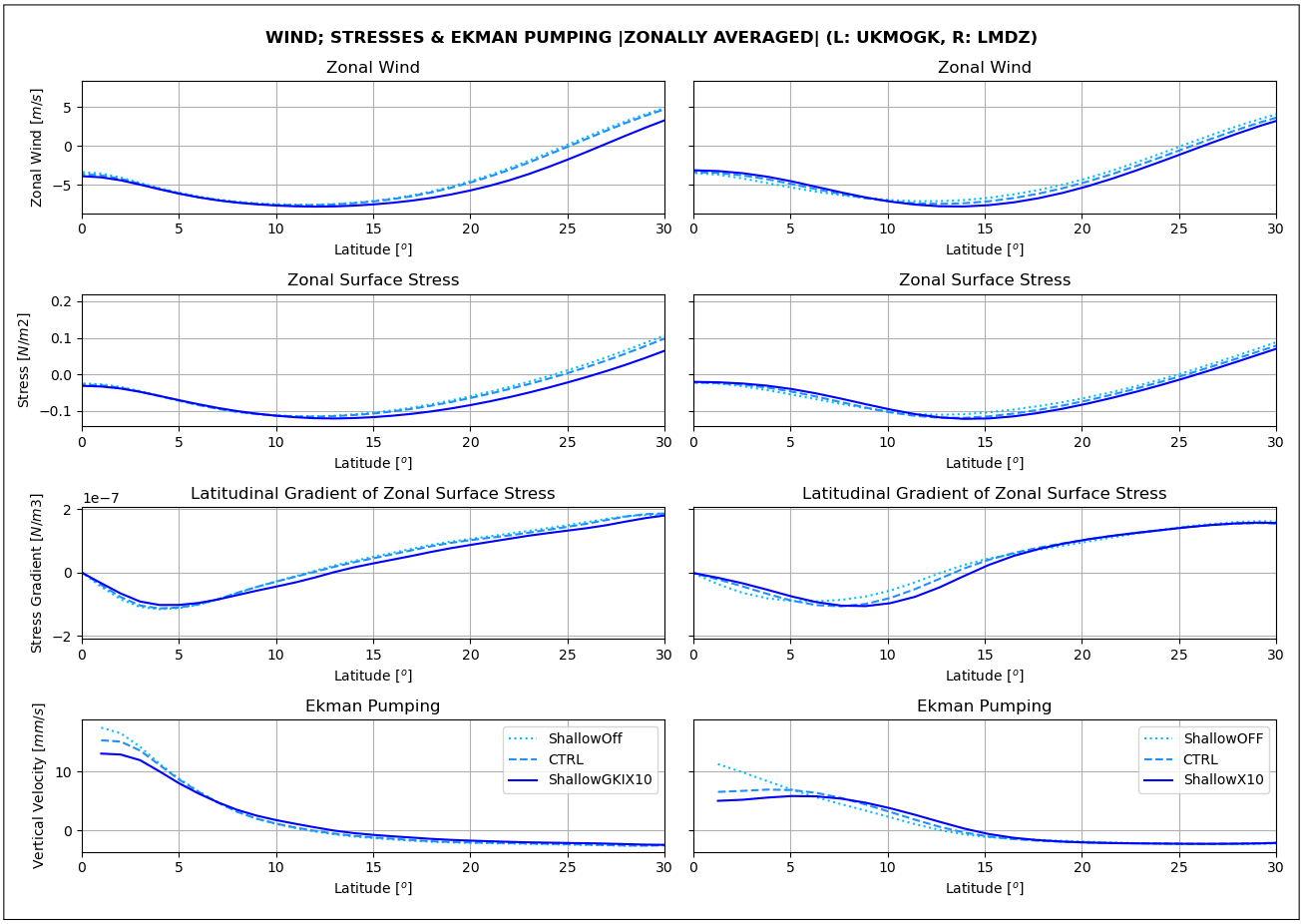

Figure 49: *Zonally Averaged Zonal Surface Wind; Zonal Surface Stress; Gradient Of Zonal Surface Stress & Ekman Pumping For UKMOGK (Left) & LMDZ (Right)*

Appendix E: Circulation

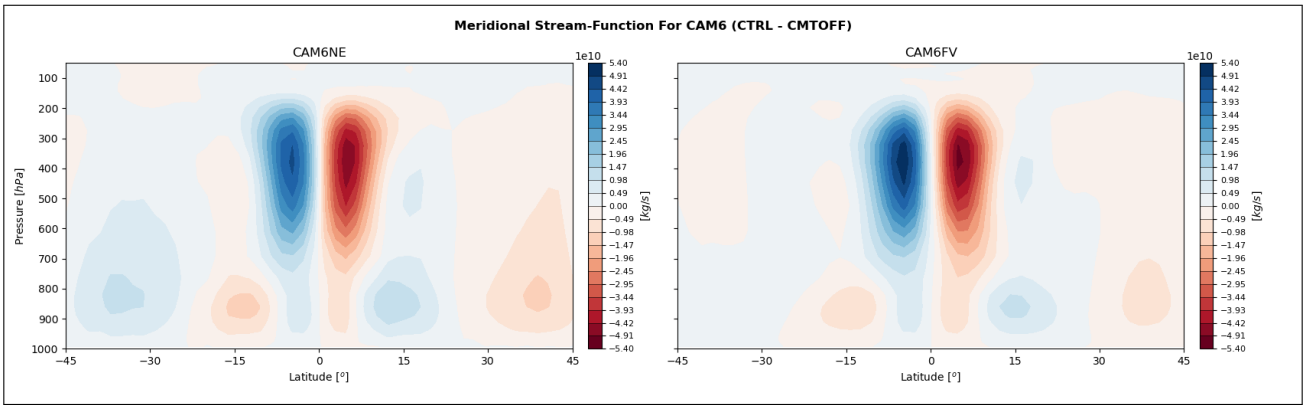

Figure 50: *Zonally Average Of The Meridional Stream-Flow Anomaly As A Result of Activated Shallow Convective Momentum Transport ($SCMT_{ctrl}$-$SCMT_{off}$) For CAM6NE (Left) And CAM6FV (Right).*

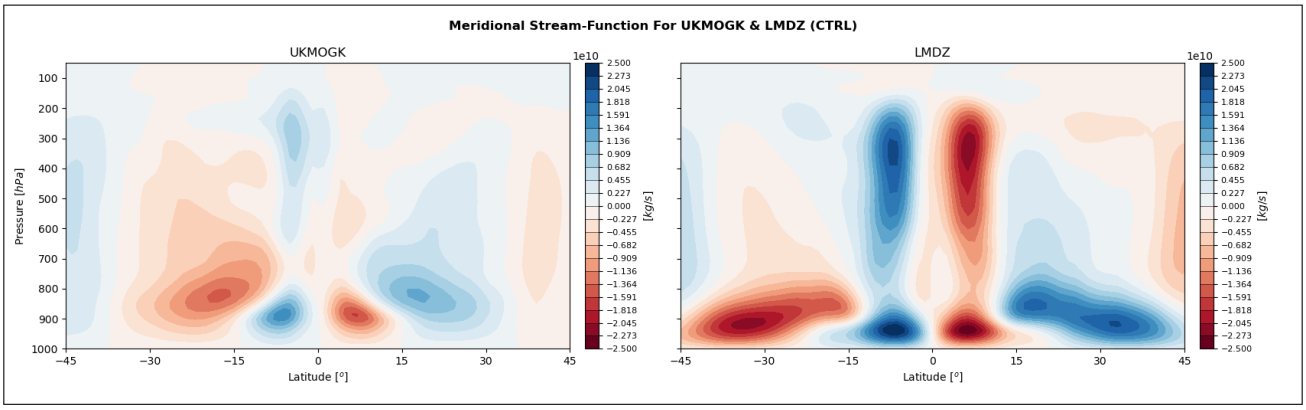

Figure 51: *Zonally Average Of The Meridional Stream-Flow Anomaly As A Result of Activated Shallow Convective Momentum Transport ($SCMT_{ctrl}$-$SCMT_{off}$) For UKMOGK (Left) And LMDZ (Right).*

Appendix F: Precipitation

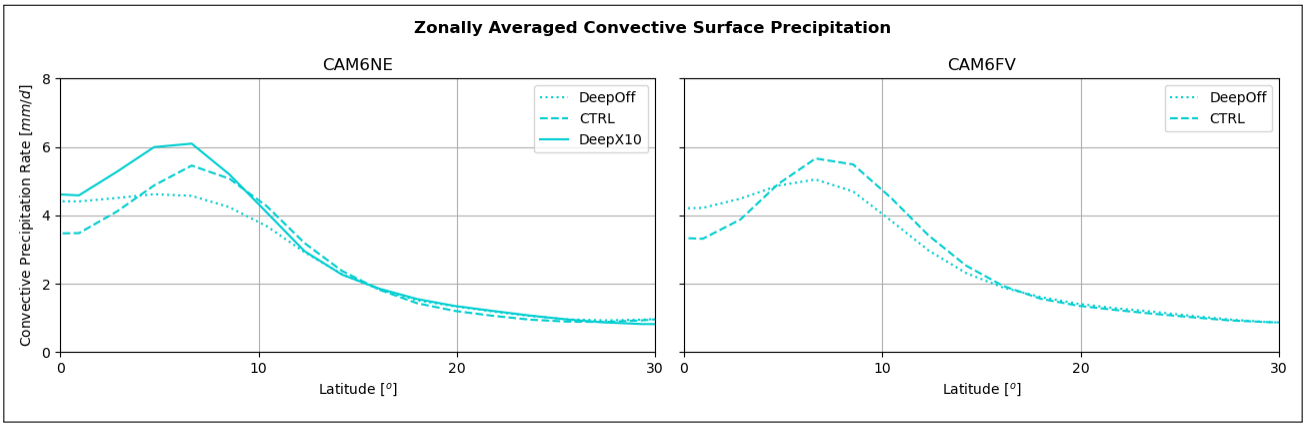

Figure 52: *Tropical Convective Surface Precipitation For CAM6NE (Left) & CAM6FV (Right).*

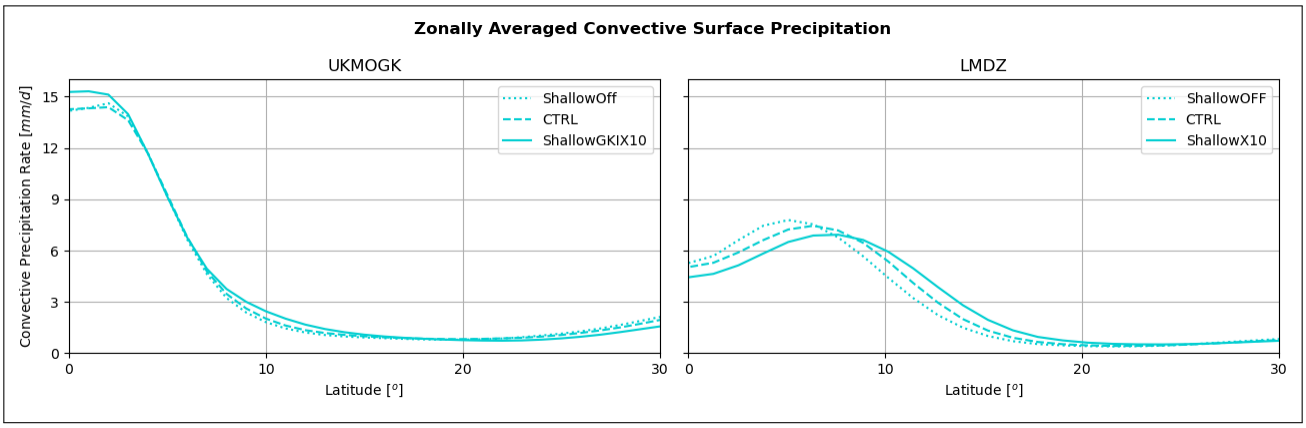

Figure 53: *Tropical Convective Surface Precipitation For UKMOGK (Left) & LMDZ (Right).*

Appendix G: MSE Budget

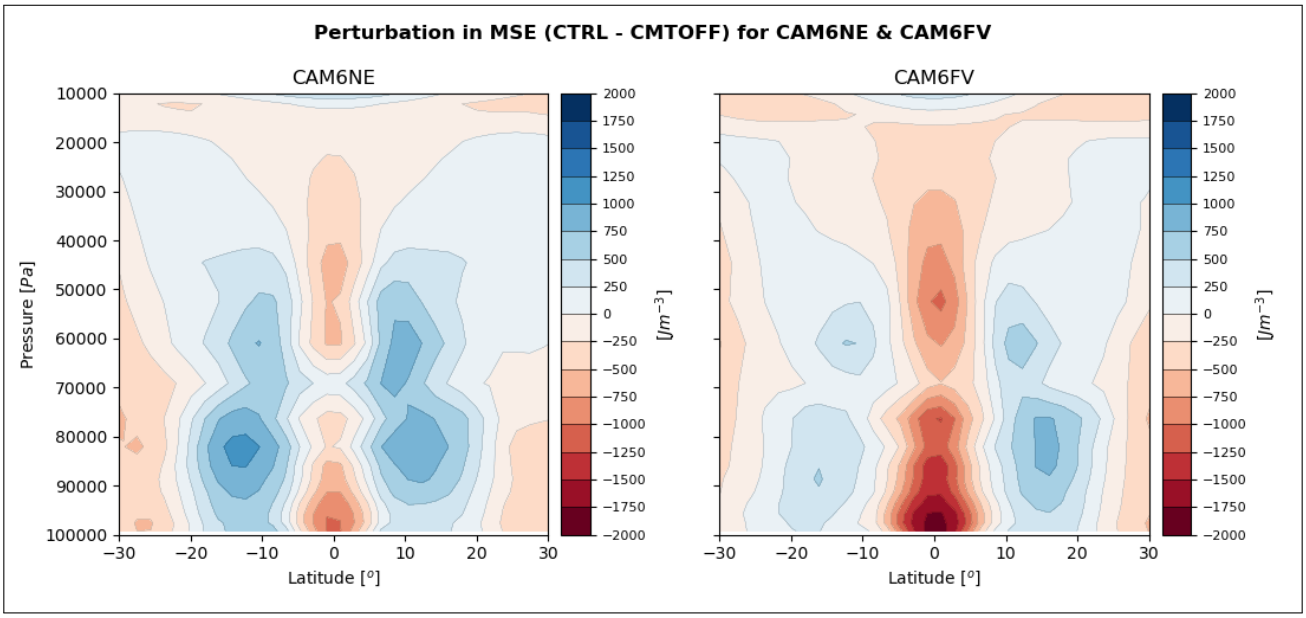

Figure 54: *Zonally Averaged Difference In MSE (CTRL-CMTOFF) For CAM6NE (Left) & CAM6FV (Right).*

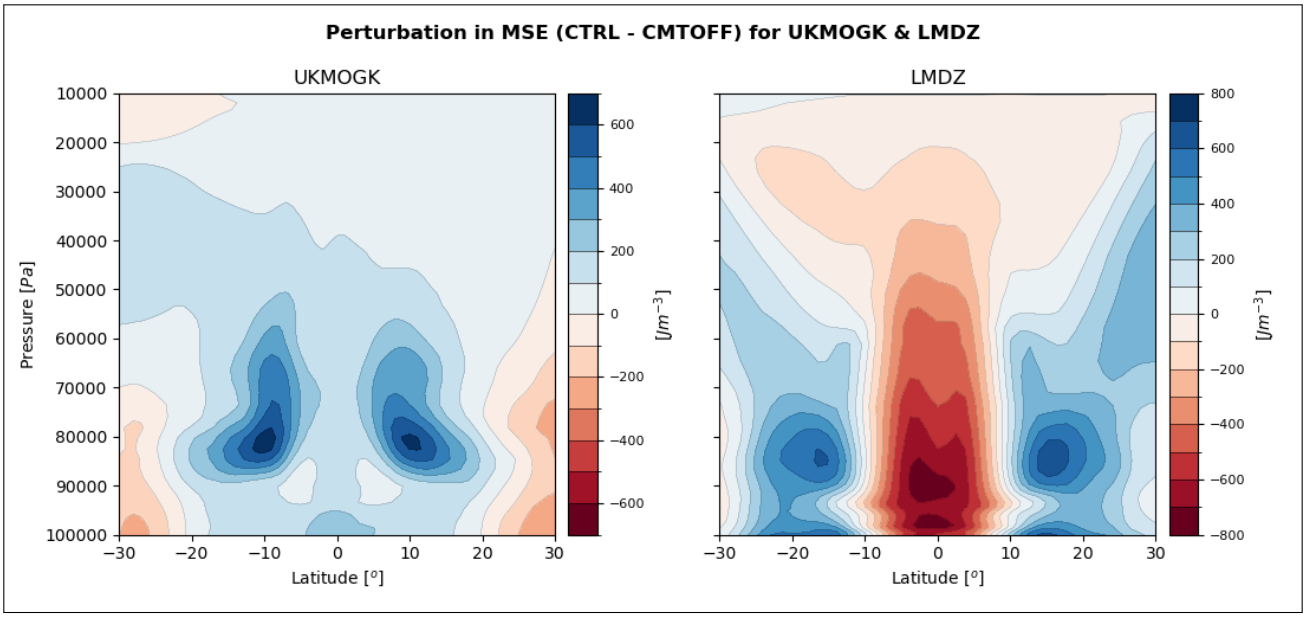

Figure 55: *Zonally Averaged Difference In MSE (CTRL - CMTOFF) For UKMOGK (Left) & LMDZ (Right).*

Appendix H: Energy Fluxes

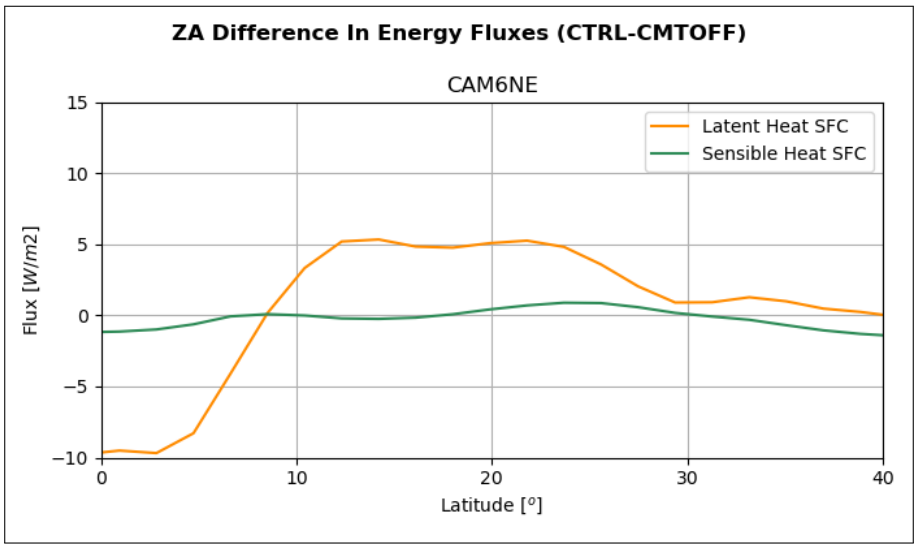

Figure 56: *Zonally Averaged Difference* ($SCMT_{ctrl} - SCMT_{off}$) *In Energy Fluxes For CAM6NE*

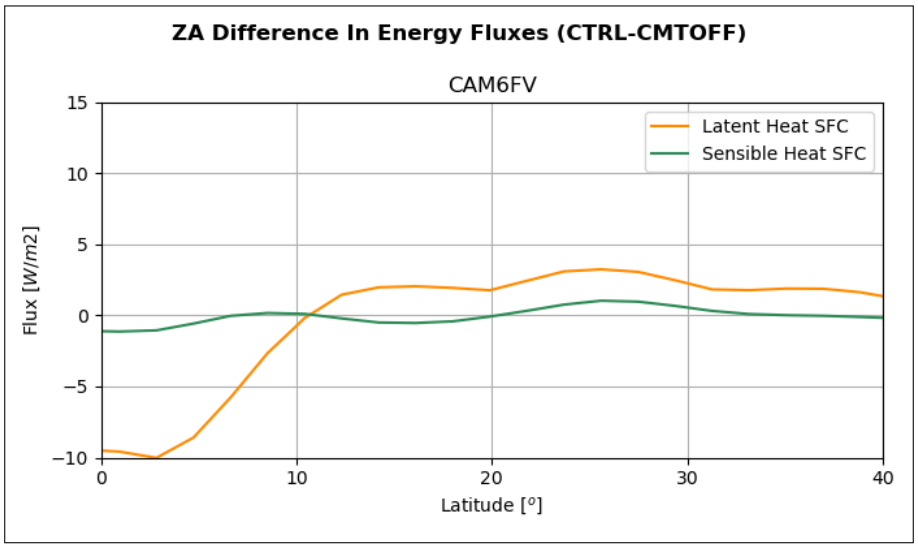

Figure 57: *Zonally Averaged Difference* ($SCMT_{ctrl} - SCMT_{off}$) *In Energy Fluxes For CAM6FV*

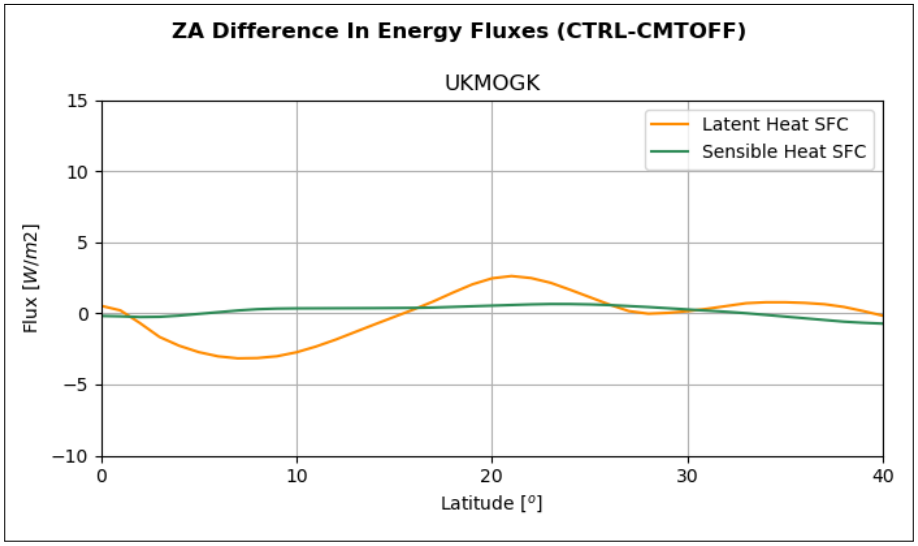

Figure 58: *Zonally Averaged Difference* ($SCMT_{ctrl} - SCMT_{off}$) *In Energy Fluxes For UKMOGK*

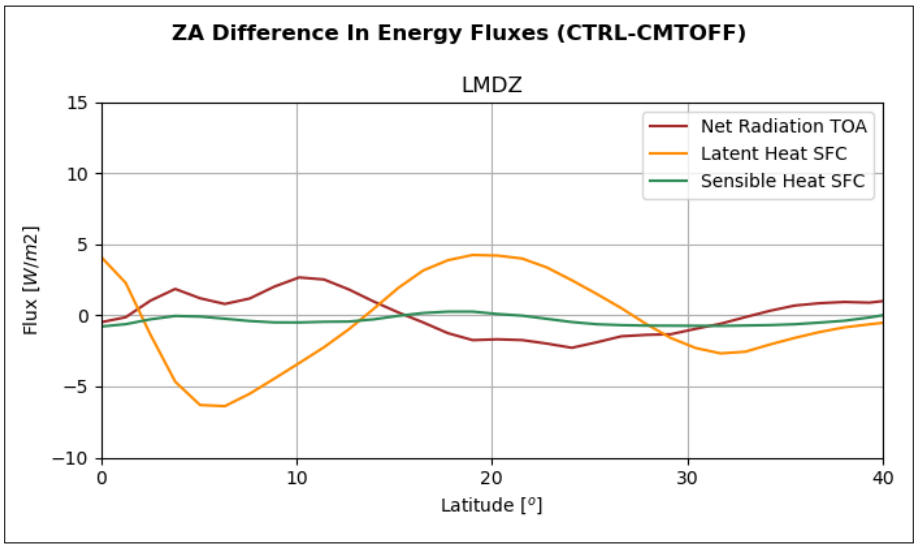

Figure 59: *Zonally Averaged Difference* ($SCMT_{ctrl} - SCMT_{off}$) *In Energy Fluxes For LMDZ*

Appendix I: MSE Advection

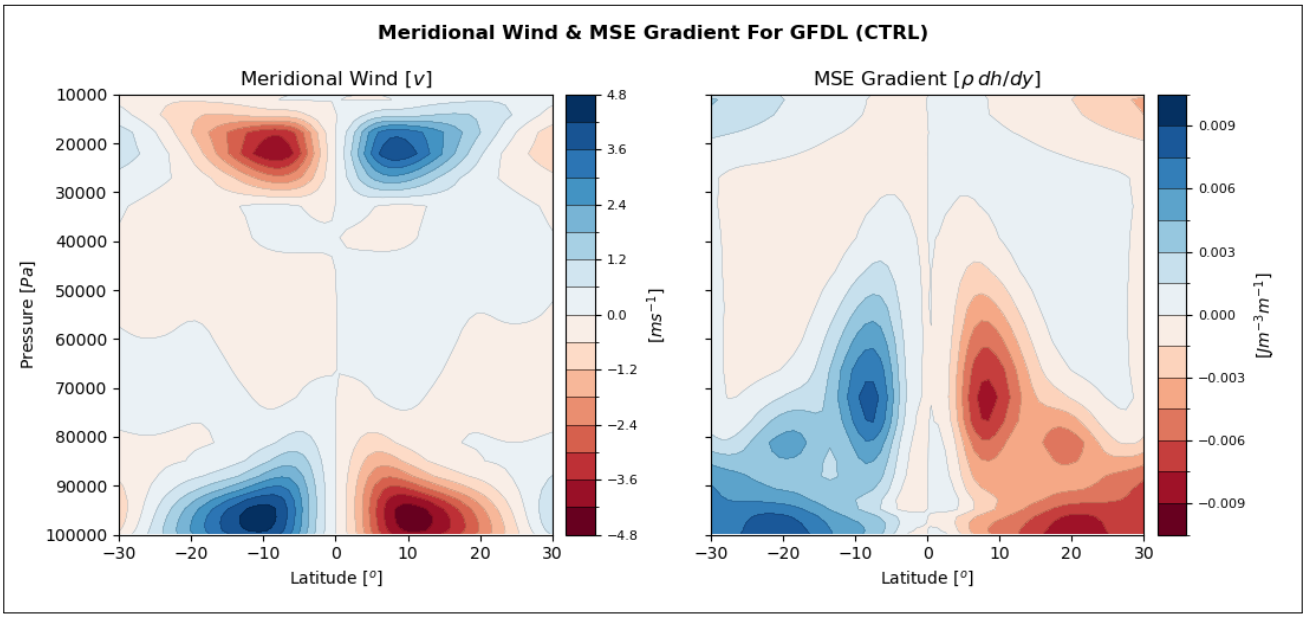

Figure 60: *Meridional Wind & Latitudinal MSE Gradient For GFDL (Control Experiment).*

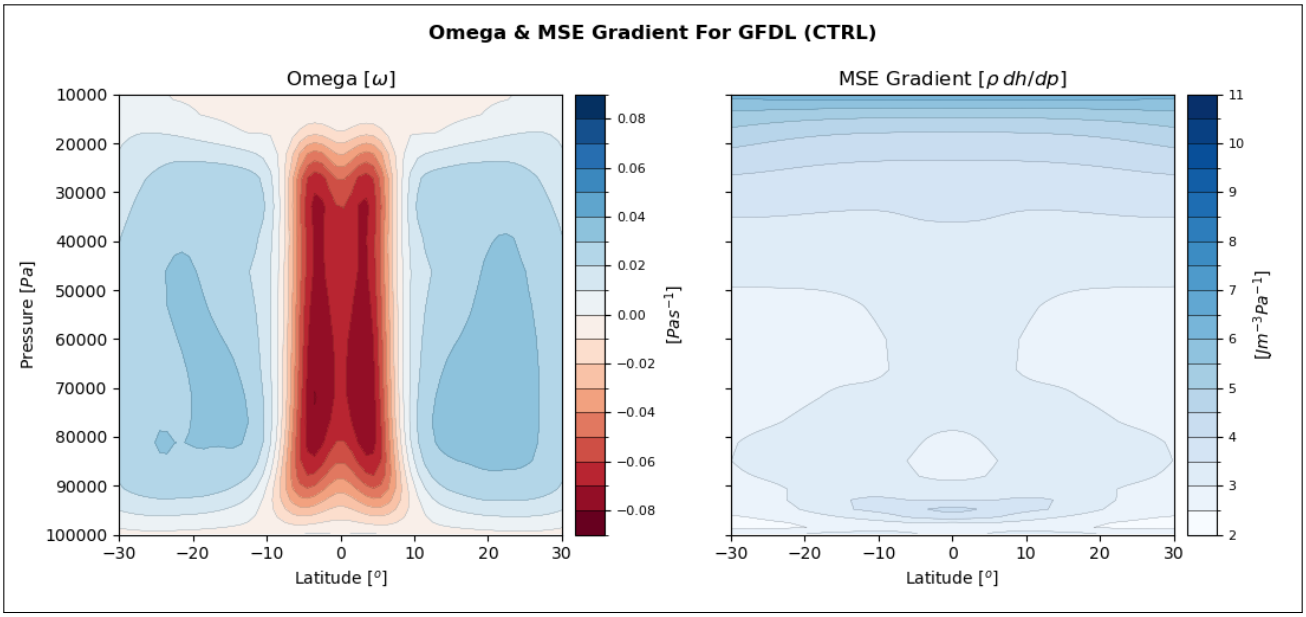

Figure 61: *Omega & Vertical MSE Gradient For GFDL (Control Experiment).*

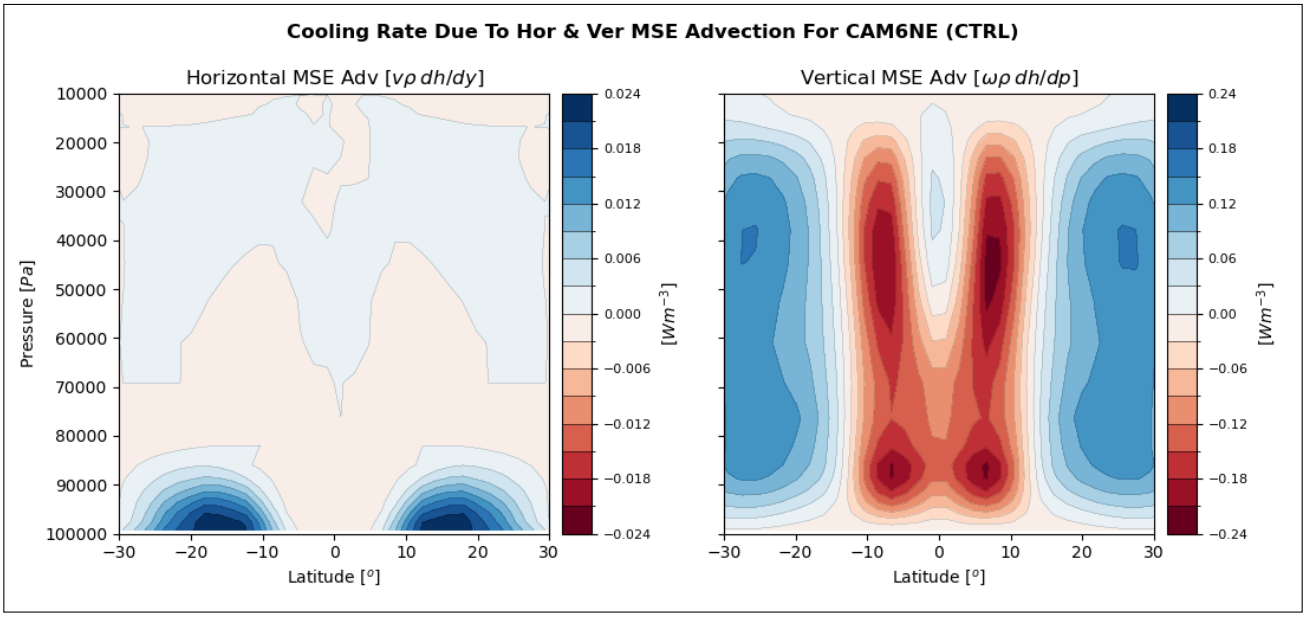

Figure 62: *Horizontal & Vertical Volumetric MSE Advection For CAM6NE (Control Experiment).*

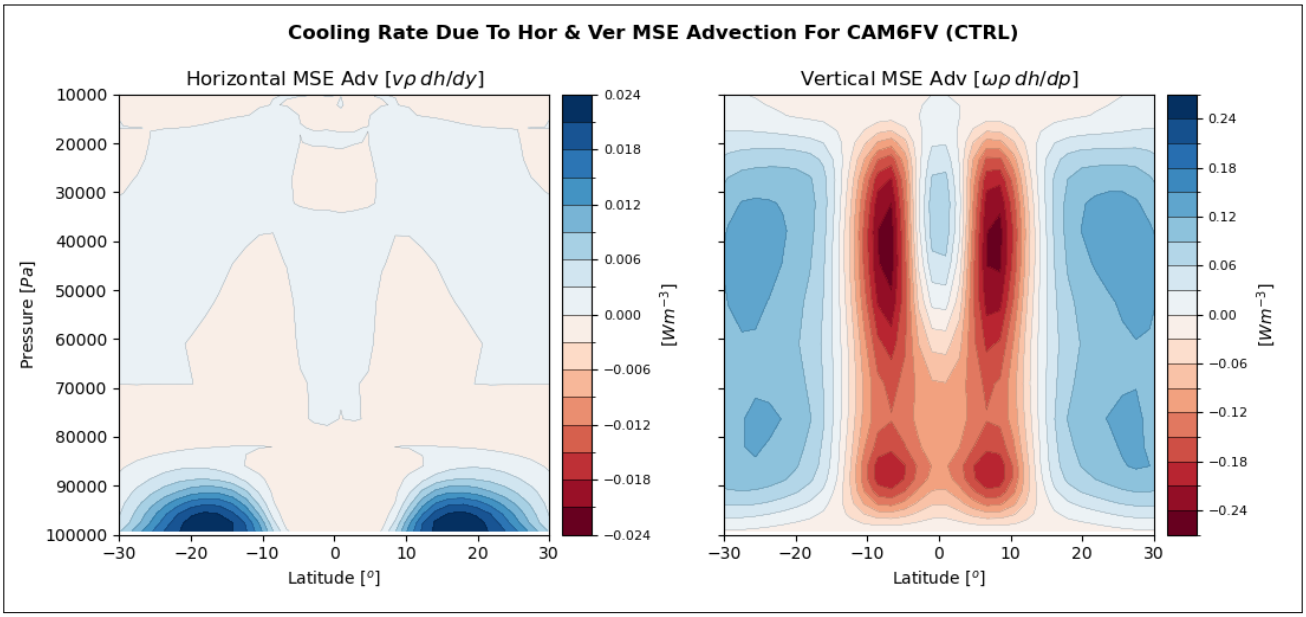

Figure 63: *Horizontal & Vertical Volumetric MSE Advection For CAM6FV (Control Experiment).*

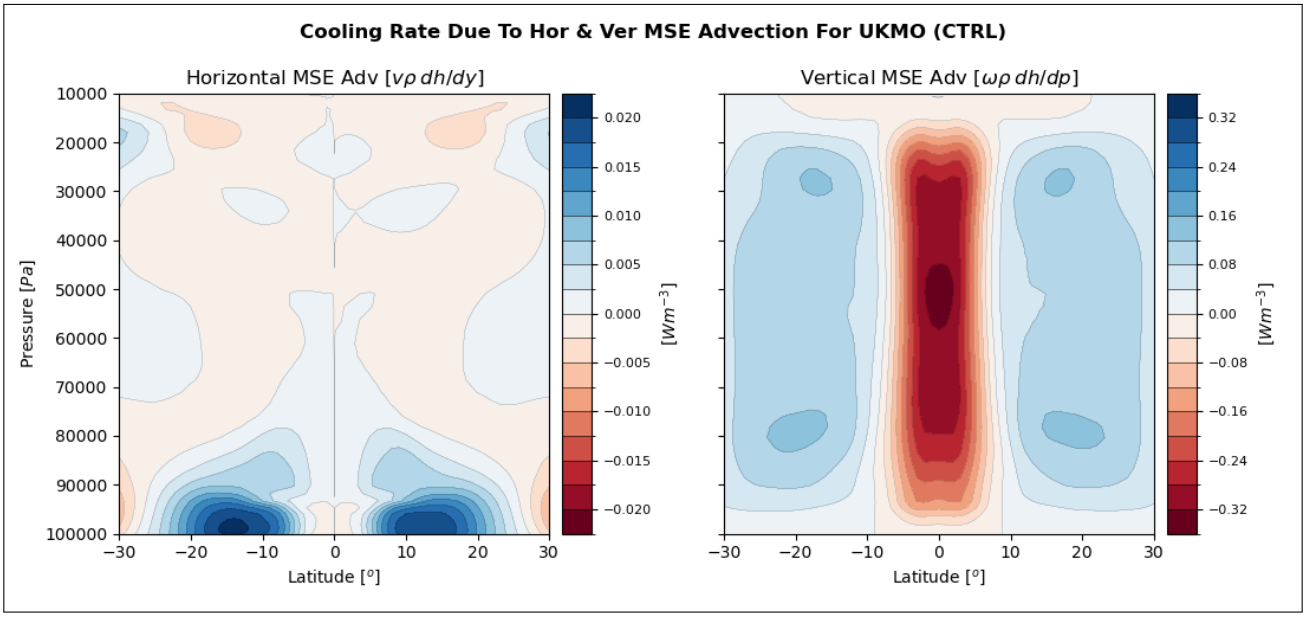

Figure 64: *Horizontal & Vertical Volumetric MSE Advection For UKMO (Control Experiment).*

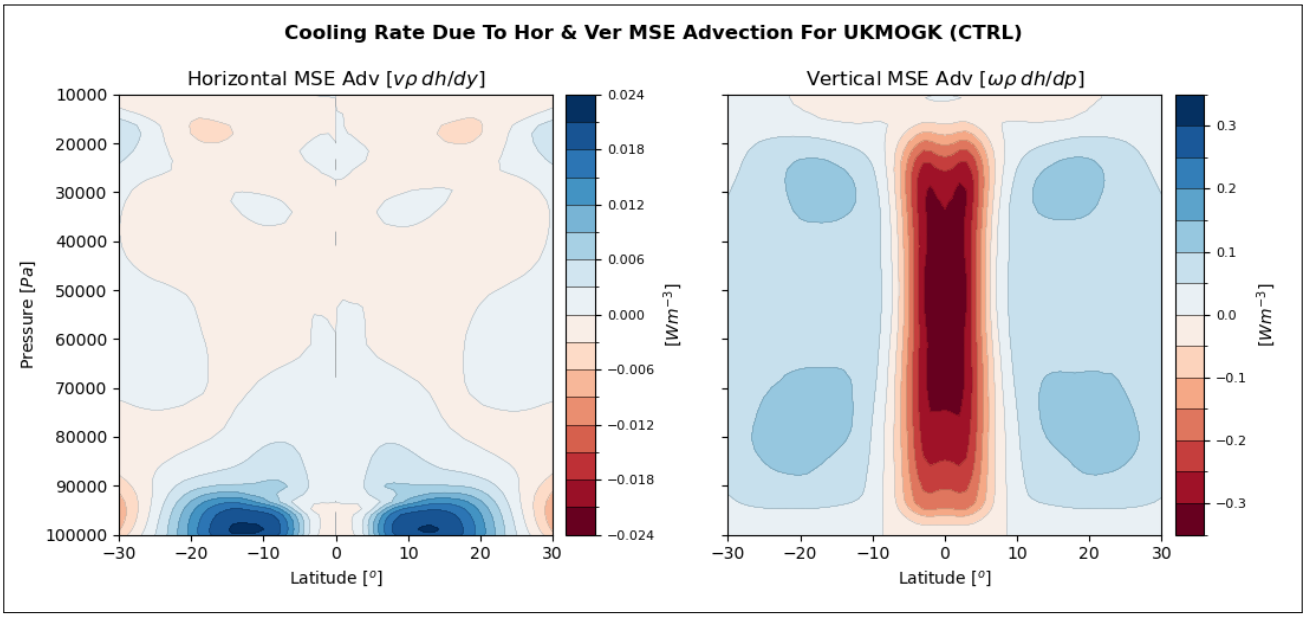

Figure 65: *Horizontal & Vertical Volumetric MSE Advection For UKMOGK (Control Experiment).*

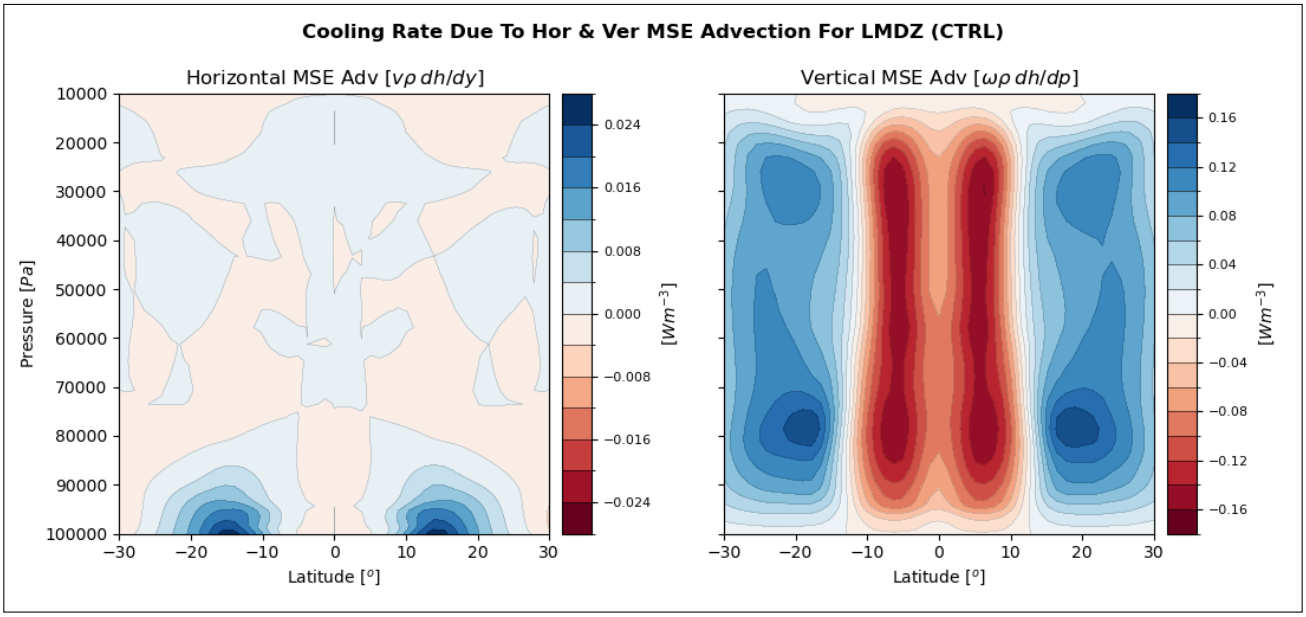

Figure 66: *Horizontal & Vertical Volumetric MSE Advection For LMDZ (Control Experiment).*

Appendix J: Change In Cooling Rates

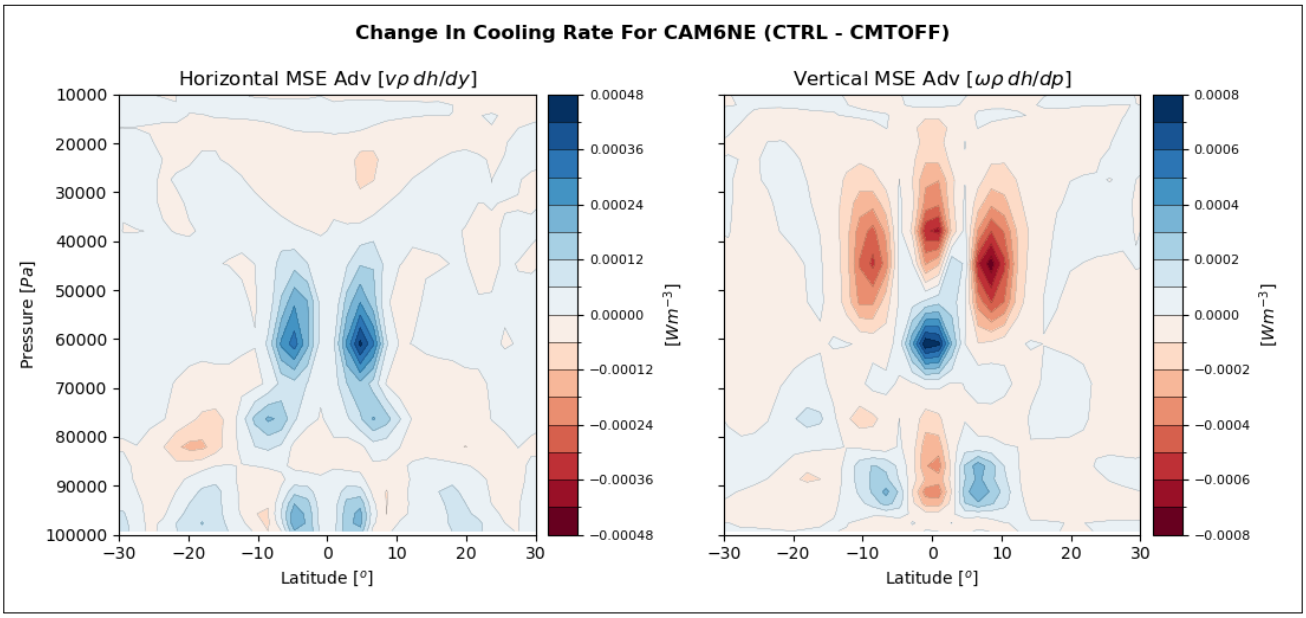

Figure 67: *Change In Cooling Rate ($SCMT_{ctrl} - SCMT_{off}$) Due To Horizontal & Vertical Advection For CAM6NE.*

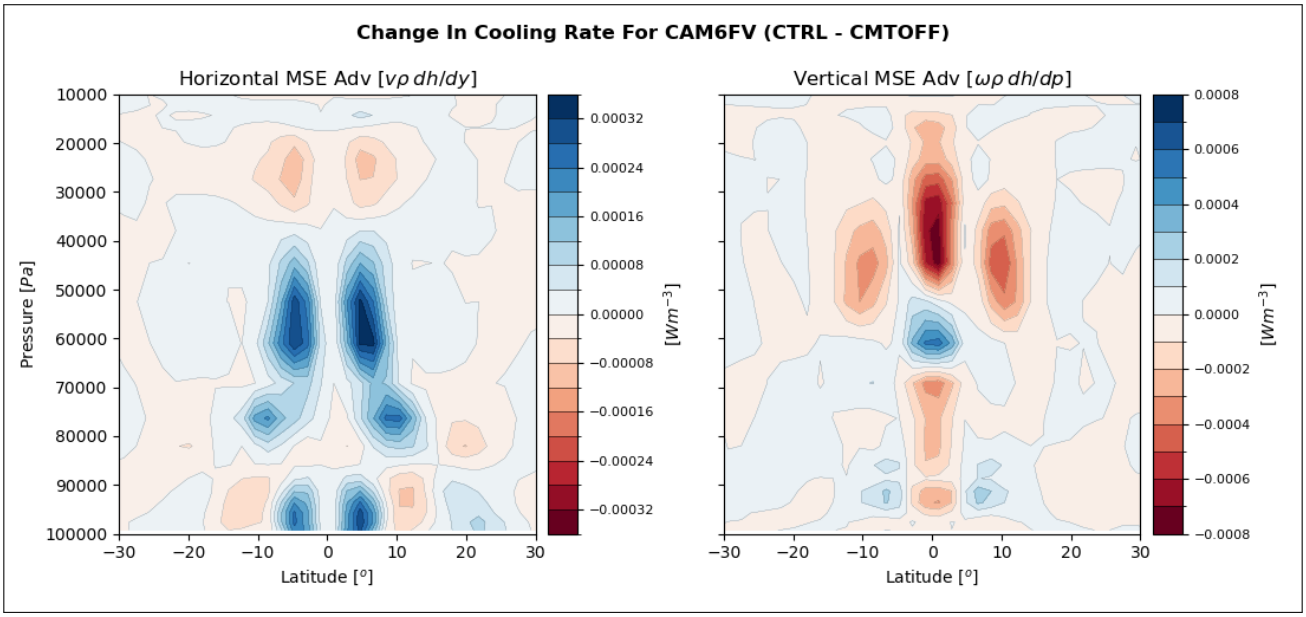

Figure 68: *Change In Cooling Rate ($SCMT_{ctrl} - SCMT_{off}$) Due To Horizontal & Vertical Advection For CAM6FV.*

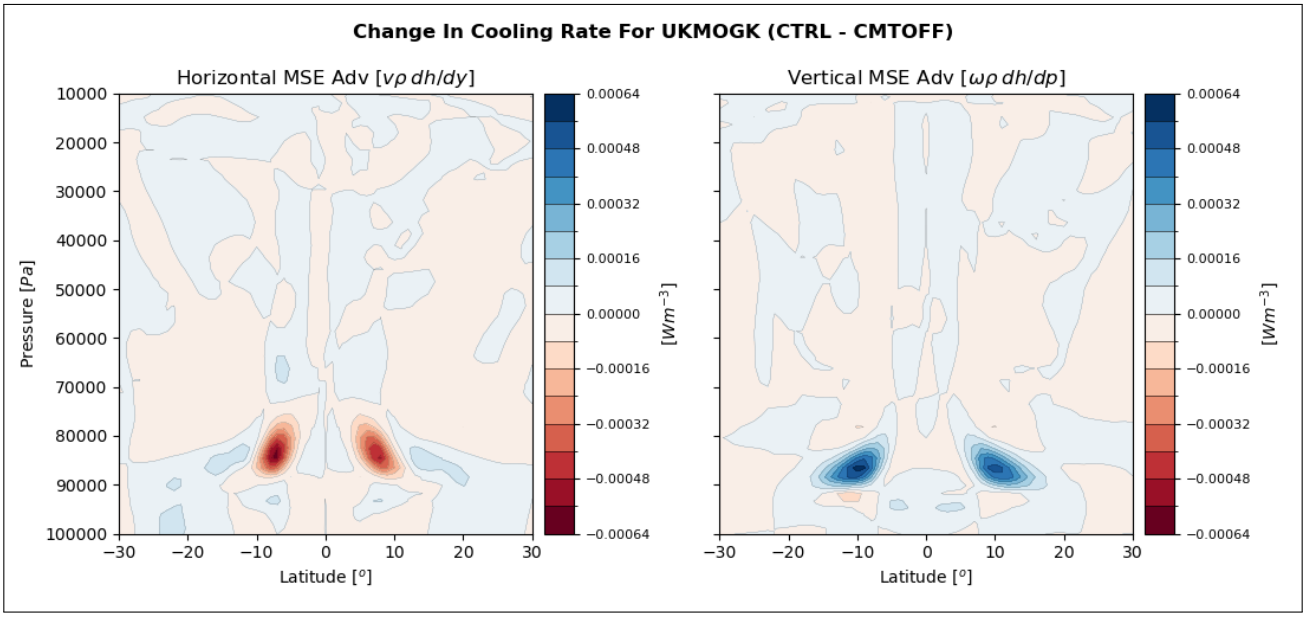

Figure 69: *Change In Cooling Rate ($SCMT_{ctrl} - SCMT_{off}$) Due To Horizontal & Vertical Advection For UKMOGK.*

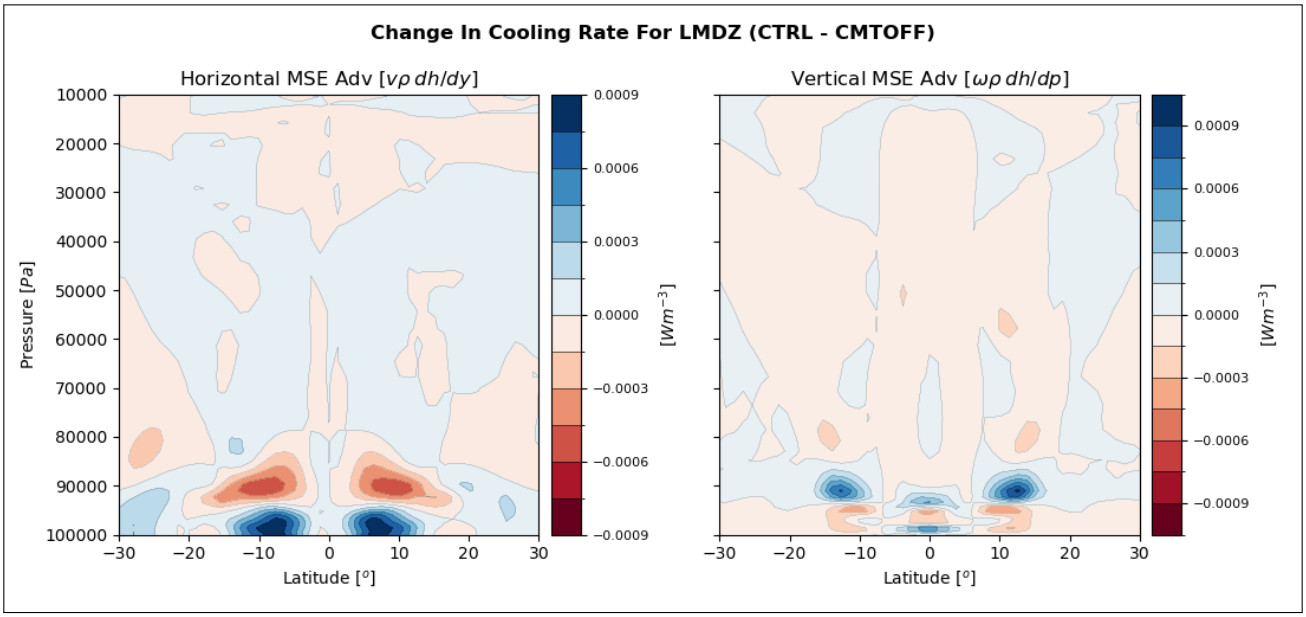

Figure 70: *Change In Cooling Rate ($SCMT_{ctrl} - SCMT_{off}$) Due To Horizontal & Vertical Advection For LMDZ.*